Measurement and Modelling of Underwater Acoustic Noise induced by Offshore Wind Turbines under the Effects of Varying Oceanic and Sea-State Conditions

Master's Thesis in Energy

Tiril Konow
University of Bergen
Geophysical Institute

June 2022

Acknowledgements

This 60 ECTS master thesis is written as part of the Integrated Master's programme in Energy at the Geophysical Institute, University of Bergen.

Firstly, I would like to thank my supervisor, Mostafa Bakhoday Paskyabi, for giving me the opportunity to write a thesis within such an interesting and highly relevant topic. Thank you for always making sure I have a deep understanding of our work, and for always pushing me to work hard and perform my best. Also thank you to the University of Bergen for providing financial support for the participation in the DeepWind Conference.

Thank you to all my friends, and fellow students especially. These five years at UiB would not be the same without you! We have had joyful times both during and outside of our studies, and I am happy for all our memories together. Throughout this last year, I am especially grateful for spending so much time together with Adrian Grotle, Christina Dimmen, Martine Rønning and Tore Skjerdal, who makes every day at the study hall an entertaining and fun journey.

Lastly, I would like to give a special thank you to my family for always believing in me and for supporting my choice of education. My parents have always shown great interest in my fields of study, and we have had many great discussions. Your endless support and love have kept me motivated to work towards my goals and best performance.

Abstract

In this thesis, we have performed several processing methods for analysing available hydrophone data. This was done in order to study the sound pressure levels in the vicinity of an offshore wind farm, and to identify energetic tones. These sound pressure levels was then compared to the environmental wind and wave conditions at the corresponding time.

Further, we have modelled how an acoustic signal from a wind turbine will propagate, and how the transmission losses will change under different forcing conditions. We have studied both scattered and continuous measurement series, and did modelling for two locations; by FINO1 offshore platform in Germany, and the location of the floating wind farm Hywind Tampen in Norway.

The ocean is a huge and valuable natural resource. Throughout the study, we have also discussed the importance of the research we have been performing. We have briefly looked into the legal framework for licensing offshore wind energy, and the importance of environmental assessment in order to live in harmony with other stakeholders. We have also looked into how we can contribute to more and deeper understanding within this field of study, especially in regard to marine species.

Contents

List of Tables

List of Figures

Chapter 1

Introduction

1.1 About Offshore Wind

Electricity generated from offshore wind plays a significant role in the future energy mix as the world transitions to a green and sustainable energy system. The installed capacity keeps increasing and is expected to increase over the next years. As the EU sets a goal of reaching at least 60 GW of installed offshore wind by 2030, it is clear that offshore wind will be a primary electricity source in the near future. EU's offshore renewable strategy also poses that Norway has great opportunities within offshore renewable energy European Comission (2020).

Offshore wind farms are already in operation along the coast of many European countries. There exist several proven technologies for offshore wind, and most of the offshore turbines are bottom fixed. As offshore farms are planning to be deployed in deeper waters, floating technology is growing in the market. Floating wind has great potential for both deep waters and challenging seabed environments, and together with the better wind conditions far off the shore, it leads to an outstanding performance compared to the remaining wind sector (WindEurope (2021)).

In June of 2020, two areas were opened for licence applications for offshore wind projects in Norway. These areas are Utsira Nord and Sørlige Nordsjø II, and the areas allow for a total installed capacity of 4500 MW. Utsira Nord is suitable for floating wind installations, whereas Sørlige Nordsjø II is of depths that allow for both bottom-fixed and floating technology (Norwegian Government (2020)). In a press release in May of 2022, the Norwegian Government presented a major initiative to promote offshore wind power, by aiming to open up areas for the production of 30 GW of power by 2040 (Norwegian Government (2022a)). They then followed up with funds for mapping of the seabed, and how existing and new industries affect each other and the ecosystems around. This aims to accelerate progress in the development of offshore wind projects (Norwegian Government (2022b)).

Even though wind power is a renewable and therefore more environmentally friendly form of energy, it also poses effects and challenges. An important problem when installing new offshore wind farms is to determine the sound disturbances from the turbines, and how it affects the marine environment. In an area of a wind farm, disturbances like construction and operational noise will occur and should therefore be studied to address and limit the environmental impact.

1.2 Underwater Acoustic Noise

In the ocean in general, there are a lot of environmental ambient sound sources. This includes both natural contributions and anthropogenic sources, i.e. sources that are caused by human activities. These sources of sound are visually illustrated in Figure 1.1. Natural contributions include weather conditions, wave breaking and sound from marine mammals and fish. Human activities also generate sound either unintentionally as a consequence of construction and shipping, or intentionally when performing seismic surveys or detecting fish and other objects. Most of the anthropogenic sound sources can be classified as noise in the ocean, as they are neither of use nor value, and don't have a biological meaning for the surroundings (Bertucci et al. (2021)).

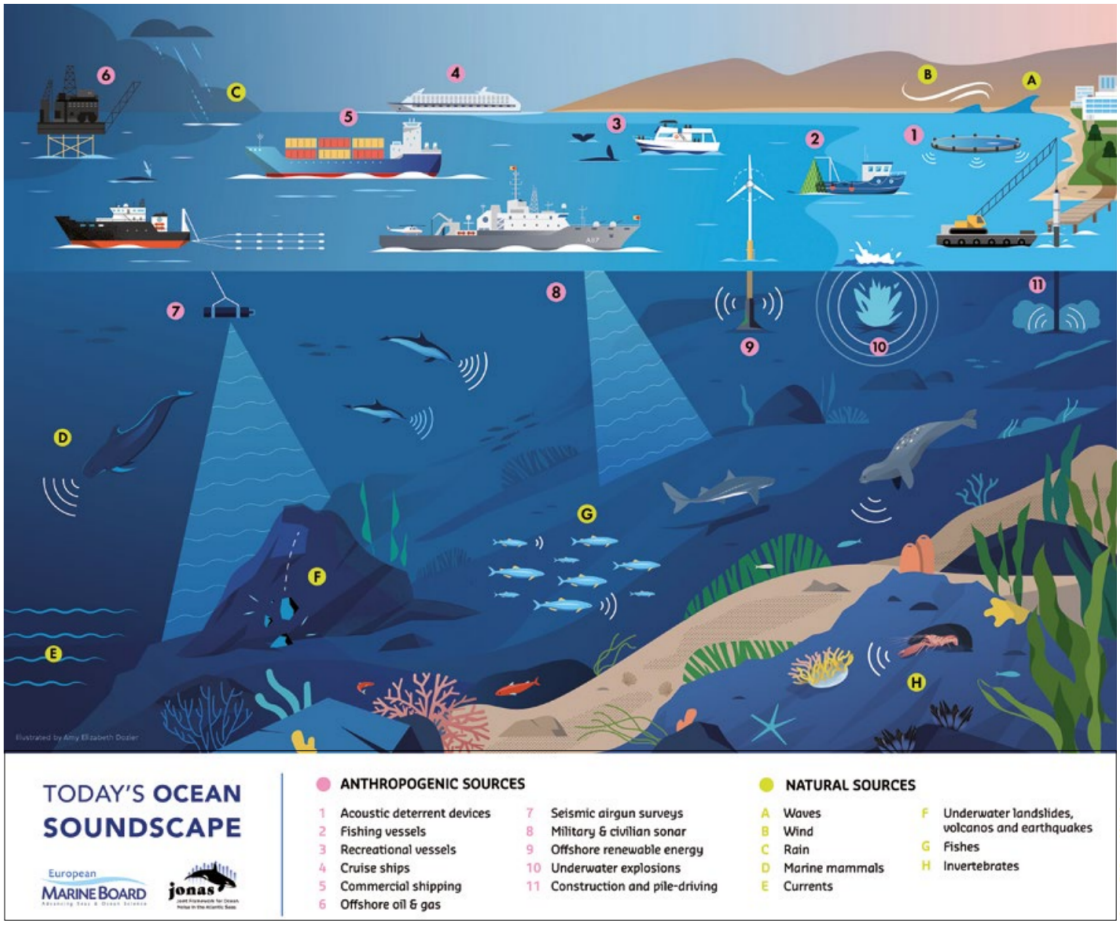

Figure 1.1: Overview of anthropogenic and natural ambient sound sources in the ocean (Bertucci et al. (2021)).

The curves in Figure 1.2 are known as *Wenz curves*, from his study on acoustic ambient noise in the ocean (Wenz (1962)). The figure illustrates how ambient noise in the ocean is distributed with frequency, and how loud it is. Man-made sources, such as ship traffic, dominates in the intermediate region of the spectra. Outside this frequency range, ambient noise is mostly due to natural sources, such as earthquakes, precipitation and breaking waves related noise. Bubble and spray noise is wind dependent and is therefore parameterized according to Beaufort sea states (Wenz (1962)).

At an offshore wind site, acoustic noise is generated by several activities such as during construction, operation, maintenance, and the decommissioning phase. There is also background noise from ship traffic, breaking waves etc. as discussed above. From the turbine itself, noise is generated through vibrations in the turbine when wind and waves are hitting the turbine. These vibrations cause pressure waves with alternating compressions and rarefactions that move fluid particles (Weissenbergen (2019)). The amount of sound generated is therefore also determined by the different oceanic and sea state conditions, as that influences the vibrations. Underwater noise from turbines can be divided into different categories, depending on which phase of the turbine's life cycle we are currently investigating. Examples are noise during construction, operation, and dismantlement.

Sound is very important for marine mammals and fish. Oceanic species depends on their acoustic sense to map their surrounding, locate food, interact and protect themselves (Dosits (2018)). For most marine animals, sound is therefore crucial for their survival and the possibility to adapt to their surroundings. The turbine-induced noise can influence during all phases of the turbines life cycle, and during construction and maintenance, ship traffic can also play a role as well. Some of the concerns regarding noise emissions from offshore wind turbines include interruption of communication abilities, habitat changes, displacement and disruption when fish and other mammals detect the acoustic surroundings (WWF (2014)).

The potential risk of deploying offshore wind farms on marine ecosystems has not been comprehensively assessed in order to inform environmental-based marine management and planning. Therefore, measurements and modelling of underwater disturbances from offshore wind turbines are important. With this kind of research, we can increase the understanding of the possible environmental impacts of offshore wind energy, and develop an effective legal framework required before licensing offshore wind energy projects and during their lifetime operation.

1.3 Objectives

Overall, the results of this study will give a site-specific overview of the acoustic noise and how the turbine induced noise change under varying oceanic and sea state conditions. Available observational data sets will be studied statistically and spectrally, and acoustic modelling will determine the propagation of sound at the site of interest. When sound pressure levels and their distributions and losses are determined, we have a basis for determining how they may influence marine species at the study site.

The thesis will directly or indirectly affect the following sustainable development goals:

- SDG 7: Affordable and clean energy.
- SDG 13: Climate action
- SDG 14: Life below water

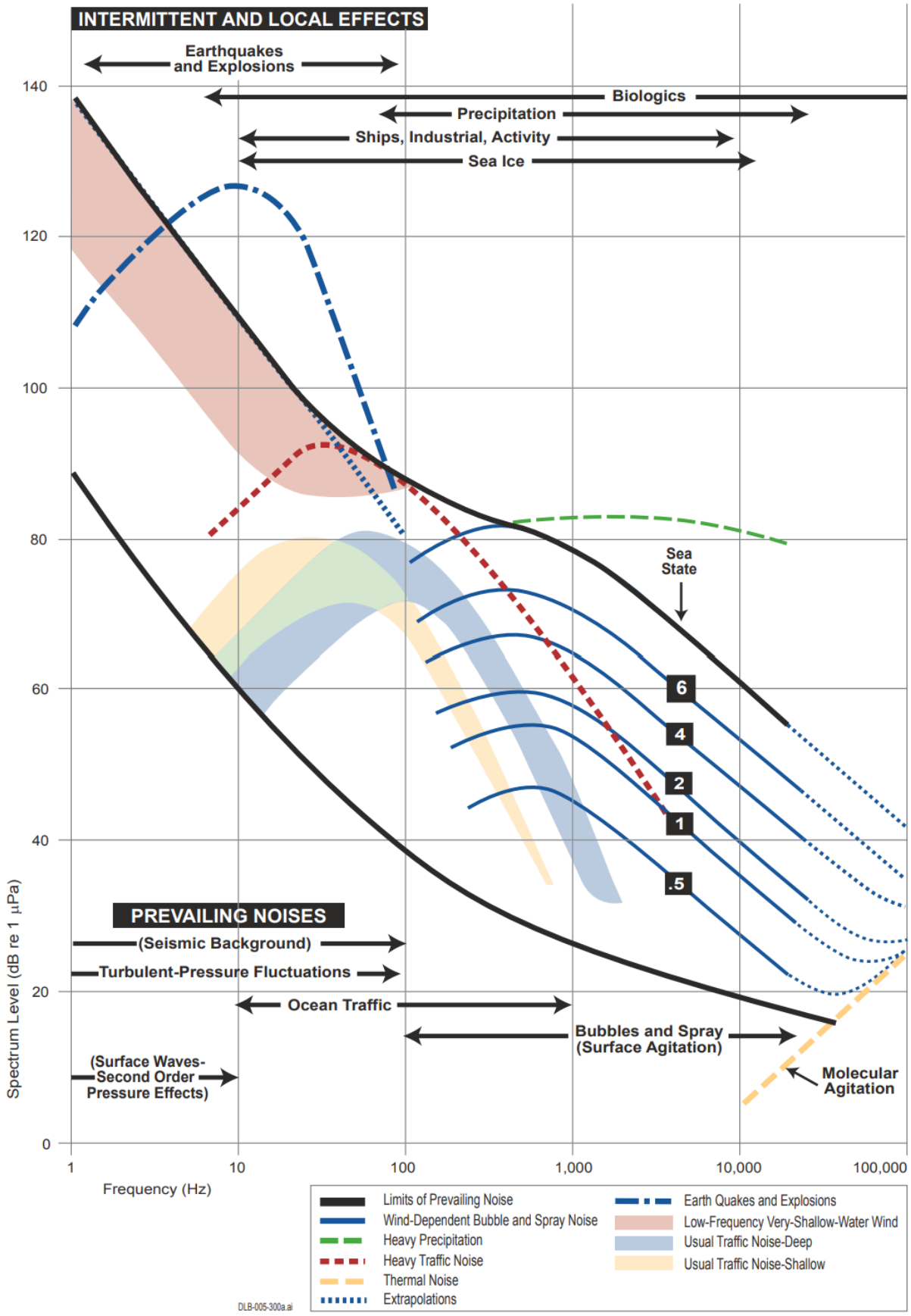

Figure 1.2: Composite of ambient noise spectra. From Bradley and Stern (2008) by Wenz (1962).

Chapter 2

Theory

2.1 The Ocean Environment

2.1.1 Properties of the Ocean

The ocean has several geographical and physical characteristics such as salinity content, temperature gradients and currents that change with the season, depth and location. The ocean surface is especially sensitive to seasonal and diurnal changes. All these properties have a great influence on the generation and propagation of underwater sound in the environment.

We can divide the ocean into different horizontal layers, based on the density profile in the area which is mainly affected by the temperature and salinity of the water. In general, dense water is situated in the deeper ocean with the lighter water on top. This layering due to differences in density is known as ocean *stratification*.

The very upper ocean is experiencing heavy mixing due to the exposed surface wind and waves. This makes the layer more uniform in terms of temperature and salt content. Below this mixed layer, the temperature is rapidly decreasing with depth. We call this a *thermocline*. In many parts of the ocean, density is a strong function of temperature, and this rapidly increasing density layer can therefore also be referred to as a *pycnocline*. In polar waters and areas where ice is present, the surface water is usually colder, making the salinity gradient more important for the density structure than the temperature gradient. This kind of salinity profile where the surface is of freshwater with increasing salinity below is known as a *halocline* (Talley et al. (2011)). This structure can also be found in areas of high precipitation.

Many processes can disturb the stratification. At the interface between air and ocean, we have interactions such as wind and waves making the environment very dynamic and full of variability. Wind and wave interactions are important for mixing in the ocean surface layer, and will further affect the distribution of ocean characteristics. Internal waves are generated from the energy in surface wind and tides. The breaking of internal waves leads to stirring and mixing in the ocean. Other examples are heat transfer, and upwelling or downwelling. This mixing of density will again affect the ocean currents (Talley et al. (2011)).

As we will discuss later, ocean stratification is important for the distribution of sound. The ocean surface is therefore an interesting interface as it is easily affected by weather conditions and variability. Another interface of interest is the ocean seabed. At most existing offshore wind farm sites, this is a relatively stable interface. Sound distribution will however be influenced by the seabed properties as rays can be reflected and scattered by the bottom surface.

2.1.2 Effect of Offshore Wind Farm on Stratification

In the vicinity of an offshore wind farm, there will be interactions between the farm and the upper-ocean currents and stratification. As a result, the sound speed and propagation of sound will therefore be affected by the turbines at an offshore wind site. Bakhoday-Paskyabi (2015) studied the interactions between an offshore wind farm, upper-ocean currents, and stratification under shallow water conditions. The study first investigated wind farm wake and vortex formations, and then related these aspects to ocean dynamics such as upwelling and downwelling currents. Such processes are significant for the climatology of the mixed layer especially.

The following figures illustrate a cross-section view of the current anomaly (v-component) and change in density. The domain has a sloping bathymetry, a water depth of 50 m and a range of 100 km. The initial mixed layer has a thickness of 10 m with a density value of 1025 kg/m^3. The wind farm consists of 5 turbines with a spacing of 1 km placed in the centre of the domain (at 50 km). From Figure 2.1 we see a difference in the Ekman drift for the simulations with (middle and bottom panels) and without (top panel) wind farm effects. The gradients are stronger in the simulation including wind farm effects.

For our study, it is interesting to look at what role the above interactions play in the change of density profiles. The change in the density profile in Figure 2.2 is displayed as density anomalies relative to 1025 kg/m^3. The simulation duration is five days, and the top panel shows the development with no wind farm effects, which we can have as a "reference" case. The previous results imply that the wind farm effects cause an Ekman drift at the sea surface. From these results, we see that this induces perturbations to the water column. These perturbations are seen as a displacement of flow and oscillations in the column. When the wind farm is present, the initial density structure has moved closer to the coast, and the density anomalies are bigger.

From the results of the vertical ocean model run, it is clear that the wind farm induced disturbances to the wind field can change the upper ocean stratification pattern, which is what Bakhoday-Paskyabi (2015) concluded within his paper.

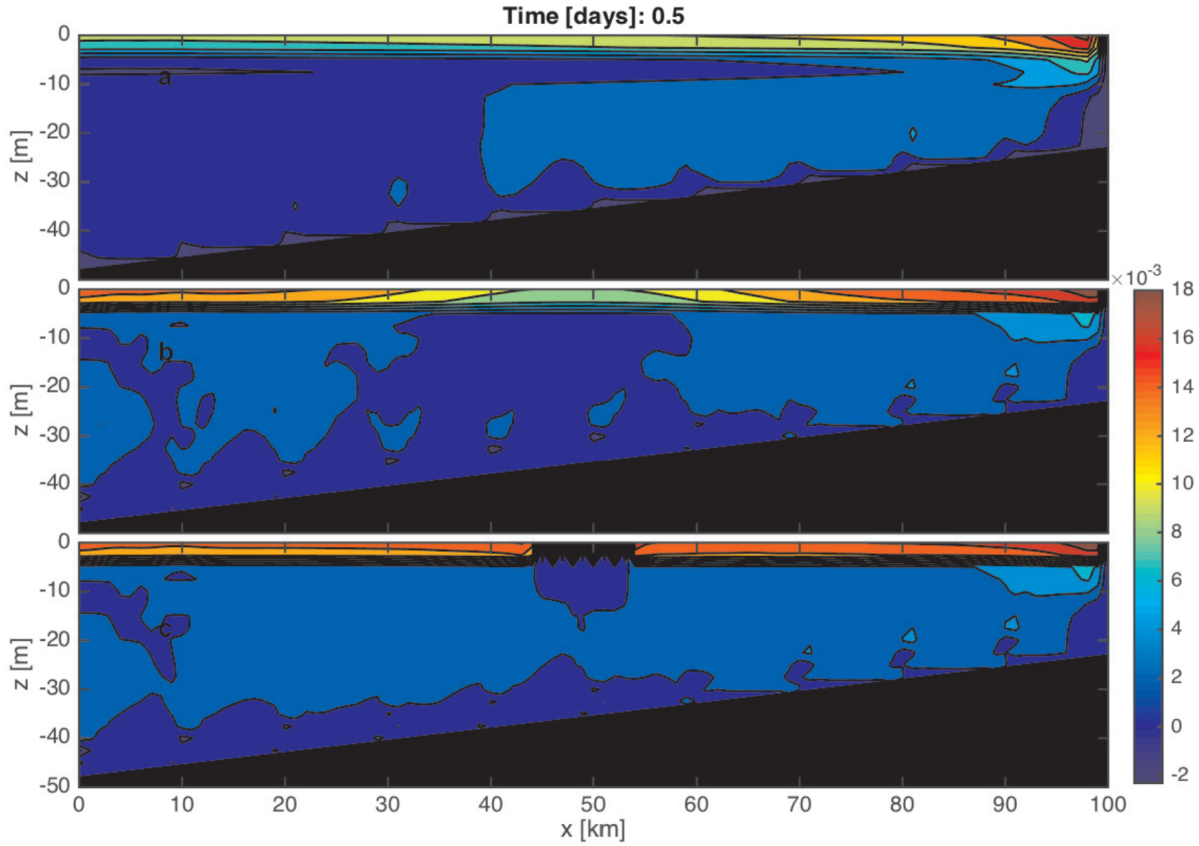

Figure 2.1: Ocean current (v-component) after 12 hours of simulation. Top: No wind farm effect. Middle: Influence of wind farm as a rigid body. Bottom: Influence of wind farm as a cluster of 5 single turbines aligned (Bakhoday-Paskyabi (2015)).

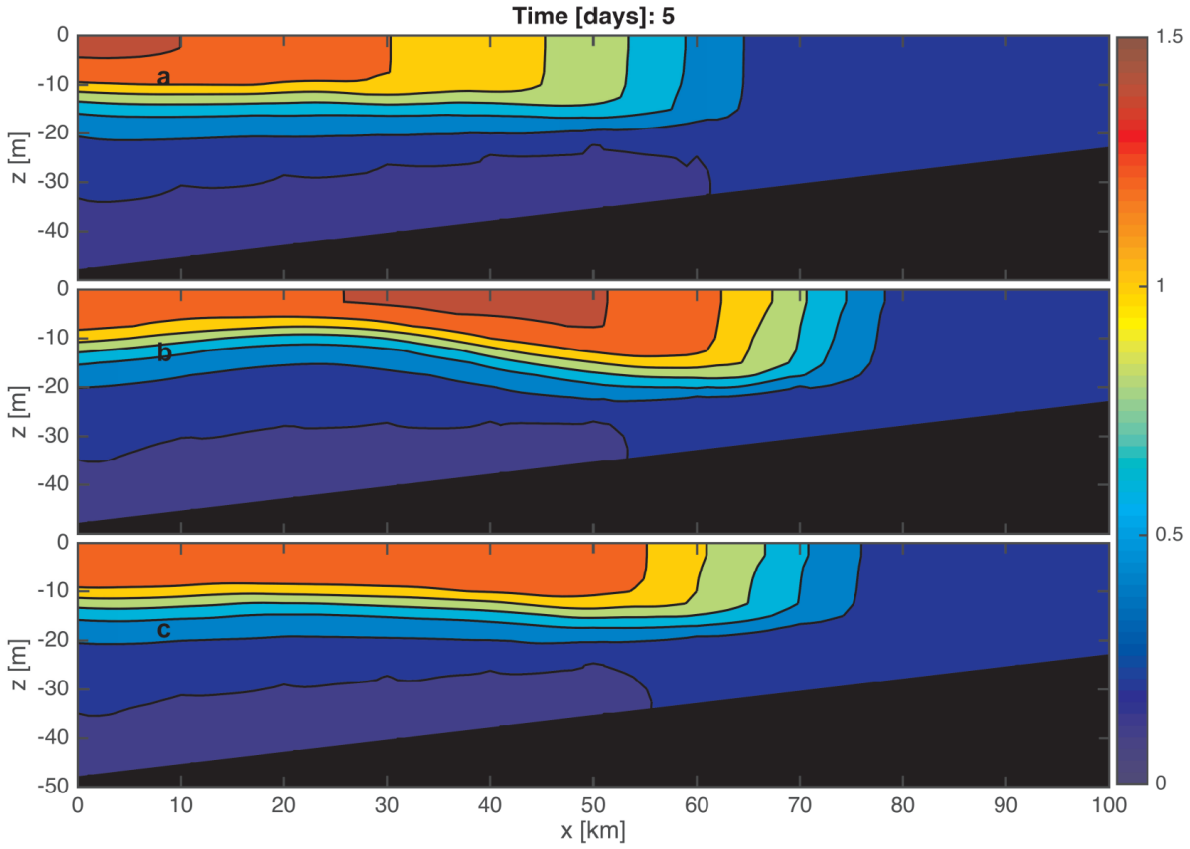

Figure 2.2: Density anomaly after 5 days of simulation, relative to 1025 kg/m^3. Top: No wind farm effect. Middle: Influence of wind farm as a rigid body. Bottom: Influence of wind farm as a cluster of 5 single turbines aligned (Bakhoday-Paskyabi (2015)).

2.2 Physics of Sound

2.2.1 Characteristics of Sound

Acoustics can be defined as the generation, transmission and reception of energy as vibration waves in the matter (Kinsler et al. (2000)). When molecules in a fluid are displaced it creates an elastic restoring force that causes oscillatory movement. These movements are essentially vibration, which is what generates acoustic waves. Since acoustic waves are pressure fluctuations they can only exist in compressible fluids, hence sound does not exist in a vacuum.

In order to describe the sound, we need different terms and equations. The following theories are mainly from the books *Fundamentals of Acoustics* by Kinsler et al. (2000) and *Computational Ocean Acoustics* by Jensen et al. (2011). When describing sound we use terms like acoustic pressure. In our case, it is the change in water pressure due to the presence of the sound that is the acoustic pressure (Bradley and Stern (2008)). The water pressure from sound will be different from the undisturbed water pressure and change with time.

One fundamental equation is the linear, lossless wave equation, Equation (2.1). It is obtained from the equation of state, equation of continuity and Euler's equation (simple force equation). It describes the propagation of sound in a fluid with phase speed c [m/s]:

$$\nabla^2 p = \frac{1}{c^2}\frac{\partial^2 p}{\partial t^2}, \tag{2.1}$$

where p is the acoustic pressure [Pa] and t is the time [s]. To drive a source we need energy. Both potential and kinetic energy are transported by acoustic waves. Kinetic energy comes from the motion of the particle that has a certain mass. The potential energy is related to the change in volume when pressure fluctuations occur. When summing these energies and dividing by the initial volume we can obtain the total instantaneous energy density ε. If we time average the energy density over one cycle T, and use the RMS values of the pressure and particle speed amplitudes P and U, we obtain the following equation for the energy density:

$$\varepsilon = \frac{1}{T}\int_0^T \varepsilon_i \, dt = \frac{1}{T}\int_0^T \frac{p^2}{\rho_o c} \, dt = \frac{PU}{2c} = \frac{p_{rms} u_{rms}}{c}. \tag{2.2}$$

This is considering a plane harmonic wave. RMS is an abbreviation of Root-Mean-Square. It is a way to characterize a sound wave as the signal will have fluctuations and different peaks. To calculate the RMS value, we take the square root of the values squared and average over a measured time (Dosits (2021)).

The rate at which this energy is transmitted through a unit area is known as the acoustic intensity I. We time average the instantaneous intensity over a period T and obtain:

$$I = \frac{1}{T}\int_0^T I(t) \, dt = \frac{1}{T}\int_0^T pu \, dt = \pm\frac{p^2}{2\rho_0 c}, \tag{2.3}$$

where $\rho_0 c$ is known as the specific acoustic impedance and has the value $1.5 \cdot 10^6 \; kg/(m^2 s)$ for seawater.

To describe the sound strength, we use sound levels in decibel (dB) scale. This is a logarithmic scale which is suitable considering the wide range of sound pressures and intensities. Since dB is a dimensionless unit we always express it together with a reference intensity I_{ref} or pressure P_{ref}. The Intensity Level (IL) and Sound Pressure Level (SPL) can be expressed as followed:

$$IL = 10\log\left(\frac{I}{I_{ref}}\right)[dB\ re\ I_{ref}]\ ,\ SPL = 20\log\left(\frac{P}{P_{ref}}\right)[dB\ re\ P_{ref}]. \tag{2.4}$$

For underwater acoustic studies, it is common to use a reference pressure of $P_{ref} = 1\mu Pa$.

2.2.2 Sound Generation from Offshore Wind Turbines

From an operating wind turbine, noise is generated through vibrations in the turbine. These vibrations cause pressure waves with alternating compressions and rarefactions that move fluid particles (Weissenbergen (2019)). From a wind turbine at an offshore site, noise is generated in every phase of the turbine's lifetime. For acoustic studies both the generation and propagation of sound are interesting. As we will discuss, there are different sources causing the generation of sound in an offshore wind turbine. An overview of vibrations from an operating turbine is given in Figure 2.3.

During the operating phase, noise is primarily generated by mechanical sources due to the machinery in the nacelle. The mechanical noise from the nacelle is emitted at low frequencies, below 1 kHz. These correspond to the frequencies and their harmonics of the gear mesh frequencies in the gearbox (Pangerc et al. (2016)). Mechanical vibrations from the turbine's generator and gearbox will propagate directly in the air, or indirectly through the tower. Corresponding underwater noise is generated by downwards guided vibrations radiated from the tower (Betke et al. (2004)). When the gearbox noise is emitted through the nacelle openings, we call it *air-borne* noise, and the indirect noise is known as being *structure-borne* (Szasz and Fuchs (2010)).

In offshore conditions, the tower vibrations can also be caused by both wind and waves. Pangerc et al. (2016) showed that the radiated sound were primarily related to the gearbox, but that the variation in amplitude varied with wind speed, and thus rotor and generator speed. As wind passes through the turbine blades, aerodynamic noise is created. There are different types of aerodynamic noise; discrete noise due to wakes or velocity gradients, self-induced noise generated by the airfoil and noise due to atmospheric turbulence (Szasz and Fuchs (2010)). This generated sound may enter the water through an airborne path, or through the turbine structure. In addition, waves will impose loads on the turbine, causing structural vibrations.

New types of foundation and increasing turbine sizes raises questions about how the generated sound may differ. The mechanical resonance of the tower and foundation is likely to change with size. However, it is not straight forward to predict the corresponding changes with generated noise as the distance from the nacelle to the water also increases with increasing turbine size (Tougaard et al. (2020)). Also, direct-drive wind turbines, i.e. turbines without a gearbox, are quieter during operation as mechanical noise is reduced, compared to a gearbox wind turbine as discussed previously (Edis Osmanbasic (2020)).

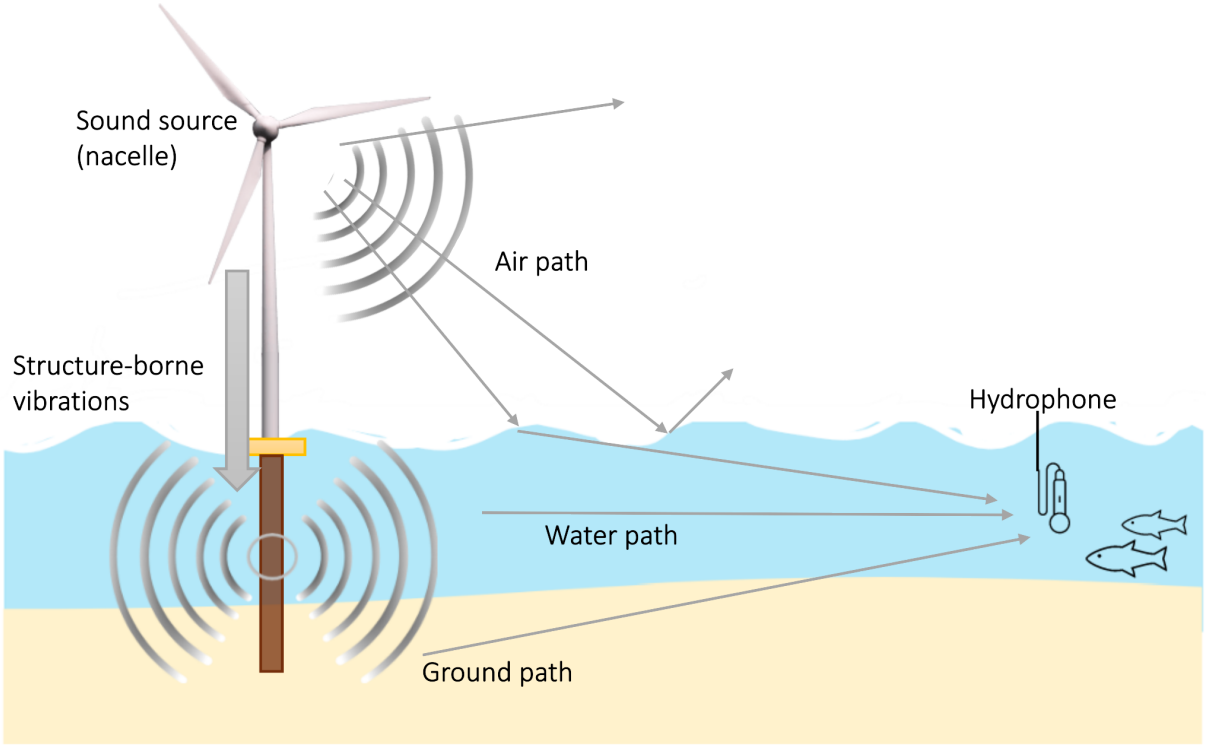

Figure 2.3: Vibrations and underwater sound generation from an offshore wind turbine (illustration inspired by Sowmiya (2018)).

At certain wind velocities, the oscillations will shed at frequencies equal to the tower's natural frequency, causing it to resonate. Sound waves will be amplified by resonance. It is therefore important to study the turbine structure's natural frequencies and mode patterns. The most important frequencies to cause structural vibrations are the excitation frequencies of the blade rotation and blade passing. These are known as the 1P and 3P frequency intervals. When designing wind turbines and their foundation, the natural frequency should be different from these frequencies to avoid resonance (Jose and Mathai (2018)). This is mainly to limit the fatigue on the turbines, but will also limit the sound wave amplitudes. Figure 2.4 shows an approximate range of the frequencies related to a typical offshore wind turbine.

The acoustic power caused by these frequencies is usually concentrated and seen in a narrow range of frequencies similar to the excited frequencies from the turbine. The connection between turbine vibration and acoustic power can be found by studying the spectral data and looking for any correlations between the vibrations and noise spectra, as will be discussed in the following subsection.

The turbine vibration characteristics described in this section are typical for the operation phase. The operational phase is the longest time period of a wind turbine's life cycle and is therefore important to assess. In the ocean, there are always a lot of ambient sound sources, such as breaking waves, tidal noise and ship traffic. These may mask the turbine's operational noise. During construction and decommission, other sound generating activities will be more relevant, such as drilling and dense ship traffic.

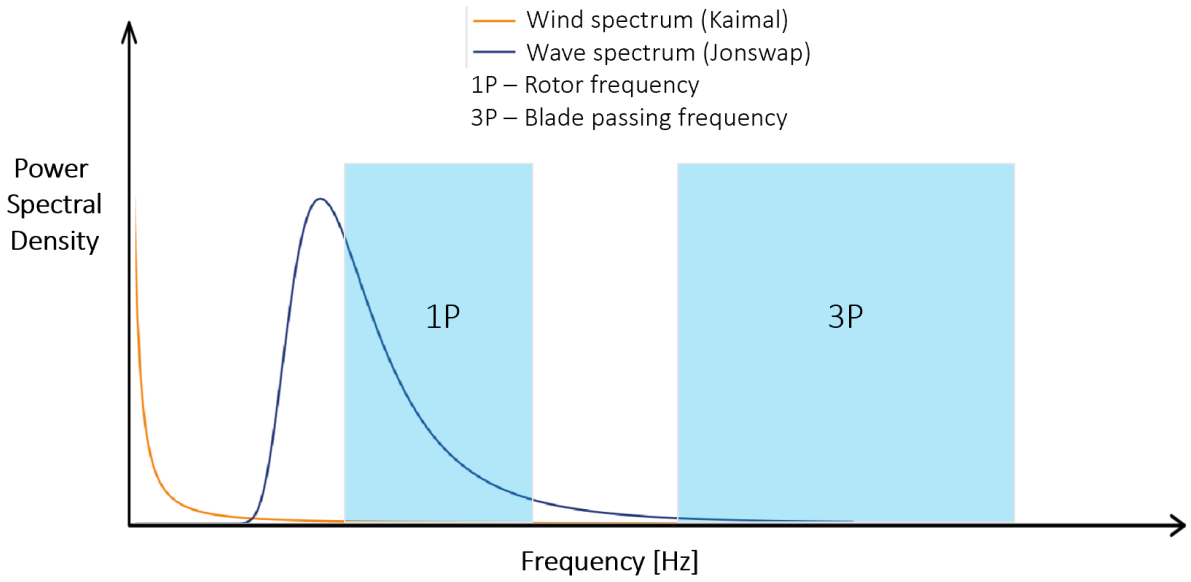

Figure 2.4: Generalized frequency diagram for an offshore wind turbine (illustration inspired by Bhattacharya et al. (2011)).

2.2.3 Vibration and Sound

To understand the connection between turbine vibrations and acoustics we study the relationship between force and pressure. By Newton's second law, the force (F) exerted on an object is the mass of the object times the acceleration of the object, $F = m \cdot a$ $[N]$. Further, we have that pressure is defined as force per unit area, $P = \frac{F}{A}$ $[Pa]$. Using these equations we can find a simple relationship between pressure and acceleration;

$$P = \frac{F}{A} = \frac{m \cdot a}{A} = a \cdot \frac{m}{A}. \tag{2.5}$$

Since acceleration a $[m/s^2]$ is the derivative of velocity, and the double derivative of displacement, it is clear that there is a relationship between acoustics (essentially pressure), and vibrations (essentially displacement) (Nedelec et al. (2016)). If a sound wave can be assumed to be propagating as a plane wave, we have the following simple relationship between sound pressure P and particle velocity c:

$$u = \frac{P}{\rho c}, \tag{2.6}$$

where u is particle velocity $[m/s]$, P is acoustic pressure $[Pa]$, ρ is density (of e.g. water, $[kg/m^3]$) and c is sound velocity $[m/s]$. Vibrational movement characteristics, such as displacement, can be derived from the particle velocity with the simple relationship:

$$\xi = \frac{u}{2\pi f}, \tag{2.7}$$

where ξ is displacement $[m]$ and f is frequency $[Hz]$.

To study the wind turbine vibrations we need to understand the dynamics of a wind turbine. All problems in structural dynamics can be formulated based on the equation of motion from Newton's 2nd law. For our tower displacement that we are interested in, we can formulate it approximately as a second-order system exhibiting damped simple harmonic motion (Dagli et al. (2018)). The total force on the system will consist of forces from wind and waves ($F(t)$), a damping force (if we choose to consider a damping system, $F_D = -D\dot{x}$) and a spring force ($F_K = -Kx$). Using Newtons 2nd law we have $M\ddot{x} = \sum F = F(t) + F_D + F_K$. Rewriting this equation, the structural dynamics can be formulated with the following equation of motion:

$$M\ddot{x}(t) + D\dot{x}(t) + Kx(t) = F(t), \tag{2.8}$$

where M, D and K are the structural coefficient matrices of mass, damping and stiffness. $x(t)$ is displacement, and $\dot{x}(t)$ and $\ddot{x}(t)$ are the derivatives with respect to time ($\frac{d}{dt}$), making them the velocity and acceleration respectively. $F(t)$ is the total external force. For an offshore wind turbine, we need to consider forces induced by both wind and waves. The natural frequency of this system will be $\omega_n = \sqrt{\frac{K}{M}}$ (Bossanyi (2000)).

Several studies have confirmed the connection between vibration and sound from wind turbines. Amongst them Lindell (2003) confirmed that there was a correlation between the mechanical vibrations of a wind turbine tower and the sound pressure, and Sigray and Andersson (2011) demonstrated the link between mechanical vibrations and particle motion in a water column. However, it was not directly proven that measured underwater noise originated from these vibrations, as turbine noise is easily masked by other ambient noise sources in the ocean (Yang et al. (2018)).

Yang et al. (2018) therefore performed a comparison of tower vibrations and underwater noise from offshore operational wind turbines emitted by China's first offshore wind farm in Shanghai. Measurements of vibration and underwater noise were measured synchronously to see if underwater turbine noise could be recognized in operational conditions. An excerpt from his article is given in Figure 2.5 showing spectrograms of tower acceleration and measured underwater acoustic data.

Figure 2.5 shows a time series based on the turbine tower of the Sinovel 3-MW SL3000. T1 and T2 correspond to two chosen time periods. From the figure, we can observe that a lot of the prominent frequencies for the mechanical vibrations are found in the spectrum of acoustic data. In the paper the conclusion was that the measurements showed a strong correlation between the two, indicating that the measured underwater noise resulted from the mechanical vibrations of the wind turbine. Yang et al. (2018) also concluded that the underwater turbine noise was very weak, and therefore difficult to measure and evaluate. During high- and low-tide the turbine noise was dominant, otherwise the turbine noise was masked by tidal noise. Further, they saw that the mechanical vibrations were mainly distributed in the low-frequency domain, and that the frequency and sound pressure amplitudes varied with wind speed until the turbine hit nominal power.

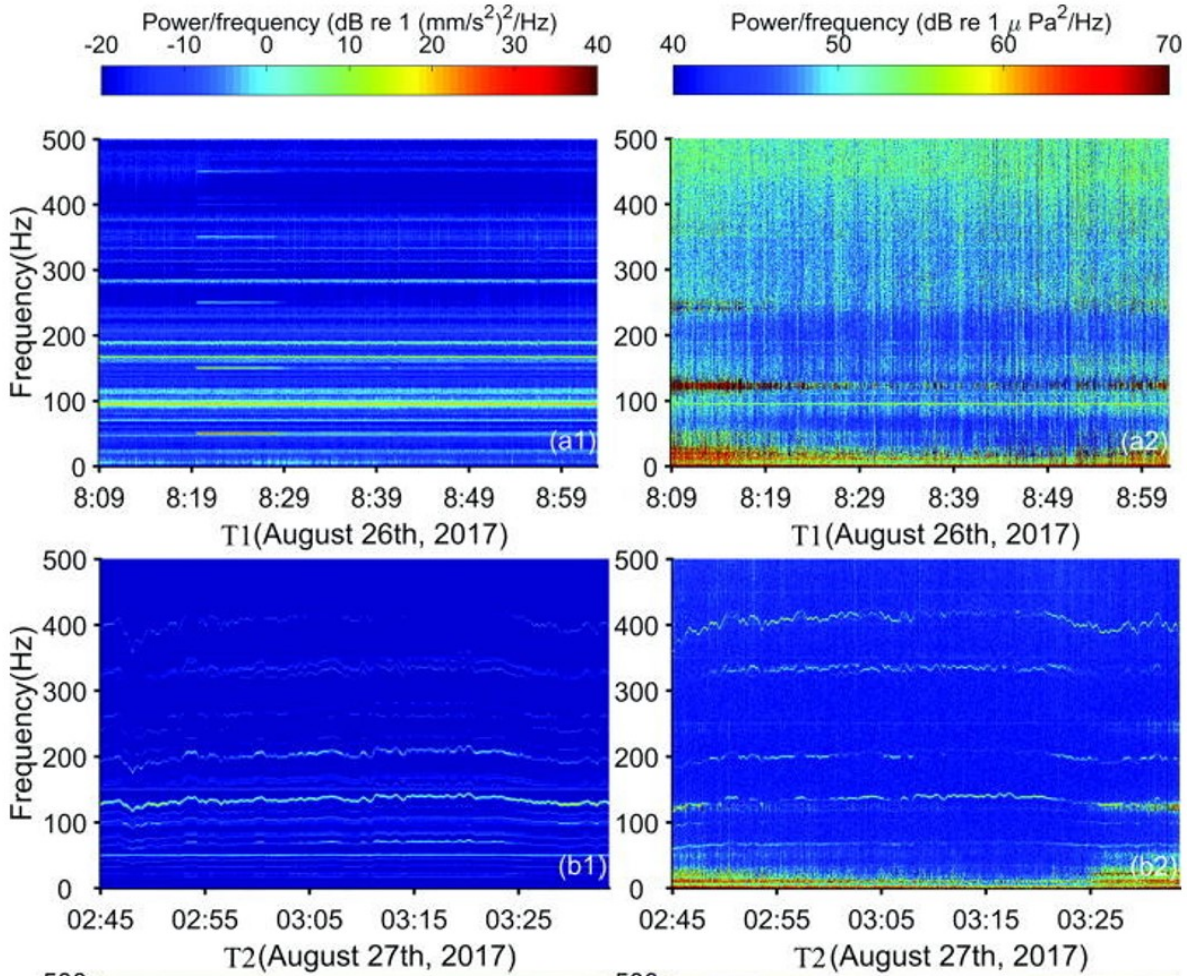

Figure 2.5: Spectral time series of 3MW turbine tower from 0 to 500Hz, two periods; mechanical vibrations (left) and underwater acoustical data measured about 50m from the wind turbine (right) (Yang et al. (2018)).

2.3 Sound Propagation

2.3.1 Sound Speed in the Ocean

The density of the ocean is related to temperature, salinity and pressure, where pressure is a function of depth. The sound speed in the ocean is related to this density and is, therefore, a function of these independent variables. The sound speed can be expressed with a simplified relation of these variables. In this study we choose to express the sound speed c in the ocean with the following relation (from Jensen et al. (2011)):

$$c(T, S, z) = 1449.2 + 4.6T - 0.055T^2 + 0.0029T^3 + (1.34 - 0.01T)(S - 35) + 0.016z, \quad (2.9)$$

where c is the sound speed in m/s, T is the temperature in $^\circ C$, S is the salinity in parts per thousands and z is the depth in meters.

The sound speed profile will look different depending on seasonal and diurnal changes, as well as if we are in a polar or non-polar region. Figure 2.6 shows a typical sound speed profile. Near the surface, wind and waves are creating turbulence which causes the first hundreds of meters of depth to mix and become more or less uniform. This is called "the mixed layer". Since the temperature and the salinity are constant in this layer, the sound speed profile will also appear constant. In warmer areas and warmer parts of the day, the temperature profile will increase near the surface, causing the sound speed profile to follow the same pattern. In polar areas the surface will be cold, causing the sound speed to decrease in magnitude near the surface. The seasonal variability has a large effect on the sound speed and is therefore very important acoustically. Diurnal heating also causes a slight difference in the profile and can lead to poorer sonar performance. This concept is known as the afternoon effect. During the night, surface cooling and turbulent mixing will allow for a more isothermal layer. i.e constant temperature with depth.

Below the mixed layer, we find the "main thermocline" where the sound speed decrease with depth. This is because the temperature also decreases with depth when we don't have turbulence to mix the water. In this upper ocean area, the temperature gradient is large, but it will eventually become constant with depth once we reach the deep ocean. In the deeper ocean the dominant variable will be depth, and as depth increases the sound speed will also increase. This layer is referred to as the "deep isothermal layer". In the case of a non-polar region where the profile is described as in Figure 2.6, we have a "deep sound channel axis" in the area between the main thermocline and the deep isothermal layer where the sound speed reaches a minimum value. For a polar region, the profile will be increasing with depth, having the minimum value at the sea surface. This is due to the cold sea surface and a constant increase in temperature with depth.

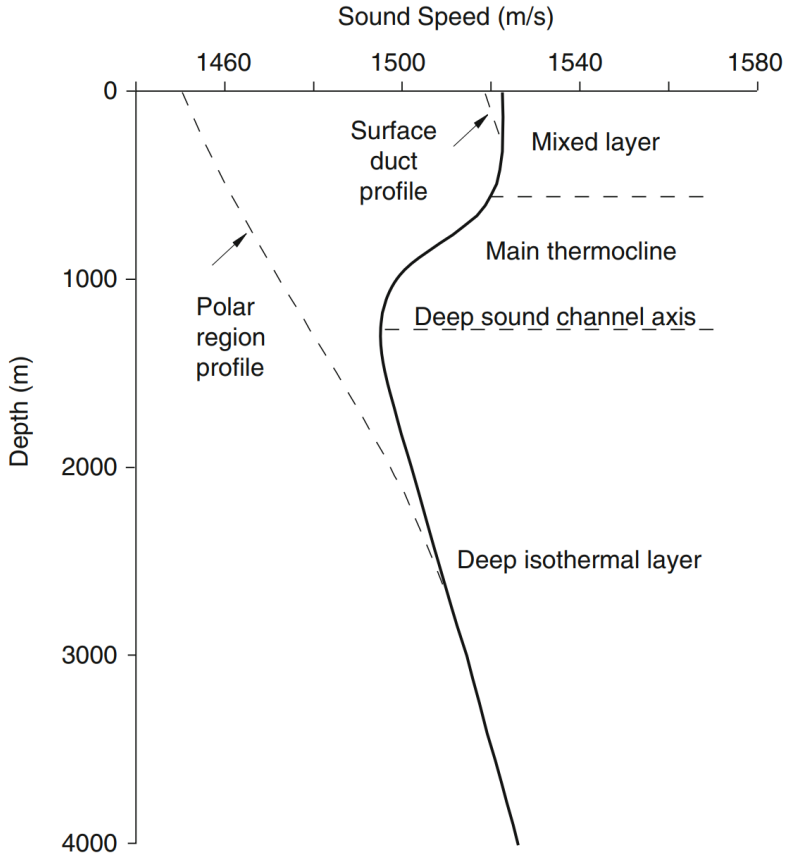

Figure 2.6: A typical sound speed profile for a non-polar region. The polar region sound profile is shown as a dashed line. Figure is from Jensen et al. (2011)

2.3.2 Propagation Paths in the Ocean

The sound waves will bend towards the lowest sound speed and are "trapped" in these regions. The theory behind this is "Snell's law", which relates the ray angle θ to the horizontal sound speed c:

$$\frac{\cos\theta}{c} = const. \tag{2.10}$$

In the ocean, there are various types of sound propagation paths depending on the sound speed profile in the region. Figure 2.7 shows a schematic representation of these types.

When the sound speed has its minimum value at the sea surface, we get "duct propagation" where the rays bend upwards with an angle of reflection equal to the angle of incidence (Kinsler et al. (2000)). Propagation path C follow a ray from a deeper sound source. It will follow the deep sound channel axis discussed in the previous subsection, where the axis is at the sound speed minimum. Path D shows a "convergence zone propagation". The sound emitted goes downwards and then reappears near the surface, where the beams converge and create a zone with high-intensity sound. This allows for long-range transmission of the sound. Path E shows "bottom bounce", where the sound is reflected from the seafloor. This phenomenon usually causes a lot of losses, meaning that the propagation distance will be short. At a continental shelf, or other shallow waters, the boundaries will act as a wave guide.

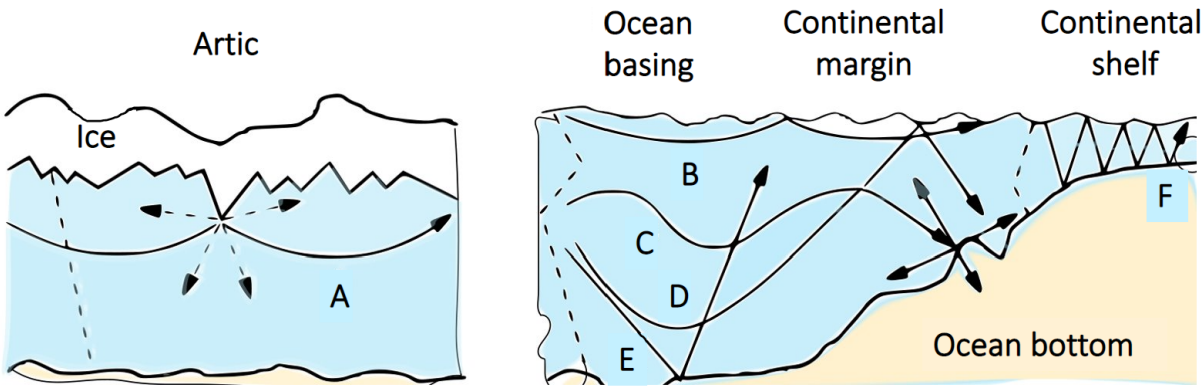

A: Artic
B: Surface duct
C: Deep sound channel
D: Convergence zone
E: Bottom bounce
F: Shallow water

Figure 2.7: Various types of sound propagation paths in the ocean, labelled A-F. The dashed lines show the sound speed profiles. Figure adapted from Jensen et al. (2011)

In general, modelling sound propagation in the ocean can be very complicated because the environmental properties have to be included in order to get reliable results. Examples of such properties are ocean stratification, topography of the seabed and wind/wave interactions at the surface. The environment varies depending on the range and the sound propagation can also differ depending on the frequency of the acoustic signal. We usually consider a stratified ocean, with each layer having constant environmental parameters in each layer. However, there will always be variability in the ocean both vertically and horizontally depending on the position and its environment.

2.3.3 Transmission Loss

As the acoustic signal propagates away from the source it will be weaker due to loss mechanisms such as geometrical spreading and attenuation. To measure how the acoustics change in signal strength with range, we use transmission loss (TL). Transmission loss can be defined as the ratio between the acoustic intensities at 1 m distance from the source and the field point of interest at the range r.

$$TL = 10\log\left(\frac{I(1m)}{I(r)}\right) = 20\log\left(\frac{P(1m)}{P(r)}\right) \ [dB\ re\ 1m]. \tag{2.11}$$

This is assuming plane waves where the intensity is proportional to the square of the pressure amplitude. In addition, the acoustic impedance must be the same at the source and field point.

The geometrical spreading loss follows geometrical spreading laws. In underwater acoustics, both spherical and cylindrical spreading is of importance. These are illustrated in Figure 2.8.

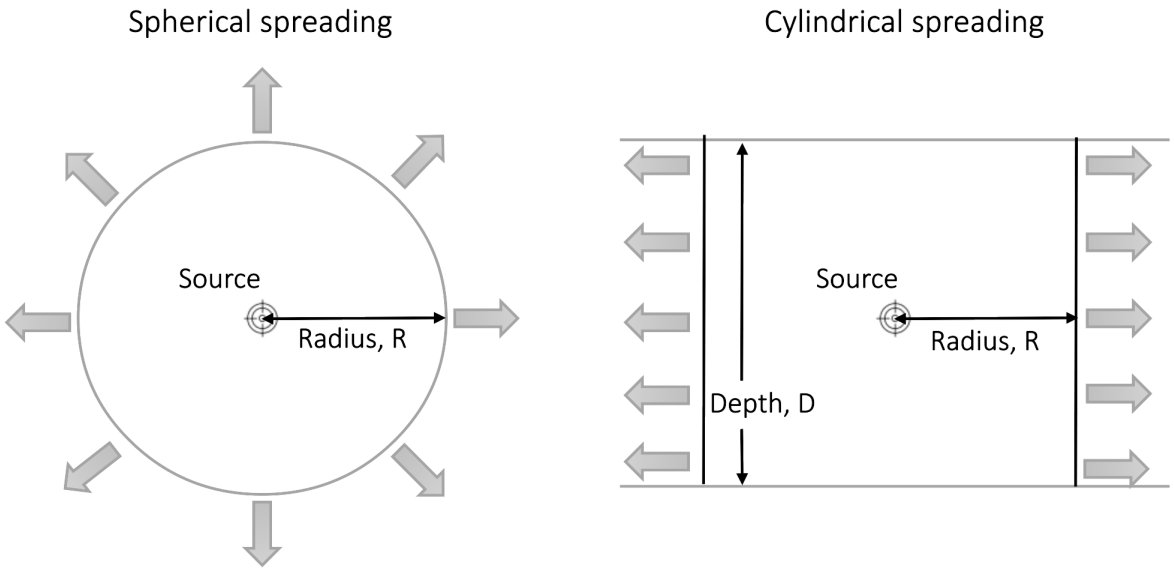

Figure 2.8: Illustration of spherical and cylindrical spreading laws

Considering cylindrical spreading we know that the acoustic intensity is inversely proportional to the surface of the sphere, $I \propto \frac{1}{4\pi R^2}$. If we insert this into Equation 2.11, we can express the transmission loss for spherical spreading as

$$TL(geom) = 20\log(r)\ [dB\ re\ 1m]. \tag{2.12}$$

Spherical spreading is a good description in the near field of a point source. If the source is in a waveguide, cylindrical spreading will apply at longer ranges. In addition to the radius, we also have to consider the depth between the waveguide boundaries. Since the far-field intensity is inversely proportional to the surface of a cylinder, $I \propto \frac{1}{2\pi RD}$, the transmission loss for cylindrical spreading can be defined as

$$TL(geom) = 10\log(r)\ [dB\ re\ 1m]. \tag{2.13}$$

.

Some factors that will affect the geometrical spreading are refraction due to the sound velocity profile, interference due to multipath propagation, and reflection/scattering from surfaces. We also have non-geometrical losses. In the ocean, both absorption and scattering contribute to the attenuation of sound. In liquids, we have a lot of absorption mechanisms, e.g. shear viscosity, thermal conductivity and molecular relaxation mechanisms. In seawater we also have chemical relaxation mechanisms from boric acid and magnesium sulphate, causing the absorption of sound in freshwater and saltwater to be different from each other, as shown in Figure 2.9. We can describe the attenuation of sound with the absorption coefficient α. For seawater, we use a formula based on the relaxation terms of boric acid and magnesium sulphate, as well as viscosity in water.

An empirical formula for the attenuation in seawater is given by Kinsler et al. (2000):

$$\alpha = \left(\frac{A}{f_1^2 f^2} + \frac{B}{f_2^2 f^2} + C\right) f^2\ [dB/km], \tag{2.14}$$

where A,B,C are values determined by hydrostatic pressure and temperature, f is the source frequency, and f_1 and f_2 are the temperature dependent relaxation frequencies.

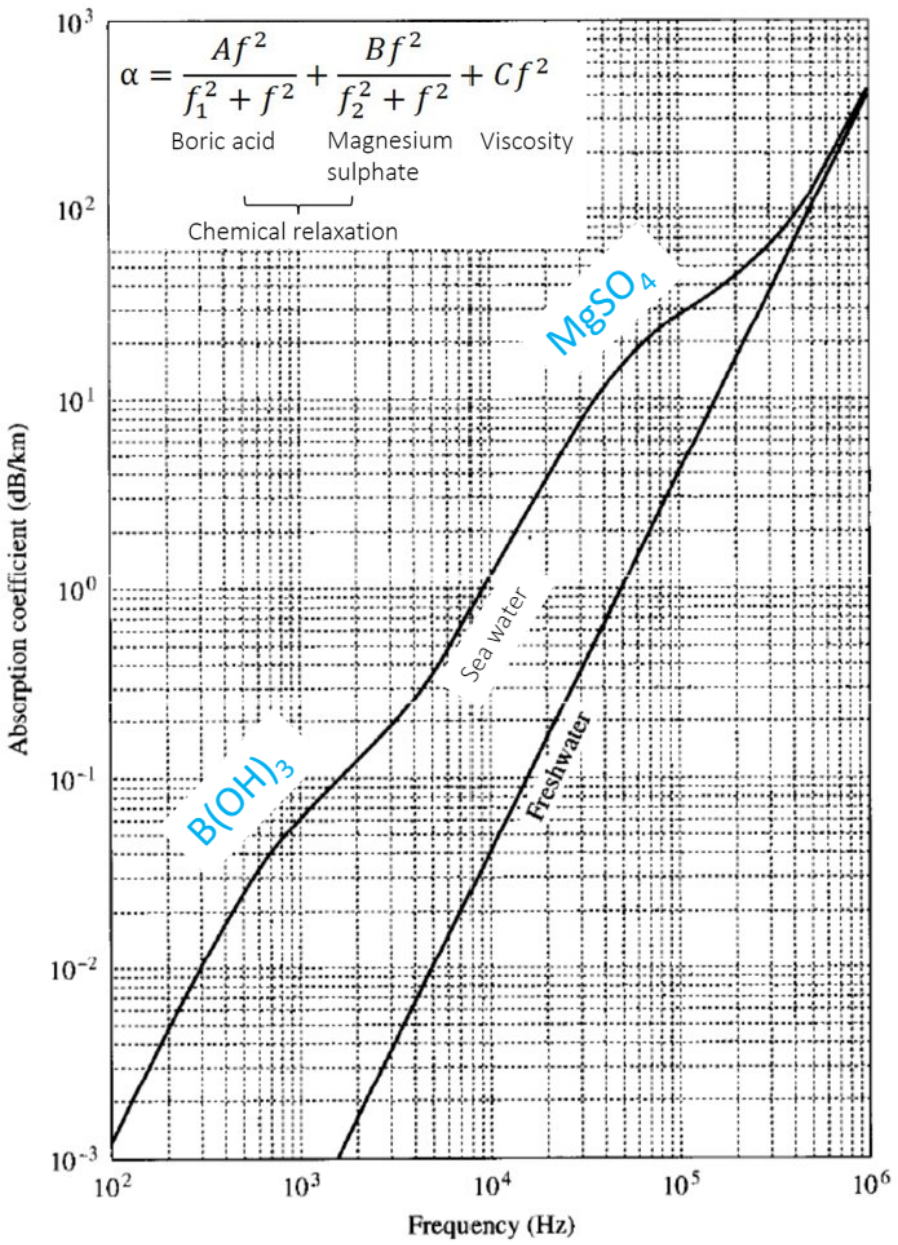

Figure 2.9: The absorption coefficient of fresh- and seawater as a function of frequency (T=5°C, Z=0km, pH=8, S=35ppt). Figure modified from Kinsler et al. (2000).

Using multiple experimental data from Fisher and Simmons (1977), a simplified expression for attenuation in seawater has been introduced (Jensen et al. (2011)):

$$\alpha \approx 3.3 \cdot 10^{-3} + \frac{0.11 f^2}{1 + f^2} + \frac{44 f^2}{4100 + f^2} + 3 \cdot 10^{-4} f^2 \; [dB/km]. \tag{2.15}$$

From the above equations, we see that the attenuation of sound in seawater is frequency (in kHz) dependent. The attenuation is also dependent on other factors such as temperature, acidity, salinity etc., but the approximation is considered sufficiently accurate for most problems within this field of study. Figure 2.10 shows how the effect of absorption is different depending on which frequency. From the figure, we see that absorption losses are very important for higher frequencies and long ranges. If we want the sound to travel far it is, therefore, best to use low frequencies.

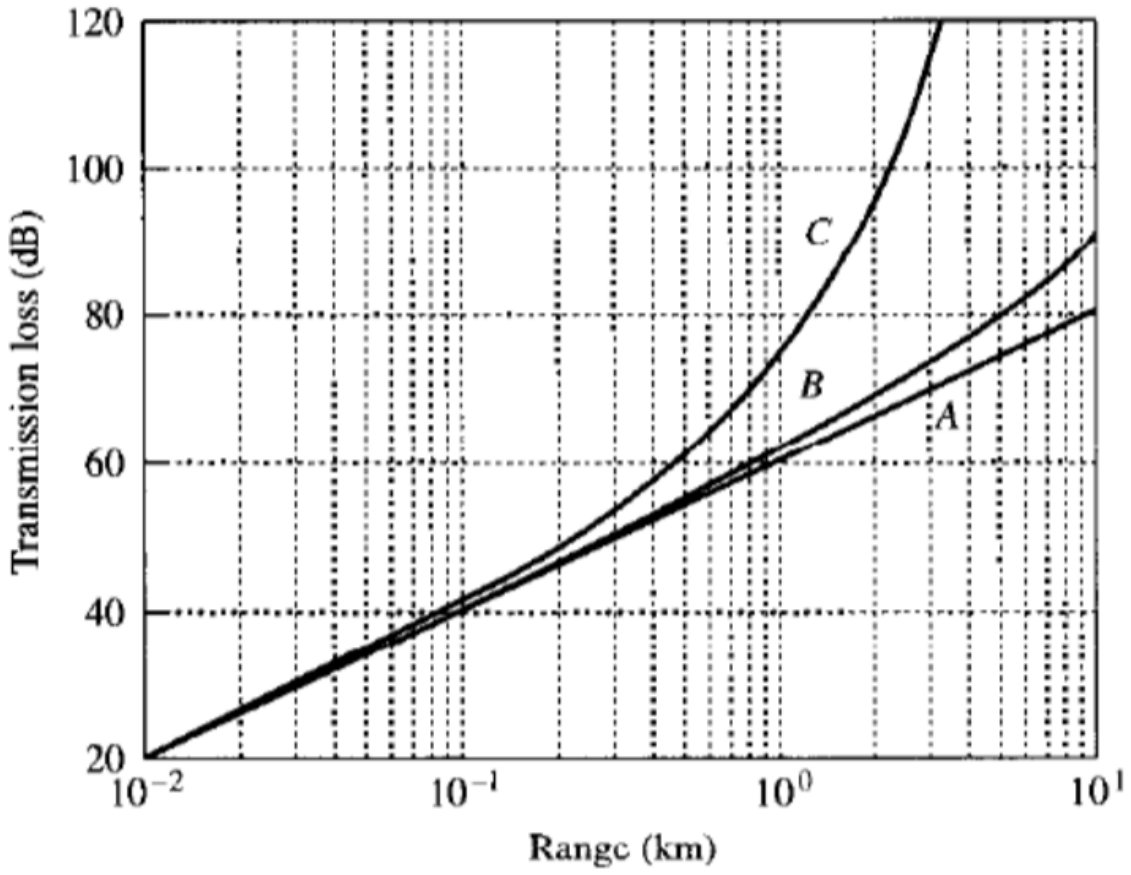

Figure 2.10: Transmission loss for spherical spreading in seawater with absorption at different frequencies. A=1 kHz, B=10 kHz, C=50 kHz (Kinsler et al. (2000)).

2.4 Propagation Model

When carrying out a noise assessment, an appropriate model is needed. Noise modelling for assessing environmental impact is often performed with limited environmental data, and without field measurements, using simplistic models (Farcas et al. (2016)) or more advanced underwater acoustic models. Factors that can influence the model selection are the dominant frequency (or frequency band) of the turbine, and oceanic characteristics. A large number of propagation models have been developed aiming to predict the received noise at given points based on the noise level and wave-field medium information. Some examples of such methods are parabolic equation, normal modes, wave-number integration and multi-path expansion (Farcas et al. (2016)). For our study, we first used the normal mode model to get familiar with simple ocean modelling. Then, we moved on to ray theory using the BELLHOP model, to include more environmental data and develop 3D results.

2.4.1 Normal Modes

The normal mode model is one of the most popular approaches for studying sound propagation. The principle behind the normal modes model is to solve the wave equation and obtain modes numerically. When studying the generated sound pressure level, it will look different depending on how many modes we choose to look at. For this study, we will use the Chebyshev-Tau spectral method when constructing the underwater acoustic normal modes (Tu et al. (2020)).

This modelling method considers a two-layer marine environment, where the water column and bottom column are both range independent. Sound velocity, density and attenuation profiles are needed from the two layers. The boundary conditions are also used as data input and correspond to a perfectly free surface at $z = 0$, and a perfectly free or rigid bottom at $z = H$. The environmental parameters are displayed in Figure 2.11, and the two layers are separated by an interface at $z = h$.

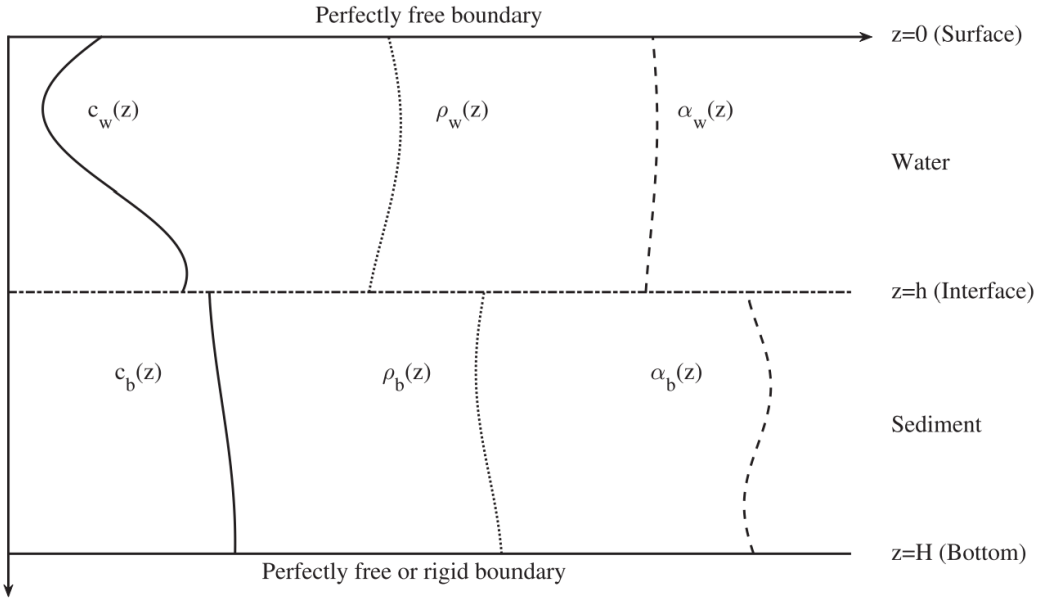

Figure 2.11: The environmental parameters sound speed, density and attenuation profiles in the two-layer marine environment. Figure from Tu et al. (2020).

An example of propagation modelling from this method is shown in Chapter 4 as we used this model when preparing results for the DeepWind conference. Since this method is not used throughout the rest of the study, we will not explain this method in further detail. However, the method is explained more in-depth in the article *A Chebyshev-Tau spectral method for normal modes of underwater sound propagation with a layered marine environment* by Tu et al. (2020), and the corresponding MATLAB code *NM_CT.m* was used.

2.4.2 Beam Tracing

We can also predict acoustic pressure fields in the ocean using a beam tracing model. BELLHOP is such a model, and for this thesis, we will be using the Matlab conversion of the code. A description of the Bellhop codes and the theory behind them is given in the *BELLHOP3D User Guide* by Porter (2016). The structure of the BELLHOP model is given in Figure 2.12.

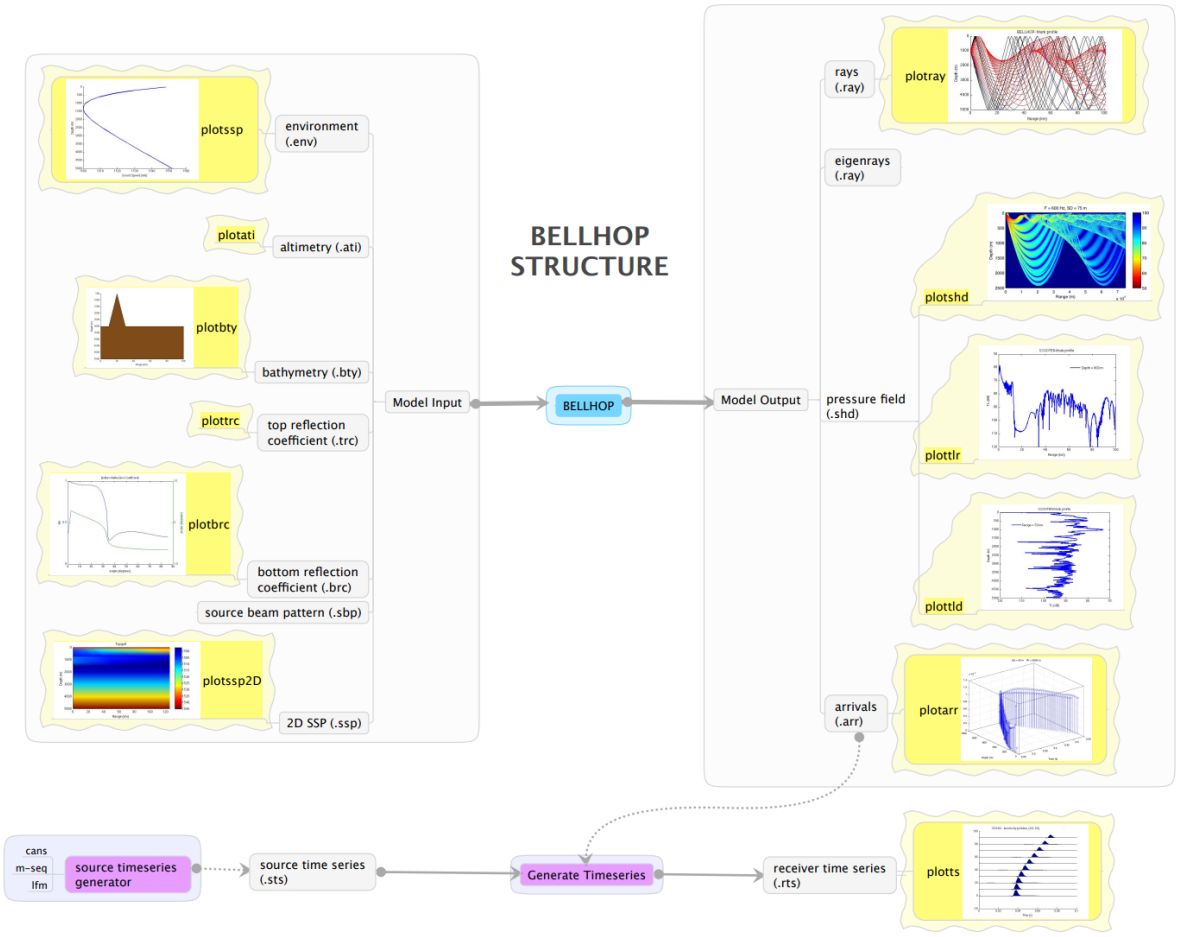

Figure 2.12: BELLHOP structure, given in the Bellhop manual and user's guide by Porter (2011).

Beam tracing is a method for studying the wave propagation paths in a system. In underwater acoustics, the rays will bend towards the minimum sound velocity, following Snell's law as discussed in Section 2.3. As a result, the rays can be "trapped" in levels where the sound speed is at its lowest. Ray theory alone does not include effects like diffraction and interference, but many models have been developed to avoid these problems.

The BELLHOP software contains several beam types. To determine the beam coordinates, the solution of the ray equations are required. We can run BELLHOP for both 2D and 3D outputs. The ray equations in 3D are given by (2.16):

$$\begin{aligned} \frac{dx}{ds} &= c\xi(s), \quad & \frac{d\xi}{ds} &= -\frac{1}{c^2}\frac{dc}{dx}, \\ \frac{dy}{ds} &= c\eta(s), \quad & \frac{d\eta}{ds} &= -\frac{1}{c^2}\frac{dc}{dy}, \\ \frac{dz}{ds} &= c\zeta(s), \quad & \frac{d\zeta}{ds} &= -\frac{1}{c^2}\frac{dc}{dz}, \end{aligned} \tag{2.16}$$

where c is the sound speed, and (x, y, z) is the trajectory from the take-off angles (ξ, η, ζ), all depending on the arc length s along the ray.

Through BELLHOP there will be several different output files depending on the input data and fields of interest. The ray trace figures will illustrate the fan of rays emitted from the source. That way we get a sense of how the sound is propagating in the environment. The distribution of sound pressure can also be displayed both vertically and horizontally.

As an input, the following files are needed:

- Environmental file
  This is the main file needed for running the BELLHOP model. The environmental file include the depth and sound speed profile that we calculate using Equation 2.9.

- Bathymetry file
  We can incorporate the topography of the seabed in both 2D and 3D modelling by making separate bathymetry files that we provide the model. This is a supplementary file.

- Altimetry file
  We can also account for rough ocean surfaces by incorporate a supplementary file containing the range dependent surface elevation.

For the environmental file we will use salinity and temperature information from CMEMS marine data. The bathymetry data are obtained from EMODnet. This will be further explained in Chapter 3. For the altimetry file, we will make a file describing the ocean surface based on mean wave information from NORA3 reanalysis data set. Ideally we should make irregular waves to get the most realistic output. However, for simplicity we will use theory for regular waves instead. Given the significant wave height H_s, peak period T_p and depth h we express the range dependent surface elevation $\eta(r)$ as

$$\eta(r) = \frac{H_s}{2}\cos(kr) \tag{2.17}$$

In this equation, k is the wave number expressed as $k = \omega/\sqrt{gh}$, and ω is the angular frequency expressed as $\omega = 2\pi/T_p$.

An example of the input and output files are displayed in Figure 2.13. The colourful shading is showing transmission loss which is our main output of interest.

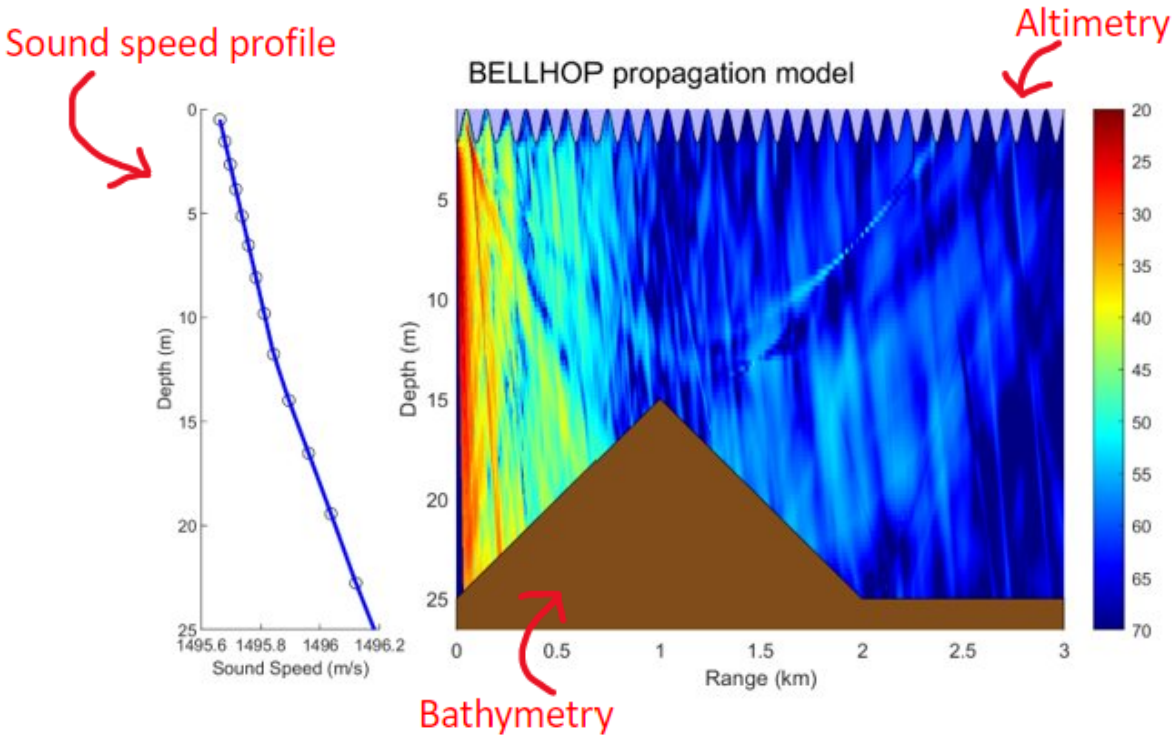

Figure 2.13: Example of the BELLHOP model. The input files are displayed on top of the shaded output showing transmission loss [dB] of an acoustic signal.

2.5 Signal Processing

In order to analyse the available underwater noise data, a series of signal processing tools in Matlab are developed. In addition to analyzing the measurements, these signal processing tools are also used to interpret results.

The acoustic signals consists of fluctuations with different frequencies and amplitudes. To extract such information we need to decompose the time series into a frequency domain. This mathematical transformation is known as a Fourier Transform (Howard (2016)). By this transformation we can display a spectrum of the Power Spectral Density (PSD) against each frequency, to show the energetic tones in the signal. This is known as an energy or power spectrum. We want to look at power in terms of dB to determine how loud the noise is. Since we are looking at underwater noise from offshore turbines, we are expecting energy at low frequencies corresponding to the vibrating frequencies of the turbine.

Another useful tool is the audio spectrogram. An audio spectrogram is a time-frequency representation of a signal. It shows the different frequencies in the signal along with their power, and how the signal varies over time.

During this study we will also develop 1/3 octave spectra and narrowband spectra as described in the report by Radecke and Benesch (2012). This will be further explained in Chapter 3.

2.6 Principle Behind a Hydrophone

One way to determine the environmental impact of turbines is to measure the underwater acoustic low-frequency noise induced by the vibrations of wind turbines. Measuring this noise under varying atmospheric and sea-state conditions is especially important when considering the environmental impact on marine life. An example of such measurements is using hydrophones where an amplifier is connected between the hydrophone and the recorder to amplify signals (Norro et al., 2009).

A hydrophone "listens" to the sound in the sea passively. Hydrophones contain a piezoelectric material. This material is able to produce electric charges from pressure changes. A sound wave has pressure fluctuations that the piezoelectric element in the hydrophone then is able to detect and transform into an electric signal that we can analyse afterwards.

A single hydrophone, as used for our study, records ocean sounds from all directions. Often, several hydrophones are placed in an array to "listen" with greater sensitivity than a single hydrophone by focusing on signals from a desired direction (NOAA (2021)). The received signals by the hydrophones will be time-shifted versions of the original signals. Signal processing tools, such as beamforming, are then used to determine the direction and strength of sources by steering the "listening" direction of the array.

Chapter 3

Method and Datasets

3.1 Overview of Approach

In this study, we consider two locations; the FINO 1 platform by the Alpha Ventus offshore wind farm, and the area of Hywind Tampen floating offshore wind farm. We will work on both observational data and modelling from this study.

From FINO 1 we have available observational data from a hydrophone. From these data, we will first conduct some simple analysis of sound pressure levels. We identify energetic tones by e.g. using 1/3 octave spectral analysis. To perform the data analysis on the pressure data, we take inspiration from the report on the *Alpha Ventus Underwater Operational Noise* by Radecke and Benesch (2012). Further, we model how the energetic tone will propagate in the area.

We then assume a source frequency propagating at the Hywind Tampen location. We do propagation modelling for a few days around an extreme event and compare it with wind and wave information at the same time period. By comparing transmission loss and wind and wave conditions we do a sensitivity analysis from these results.

We use available oceanic reanalysis data of salinity and temperature for the acoustic model simulations. To study sound propagation, we will use the BELLHOP model as described in Section 2.4.

We want to investigate the noise propagation during selected forcing events. Therefore we also study the wind forcing at the same measurement time. To obtain wind speed and wave information at the given time and location we use NORA3 data. NORA3 (The 3 km Norwegian reanalysis) was developed by Solbrekke et al. (2021) and is a climatological wind power data set.

3.2 Study Site, Dataset and Methodology Details

3.2.1 FINO1 area

We have obtained observational data from FINO1 offshore platform in the North Sea. Underwater acoustic pressure data were recorded between 2010 and 2012, after the start of operation of the Alpha Ventus Offshore Wind Park nearby in the Southern North Sea. The sound data was made available by the RAVE (Research at Alpha Ventus) initiative, which was funded by the German Federal Ministry of Economic Affairs and Energy on the basis of a decision by the German Bundestag and coordinated by Fraunhofer IWES (see: www.rave-offshore.de).

A map showing the FINO1 location is presented in Figure 3.1. The exact site coordinates of the FINO1 platform are N 54°00′53, 5” E 6°35′15, 5”. The depth is approximately 30 meters.

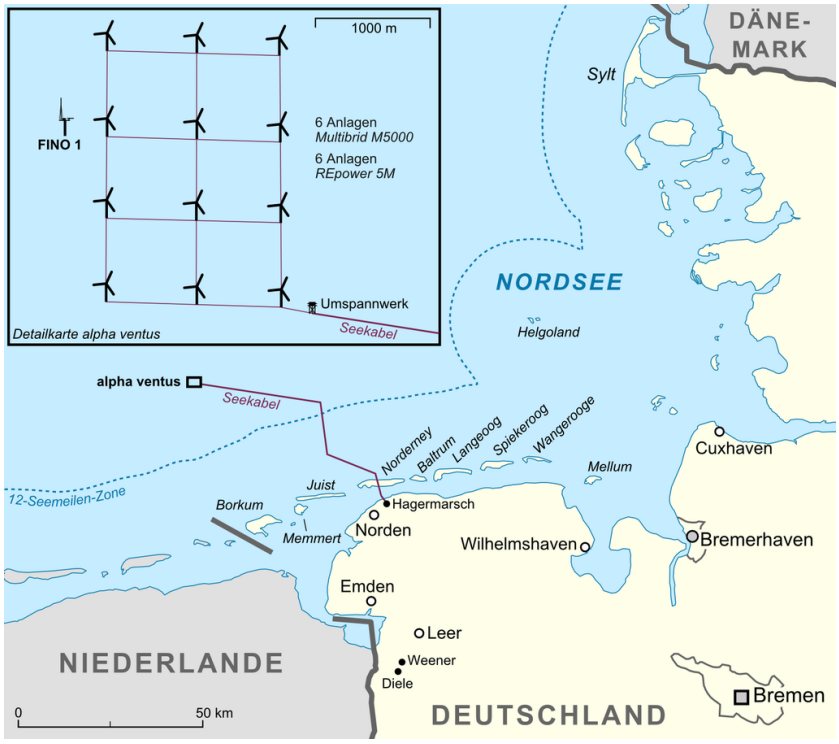

Figure 3.1: Map showing the location of FINO 1 research platform and Alpha Ventus Offshore Wind Farm in the North Sea (Von Lencer (2009)).

RAVE has provided several months of measured data. For our study we first used data from the 15th and 16th of November 2010. Then we also studied selected measurements from every month in 2011, a ten-days period in November 2010, as well as a couple of extreme events. This allowed us to do more detailed research on sound pressure levels and environmental conditions, as wind and wave characteristics change both daily and with the seasons. Underwater pressure data were recorded from several locations, but we were provided with the data from the hydrophone by the FINO1 offshore platform. This platform is situated in the vicinity of the Alpha Ventus Wind Farm, as indicated in the map from Figure 3.1.

The sampling frequency is set to 50 kHz. Each measurement segment is 5 minutes, and the sound data were recorded three times a day. The FINO1 platform is situated left of one of the turbines, as indicated by Figure 3.2 where we also see the hydrophone as a yellow dot besides the platform. The hydrophone was placed 3 meters above the sea bed. Originally it was placed 400 meters left of the turbine, but by the time it was removed it was approximately 450 meters away.

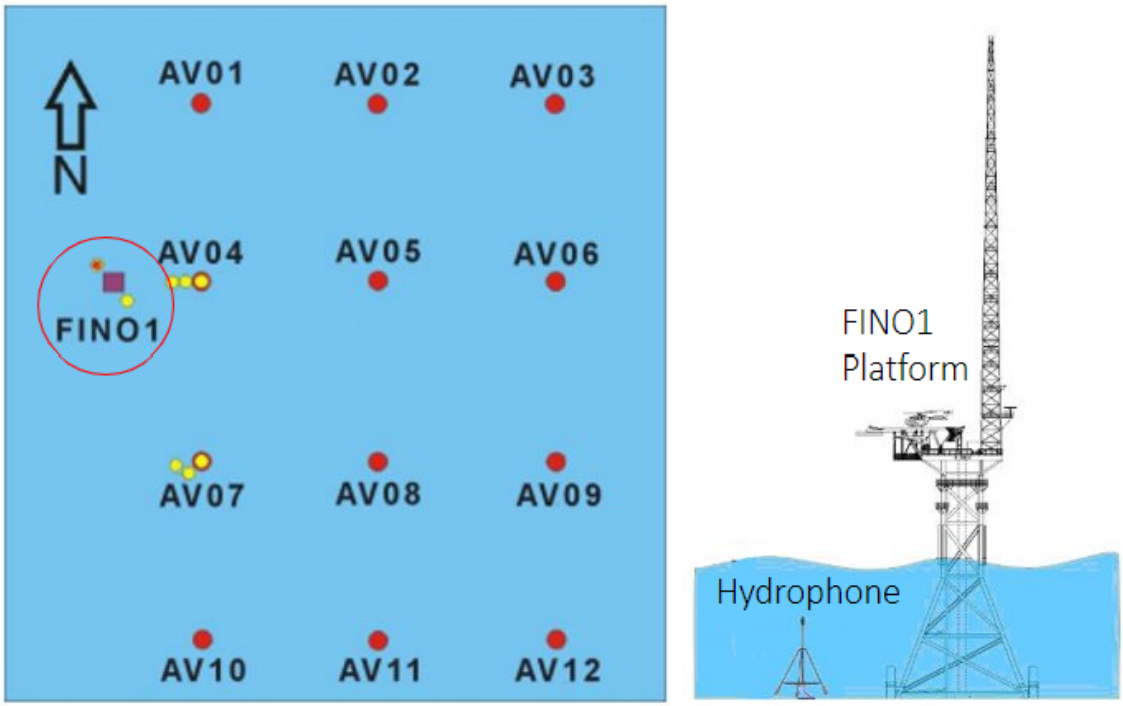

Figure 3.2: Hydrophone placements. The yellow dot by the FINO1 platform is the hydrophone that our measurements are recorded from. The illustrations are taken from Radecke and Benesch (2012) and adapted (dimensions are not accurate).

The type of sensor used was the hydrophone of Brüel & Kjær 8106.

An overview of the FINO1 measurement system is given in Table 3.1.

Table 3.1: FINO1 measurement system

FINO1	
Measuring system installed:	08.09.2010
Hydrophone installed:	08.09.2010
Accelerometer installed:	08.09.2010
First measurement:	08.09.2010 18:00
Remark:	- Power failure: 27.09.2010-05.10.2010 - Change of hydrophone: 11.11.2011
Last measurement:	18.09.2012
Uninstalled:	18.09.2012

Detailed information about the data file structure and installation, and operation remarks were given in separate user guides that followed the provided data from RAVE. In the file header of each measurement segment, there was given information about the sampling rates, the number of measurements, channels and conversion rates to go from binary numbers to volts, acceleration and pressure.

As mentioned, we were given files from the measurements at FINO1 platform. In the given files we had two channels of data. Every other binary number belonged to channel 1 and channel 2 respectively. The numbers were first converted from binary numbers to volts, and then to acceleration and pressure. In our data set, the first channel belonged to the pressure sensor/hydrophone, and the second channel was the acceleration measurements. In the header of each data file was a table showing simple statistics such as mean, standard deviation and minimum/maximum values in volts. We, therefore, calculated the same statistics to make sure that the data was correctly extracted from the binary file.

After converting the binary numbers in the channels to volts, we calculated the pressure using a sensitivity of 2.24 mV/Pa, as indicated by the instrument. To display and demonstrate the data, a time series of the first measurement segment from 15/11-2010 is given in Figure 3.3. By manual screening of the data set we could see some spikes in every bulk of measurements. Some of the bigger spikes were removed before we calculated the sound strength.

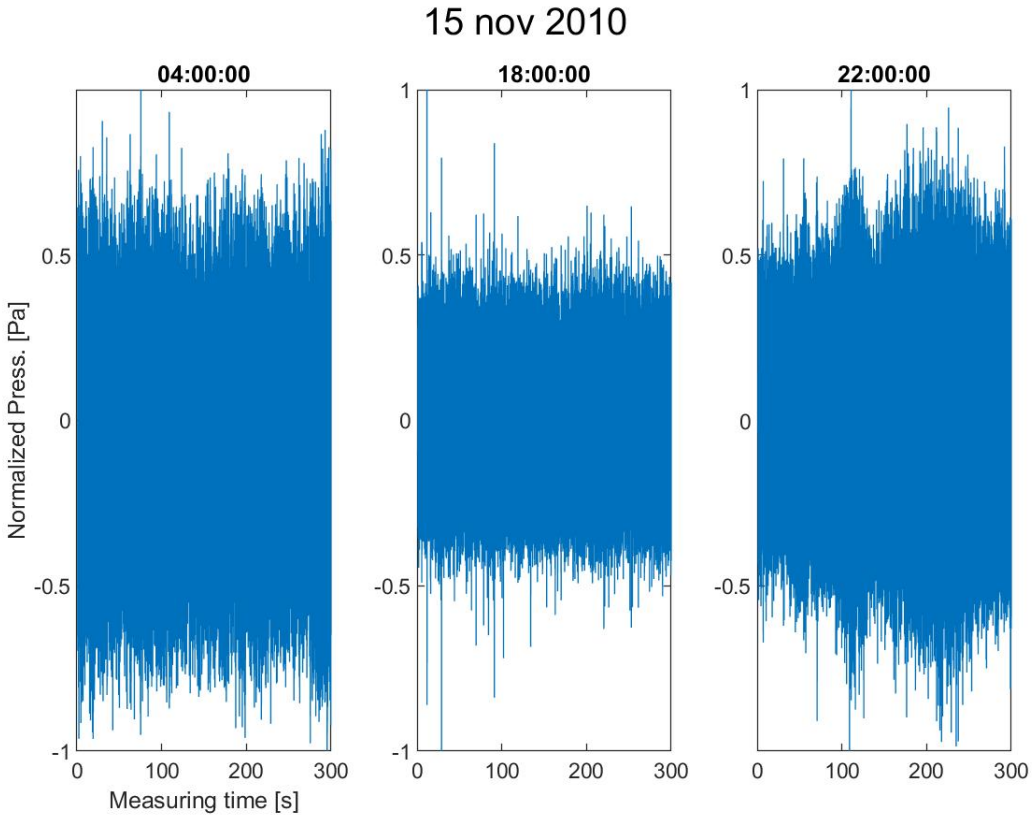

Figure 3.3: Pressure [Pa] time series of the three measurement segments for 15. November 2010. This raw pressure data is normalized for confidential reason.

As discussed in Section 2.2, we can describe the sound strength in terms of intensity or sound pressure level. We then obtain dB relative to a reference pressure, in our case 1 μPa for underwater studies. Our time series of pressure, $p(t)$, is fluctuating and of very high resolution. We, therefore, split the data into bulks of 5 seconds and 300 seconds of measurements, and calculate the equivalent sound level, Leq, using the following formula:

$$Leq = 10 \cdot \log \left(\frac{1}{T} \int_0^T \frac{p(t)^2}{p_{ref}} dt \right) [dB]. \tag{3.1}$$

This formula is essentially the same as Equation (2.4), but here we use a temporal integral of the pressure time series for our chosen time intervals T of either 5 or 300 seconds (with dt as time steps). We also calculate a peak sound pressure level, Lpeak, where we use Equation (2.4), but with pressure p being the peak pressure in the time interval.

Further, we study the 1/3 octave spectra of the sound pressure levels calculated from the 300 second segments. This is to get a more in-depth view of the sound level across the frequency domain. The next step in the spectral analysis is to study the narrow band spectra. We obtain the spectral density by using Welch (1967) power spectral density estimate with a Hanning window of 50% overlap and 50000 discrete Fourier transform points.

We perform bandpass filtering to the sound level values. The bandpass filter consists of a high-pass with a cut-off frequency 10 Hz, and low-pass with a cut-off frequency of 3 kHz. This way we filter away low-frequency and high-frequency contributions such as current interference and electromagnetic radiation.

We also plot the bulks of sound pressure levels against both wind speed and wave height. This is to see if we can observe a connection between source levels and forcing conditions in the area. A simple correlation study of calculating the correlation coefficients is therefore performed.

As a last step we do propagation modelling using BELLHOP and compare to the observational data. Oceanic information about salinity and temperature are from the EU Copernicus Marine Environment Monitoring Service (CMEMS). The data set contains a daily mean of these variables. To run the BELLHOP model we need environmental input data containing the sound speed profile among other things. This sound speed profile is calculated using Equation (2.9). Figure 3.4 displays the ocean profiles for 15th and 16th of November 2010, that we will be using in the sound propagation model. The ocean depth is about 27 meters, and for bathymetry we assume a constant bottom for simplicity. We will account for altimetry using NORA3 data set to obtain mean significant wave height and peak period, as well as comparing it to the mean wind speed.

The results will be presented in Chapter 5.

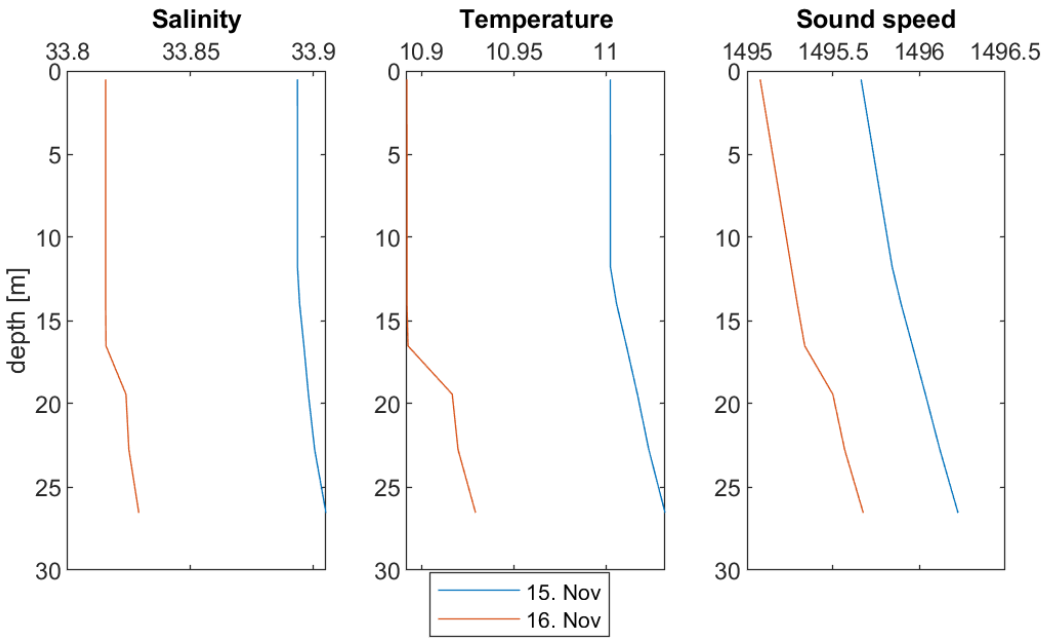

Figure 3.4: Daily mean profiles of temperature, salinity and sound speed for FINO1 location.

3.2.2 Hywind Tampen area

The second study site of this project is in the area of Hywind Tampen. Hywind Tampen is located between the Snorre and Gullfaks fields, approximately 140km off the Norwegian coast. The location is shown in Figure 3.5

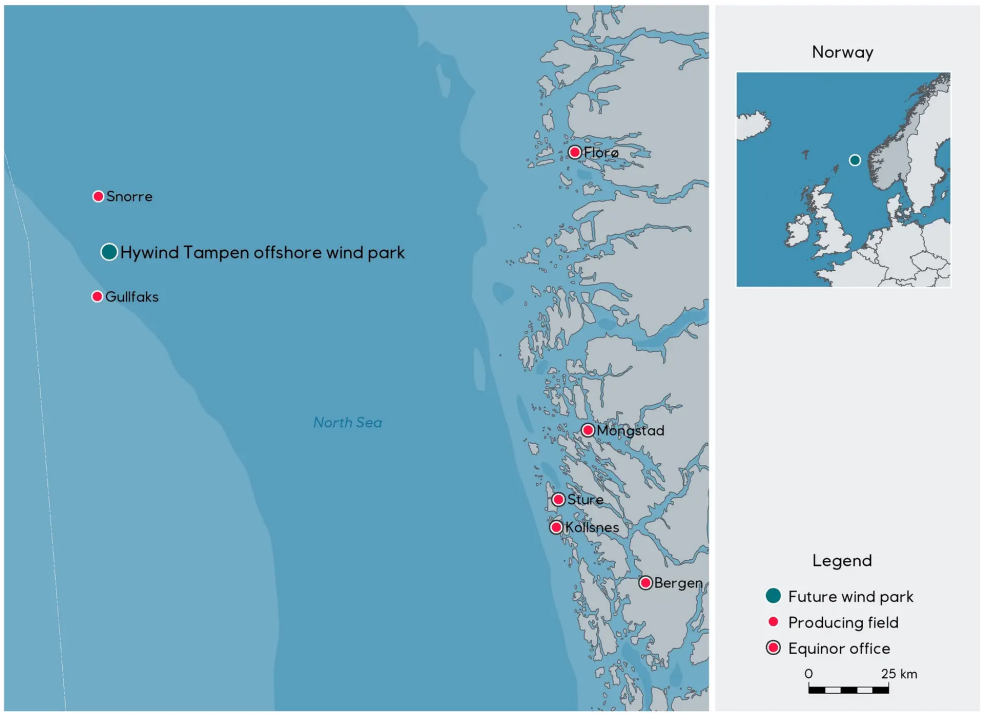

Figure 3.5: Location of Hywind Tampen, located approximately 140km off the Norwegian Coast (from Equinor (2022)).

This will be the world's first floating offshore wind farm that aims to supply renewable energy to offshore oil and gas. The farm consists of 11 turbines, with a total installed capacity of 88MW. The site is of great water depth, ranging between 260m and 300m (Equinor (2022)).

Oceanic information about salinity and temperature are from the EU Copernicus Marine Environment Monitoring Service (CMEMS). For this study we extracted daily averaged data. Ideally, we would use the newest available oceanic data, preferably from 2020 or newer. However, our wind and wave data set are from the year of 2016, and we will therefore use CMEMS data from this year.

We obtain mean wind and wave information from the NORA3 reanalysis data set. In the propagation model we will account for surface waves. The wind and wave data will form a basis for doing sensitivity analysis of transmission loss and environmental forcing conditions.

For the BELLHOP modelling, we can also account for bathymetry data, which is showing the topography of the seabed. Bathymetry data used in the model are from European Marine Observation and Data Network (EMODnet). EMODnet offers a very high resolution of bathymetric data. The bathymetry is displayed in Figure 3.6.

As we can see from the figure, the seabed over the Tampen area is not uniform, and the farm is placed over a slight hill. The star indicates the location of the turbine placed over the greatest depth of the farm. Figure 3.7 shows a slice of the topography at this location, ranging 3 km west of the location. For the BELLHOP propagation model we accounted for this bathymetry. However, for a short range of 3 km we could assume constant depth as the change in elevation is really small.

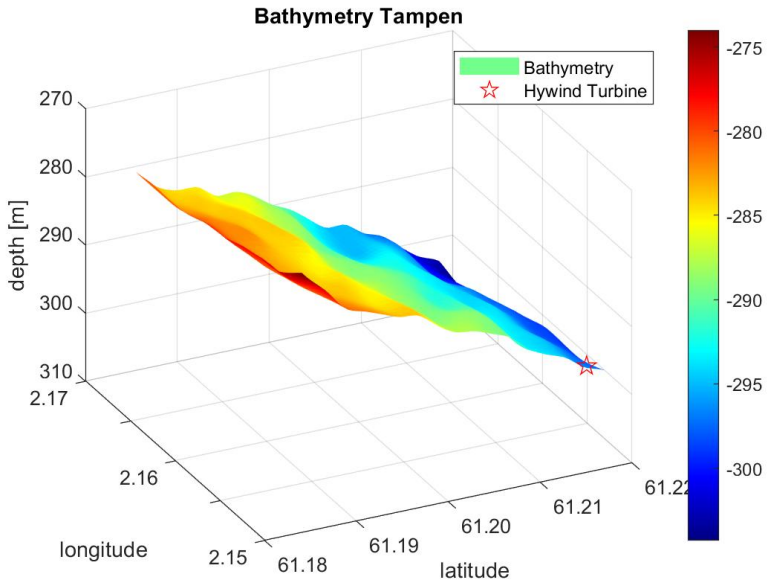

Figure 3.6: Displayed bathymetry data from EMODnet for the location of Hywind Tampen. The star is indicating the location of the turbine placed over the greatest depth of the farm. The colourbar is showing the depth [m].

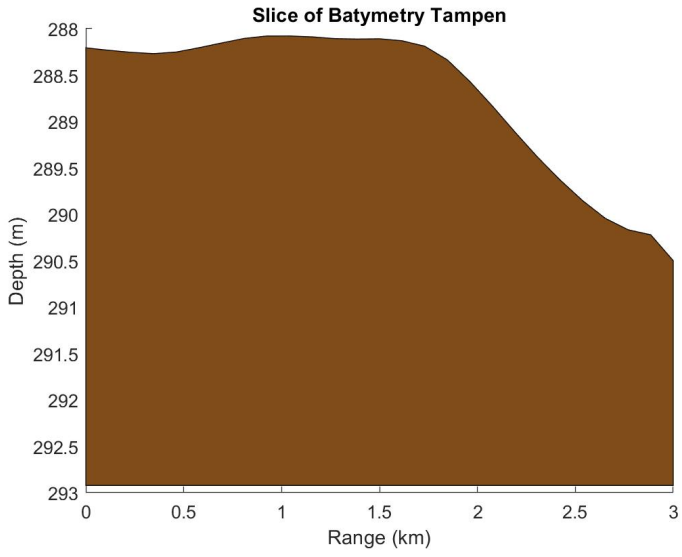

Figure 3.7: Slice of bathymetry data at the location below the Hywind turbine placed over the largest depth. The range is 3 kilometres west of this location.

Chapter 4

EERA Deepwind conference

The 19-21. January 2022 we participated in the European Energy Reseach Alliance (EERA) Deepwind conference. This is an international research & innovation conference that is being held in Trondheim every year. Due to covid, it was being held as a hybrid conference, and our participation was online. Originally we were going to make a poster and present it in the poster sessions while networking. Instead, we made a video that was being distributed on the conference platform and held a short presentation on zoom in parallel sessions.

The topics discussed at the conference were:

- New turbine and generator technology
- Grid connection and system integration
- Met-ocean conditions
- Operation & maintenance
- Installation and sub-structures
- Wind farm control
- Wind farm optimization
- Experimental testing and validation
- Sustainable development

My presentation was within the topic of "sustainable development". Since this is a slightly broad topic, we had many different disciplines and tasks in my session, and we represented different universities. Both technical and non-technical challenges was addressed, such as impacts of competitive seabed allocation, reducing carbon emissions in floater manufacturing and harnessing Norwegian maritime capabilities. It was very nice and educational to hear the other contributions. At the end of the poster presentations, we had a joint discussion where we tried to link all the topics together.

For the presentation, focus was put on the modelling part of the thesis. At this time we worked with the Chebyshev-Tau Spectral method for Normal Modes Modelling. After explaining the thesis approach and input for the normal modes model, a few sound propagation examples were shown. The study site was Hywind Tampen. The sound speed profiles were extracted from the Hywind Tampen Environmental Assesment (Weissenbergen (2019)). We modelled for two months (July and December) at different source frequencies and source depths. The results are shown in Figure 4.1.

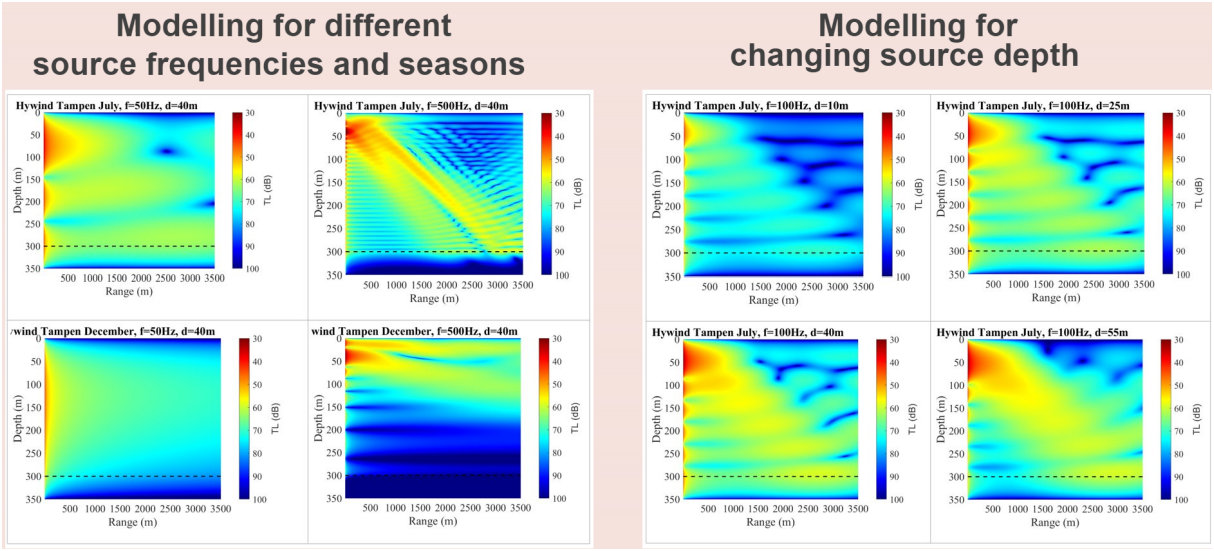

Figure 4.1: Screenshot of presentation at DeepWind Conference, showing modelling of sound propagation at Hywind Tampen. Modelled for different frequencies (left) and changing source depth (right).

From the left side of Figure 4.1, we see two low frequencies modelled for both July and December. Frequencies damp out differently, so as expected these patterns look different. One important theory is that sound bends towards the lowest sound speed, which is why the sound stays on the surface in winter, and towards the bottom in summer. On the right side of the figure, we have modelled for changing source depth, and the variation in sound velocity will again affect how the waves propagate, as well as where in the profile we have a generation of internal waves and other influences.

Chapter 5

Results and Interpretation

5.1 FINO1 Underwater Noise Measurements

5.1.1 Observational Data

For this section, we will present the results based on an analysis of the hydrophone data from FINO1. We have analysed the observational data in terms of sound pressure levels and energy spectra, as well as studied the forcing conditions at the corresponding time. We had numerous measurements from 2010 and 2011 available, and have chosen to present a few different time periods. The following results are based on a short two days period in November 2010, selected measurements throughout the months of 2011, a detailed period of 10 days in November 2010, and a couple of extreme events.

The following figure and table are presented as an overview of the measurement data from the 15th and 16th of November 2010. The data files were combined, and the peak and equivalent sound pressure levels were calculated in bulks of 5 seconds and 300 seconds. Before beginning any calculation we removed some of the spikes in the dataset, based on a manual screening of the data. The full time series of these results are presented in Figure 5.1. Table 5.1 contains the mean values of these bulks.

Table 5.1: Mean values of Leq and Lpeak values for the bulks of 5 seconds and 300 seconds. Decibels [dB] are re $1\mu Pa$.

SPL	**dB**
Leq 300s	123.13
Lpeak 300s	136.89
Leq 5s	123.01
Lpeak 5s	132.27

Each measurement segment is of 5 minutes (300 seconds), but by also studying the shorter averaging time of 5 seconds we get more scatter points and obtain a better impression. The results in Table 5.1 show that the sound level Leq averaged over 300 seconds for the two dates in November are 123 dB re 1 μPa with peak values about 14 dB higher.

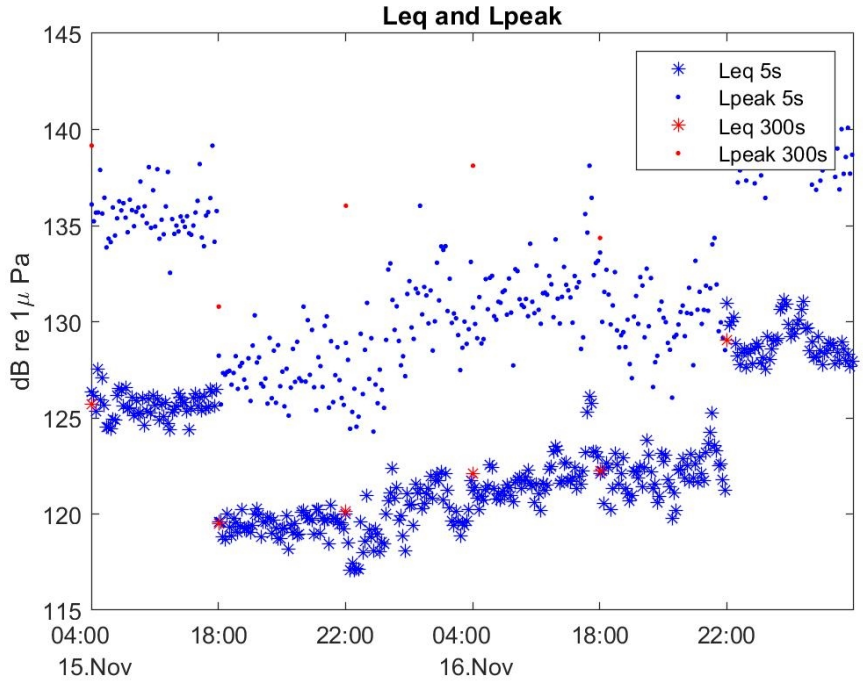

Figure 5.1: Sound pressure levels, equivalent and peak values for bulks of 5 seconds and 300 seconds. The blue colour is indicating values for the 5 seconds bulks of data, and the red colour indicates the bulks of 300 seconds.

In addition to the time domain, it is also interesting to look at the frequency composition of the sound field. To get a more in-depth view of the sound level across the frequency domain, we look at the 1/3 octave spectra, shown in Figure 5.2. This figure is showing the spectra of the Leq values for the bulks of 300 seconds. In Figure 5.2, we use the Leq values calculated based on the raw time series. We also plotted the same spectra for the spike removed time series to see the difference between the two. This is displayed in Figure 5.3

From the spectra figures, we see that most of the spectra peak at about $50 - 100$ Hz. In Figure 5.2, we see more energy for low frequencies and a lot less energy for the higher frequencies. After 100 Hz the spectral density drops for both spectra. In terms of environmental conditions, all measurements are done with a wave height less than or equal to 2 meters for our two days. Spectral components above 100 Hz are typical for ship noise (Radecke and Benesch (2012)) as well as the wind dependent bubble and spray noise which is typical for the higher frequencies (Wenz (1962)). We also see energy in very low frequencies, and in addition to the turbine noise, this is typical for other sources of background noise as indicated by the Wenz-curves shown in Figure 1.2 from Section 1.2.

The results of the narrowband spectra are shown in Figure 5.4

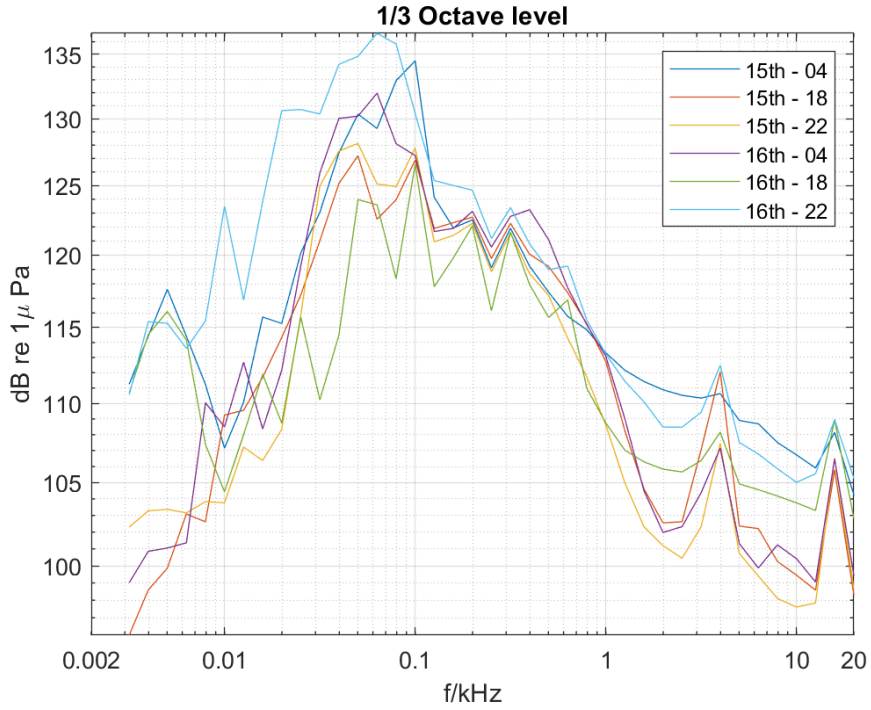

Figure 5.2: 1/3 octave spectra of Leq 300sec values. The spectra provide an overview of sound level in the frequency domain, with frequencies [kHz] on the x-axis. The values are calculated based on the raw pressure time series.

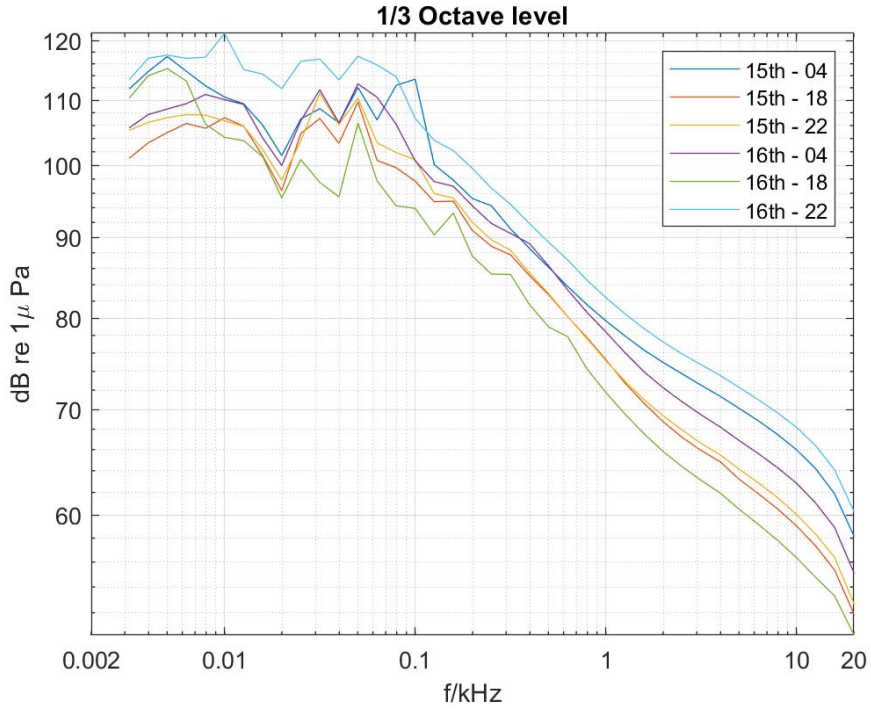

Figure 5.3: 1/3 octave spectra of Leq 300sec values. The spectra provide an overview of sound level in the frequency domain, with frequencies [kHz] on the x-axis. The values are calculated based on the spike reduced data.

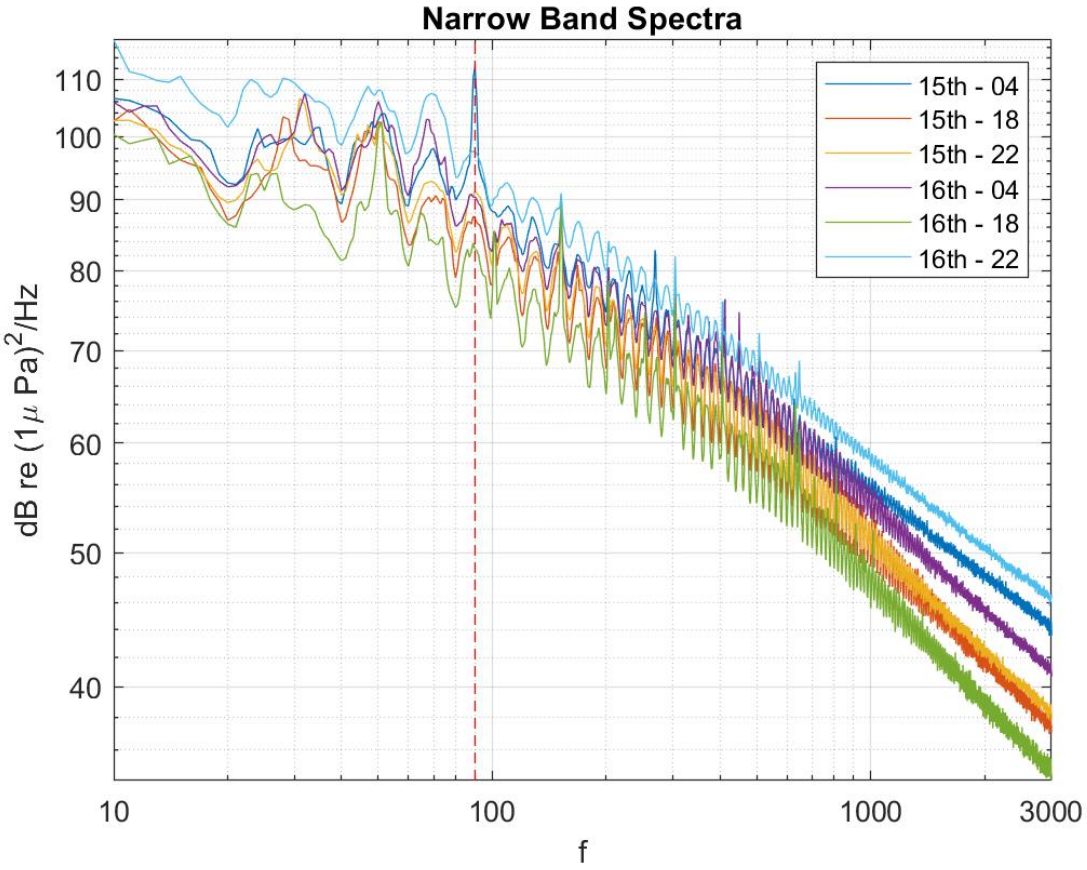

Figure 5.4: Narrowband spectra of all Leq 300sec values. The red dashed line is showing the 90 Hz frequency.

From the narrowband spectra, some peaks are revealed at different frequencies. The narrowband analysis reveals a larger number of dominant frequency components compared to the 1/3 octave spectra. From this analysis, we see a very prominent tone at $90 - 100$ Hz, as we also saw in the 1/3 octave spectra. Some other peaks across the frequency domain are also seen, especially around $300 - 800$ Hz for some measurement series. Higher levels of energy are also seen for very low frequency. As discussed earlier, this can be contributed by different sources of background noise in addition to the turbine itself, as indicated by the Wenz-curves. A study of operational noise at the Alpha Ventus wind farm was performed by Betke (2014). From this study, a tone of 90 Hz could be traced back to one of the turbines. Depending on the weather conditions, both the frequency and magnitude of this signal varied by a few Hz and dB. Regardless, it is natural to assume that the 90 Hz peak in our spectra is coming from the operating turbines nearby.

As mentioned in the method section, we will also filter the sound levels with a bandpass filter with cut-off frequencies of 10 Hz and 3 kHz. This is to reduce the energy of frequencies outside this range, that corresponds to contributions outside our scope. A visual representation of this bandpass filtering is shown in Figure 5.5.

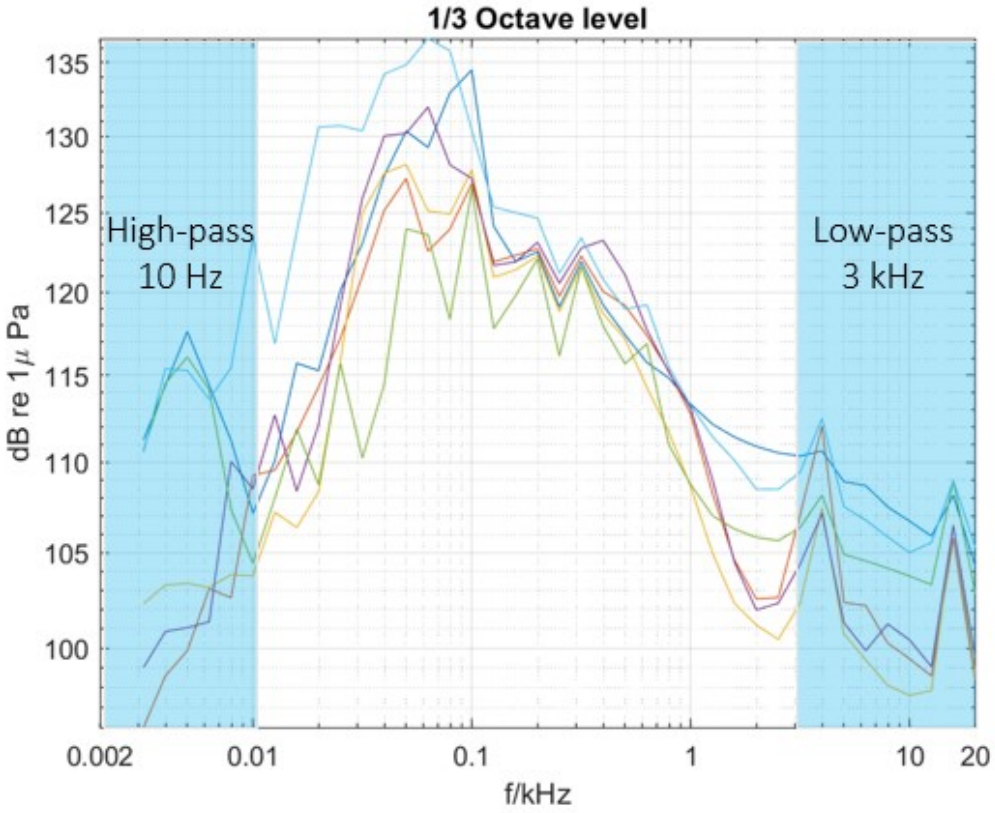

Figure 5.5: Visual demonstration of the bandpass filtering of $10 - 3000$ Hz. Inspired by Radecke and Benesch (2012).

This filtering will lower the values of Leq and Lpeak, as shown Figure 5.6. To see how much dB attenuation the filtration causes we also plot the difference between the unfiltered and filtered values, shown in Figure 5.7.

As seen in this figure, the difference is very small and doesn't contribute to a large change in the overall averaged values. At peak values, the difference due to the bandpass filtering is stronger. This is expected as the filter removes the bigger fluctuations. A summary of these results is given in Table 5.2. As we see from the visual representation of the filter in Figure 5.5, the energy level is already quite low within these ranges. This explains why the difference between the unfiltered and filtered values is so small. The limits of the bandpass filter were chosen based on the report from Radecke and Benesch (2012). In general, the bandpass filter limits are chosen based on our frequency range of interest, and for our case, we could have narrowed it even more. However, the filter chosen still fits our interests well. The biggest difference in filtering is found in the measurement segment for the 16th of Novemeber at 16:00. At this time, noise is also generated by sources within the frequency range we filtered away.

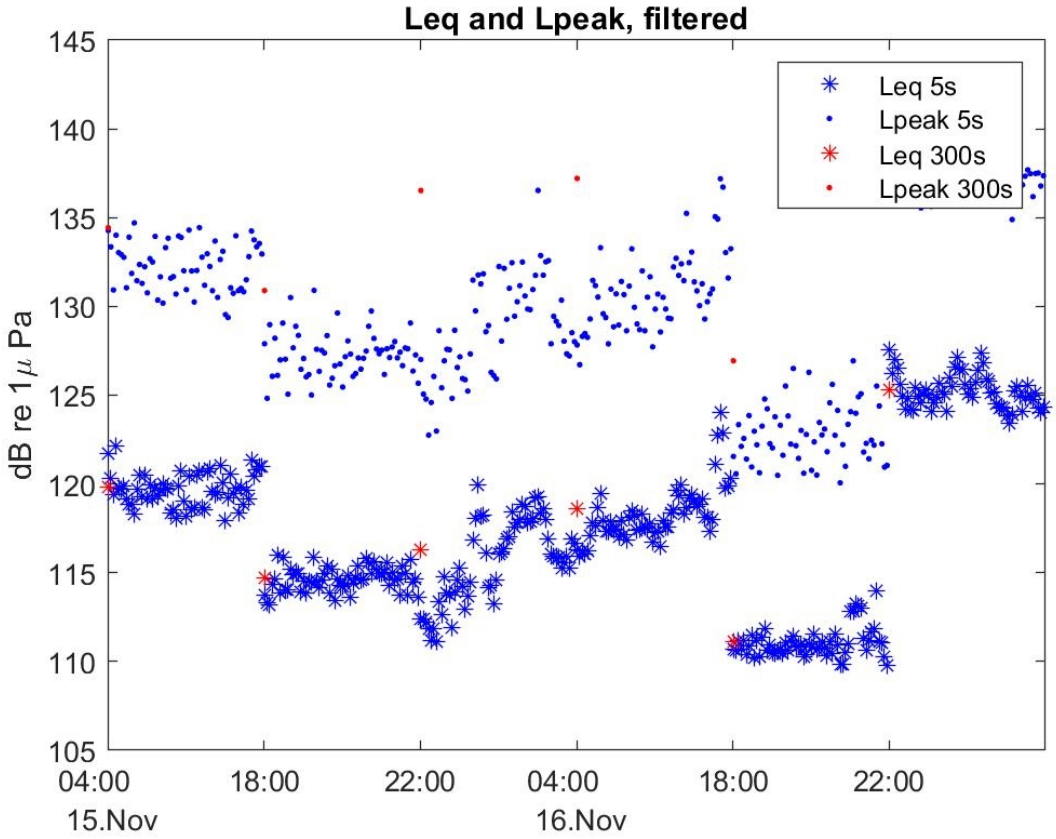

Figure 5.6: Sound pressure levels Leq and Lpeak based on filtered data for bulks of 5 seconds and 300 seconds. The blue colour is indicating values for the 5 seconds bulks of data, and the red colour indicates the bulks of 300 seconds.

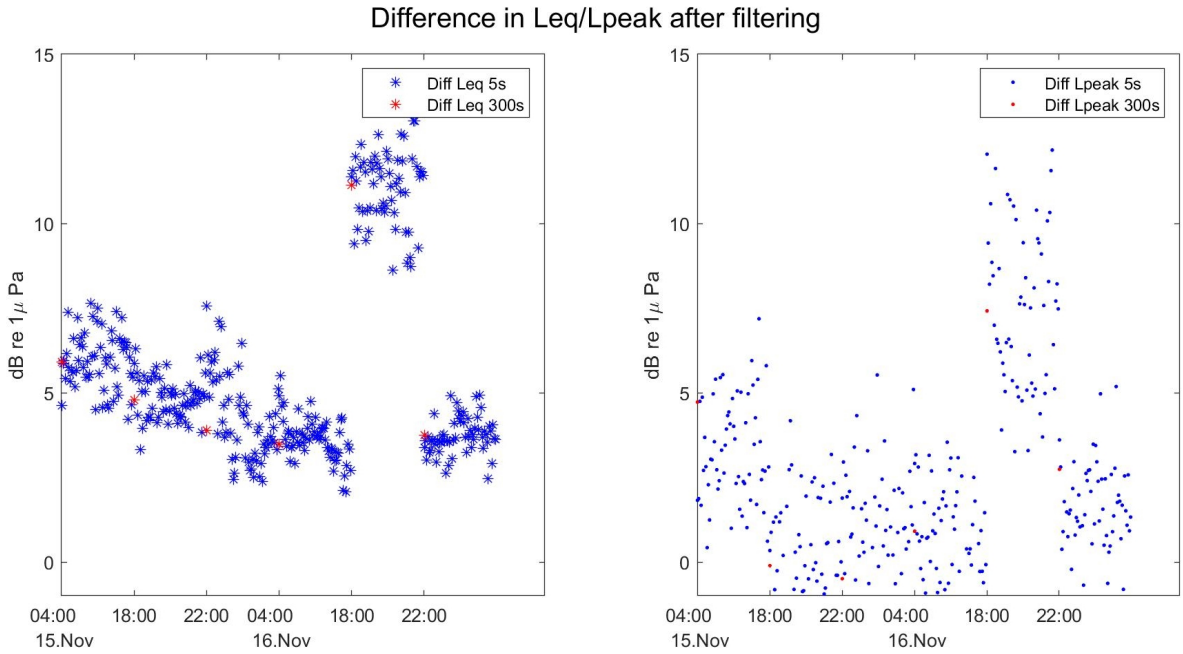

Figure 5.7: Difference in Leq and Lpeak after filtering the data set.

Table 5.2: Summary of mean values of Leq and Lpeak for the bulks of 5 seconds and 300 seconds. Showing both unfiltered and filtered, as well as the difference between them. Decibels [dB] are re 1 μPa.

SPL	**Original [dB]**	**Filtered [dB]**	**Difference [dB]**
Leq 300s	123.13	117.64	5.49
Lpeak 300s	136.89	134.36	2.53
Leq 5s	123.01	117.43	5.58
Lpeak 5s	132.27	129.95	2.32

A study performed by Tougaard et al. (2020) used available measurements of underwater noise induced by different offshore wind turbines and reviewed their source levels. The study showed that the turbine radiated noise was low, at least compared to ship traffic which was 10-20 dB higher in the same frequency range. The study also revealed smaller effects on the measured sound pressure coming from wind speed and turbine size, but with distance being the most important factor.

The noise emitted from the Alpha Ventus offshore wind farm was also included in the paper. It showed a mean value of 118 dB re 1 μPa based on the findings from Radecke and Benesch (2012) and Betke (2014). The source levels from the different turbines all varied by some dB depending on the environmental conditions. The highest value found was 137 dB re 1μPa 40 meters away from the turbine. This level of sound is closer to our result for completely raw data, and for the filtered data we are slightly above the findings of the FINO1 report. However, our higher levels could potentially be explained by a few reasons. The measurements that gave an average sound pressure level of 118 dB 1 μPa were measurements from two additional hydrophones placed by a wind turbine each, and not the FINO1 hydrophone alone. From the FINO1 tower, we could experience resonance from the tower or filtration of frequencies by the structure that could affect the signal. Also, the sound pressure levels are based on the total background noise which could be different at the FINO1 location than that for the other hydrophones.

Madsen et al. (2006) performed a similar study based on the measurements available at that time. Both Madsen et al. (2006) and Tougaard et al. (2020) concluded that the operational noise was limited to low-frequency noise, typically with dominant peaks corresponding to the mechanical frequencies (and their harmonics) in the nacelle. The dominant peaks of the different wind turbines vary a lot, but they were all below 1 kHz. For the Alpha Ventus offshore wind farm the dominant frequency was 90 Hz. Wind-induced vibrations also had a slight impact, which is expected as the tower vibrations move down the structure and into the water.

In general, wind itself will contribute to the overall sound pressure level in the ocean, as wind induce and increase noise as the forcing gets stronger. This is also because wind will affect the wave breaking and bubbles, which again increases noise levels. What kind of waves that are present will also affect the overall noise. This is why it is interesting to study how sound pressure levels will change under varying forcing conditions. Far off the shore, including our study sites, we are expecting well devolved waves. When studying forcing conditions we will be using significant wave heights, but identifying wave properties such as wind sea or swell would also be of interest.

The types of energy spectra we showed previously are useful for checking if these tones are equally prominent under different forcing conditions. Since this 90 Hz tone belongs to the turbine, it is expected to be dominant under full load hours. For a wide range of measurements, it would be interesting to sort these measurements after environmental parameters such as wave height and wind speed. We therefore also arrange the sound values in order of various parameters such as wind and wave data. The wind and wave data are from NORA3 reanalysis data set, and in Figure 5.8 we see a 10-day period of the data for November 2010. These data are very correlated, with a correlation coefficient of 0.88 for the whole ten-day period, and 0.77 for the 15th and 16th of November which are our dates of interest. This can imply that the waves are wind-generated and not just swelling waves.

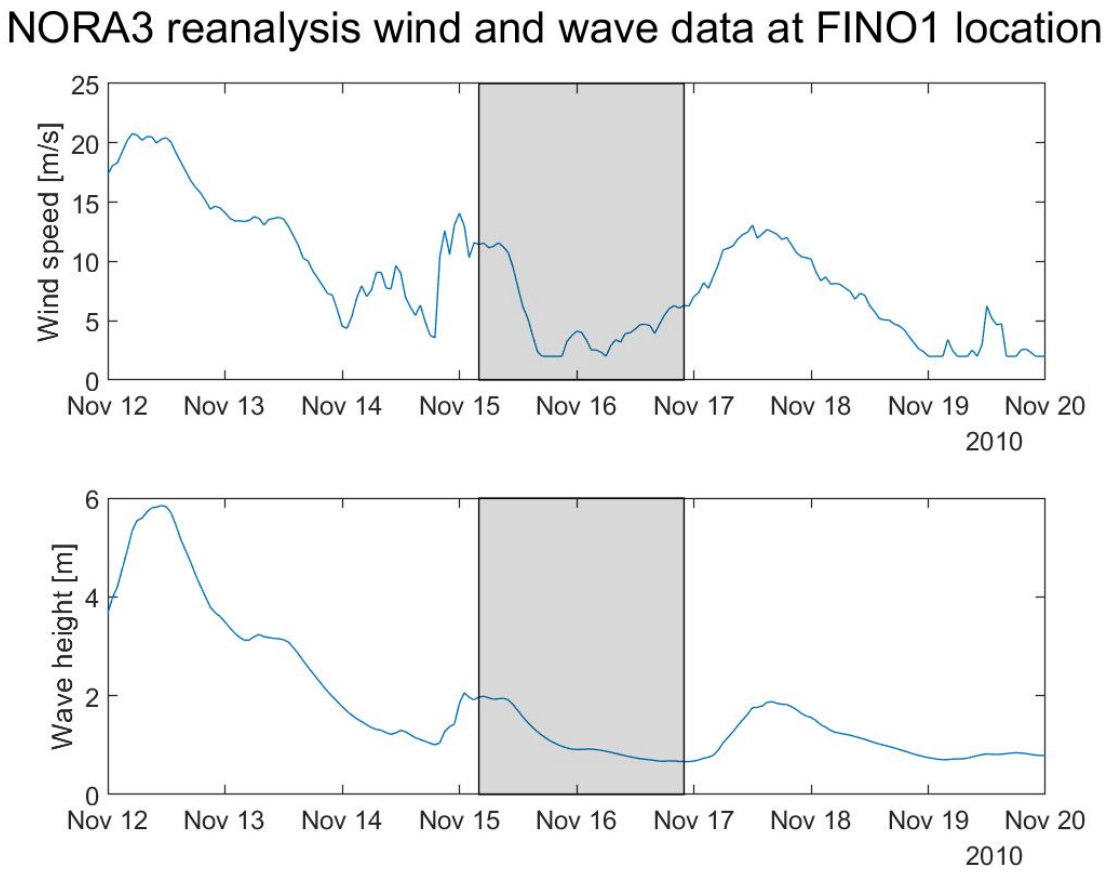

Figure 5.8: Wind speed and wave height data from NORA3 at the FINO1 location. A time series of ten days in November is shown, and the grey boxes show our time period of interest.

The following figures show the sound pressure level plotted against the wind speed and significant wave height for the respective time. As mentioned in Section 3 this data is from NORA3, and the wind speed is at an altitude of 10m, see Figures 5.9 and 5.10.

Looking at the Figures 5.9 and 5.10, the plotted values are all very scattered and not particularly correlated. To explore this further, we look at the correlation coefficients shown in Table 5.3.

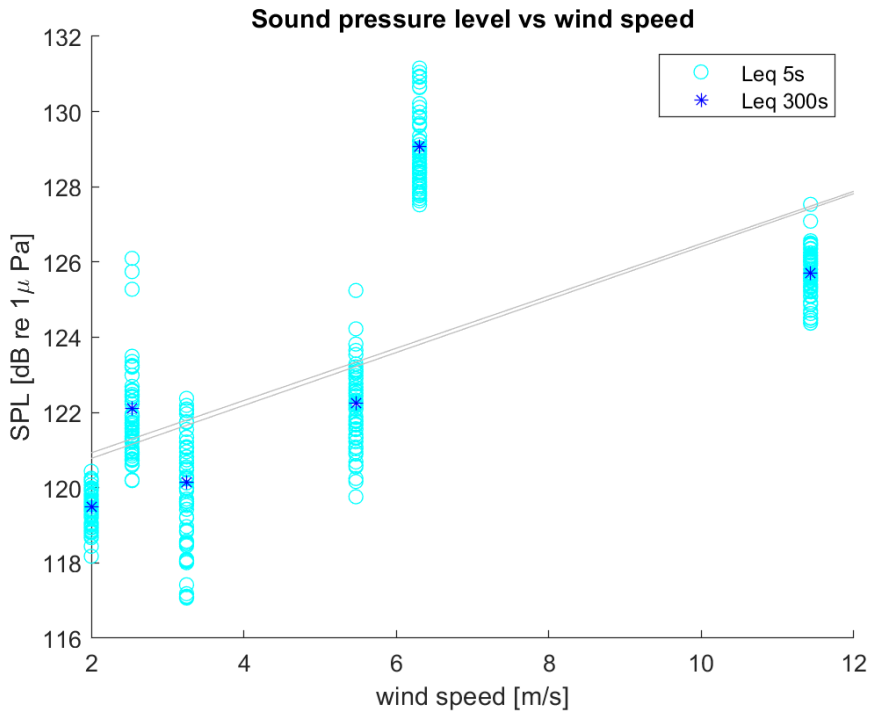

Figure 5.9: Sound pressure levels Leq averaged at 5 seconds and 300 seconds, sorted against corresponding wind speed [m/s] at 10m height from NORA3. The line is showing a linear fit of the scattered data points.

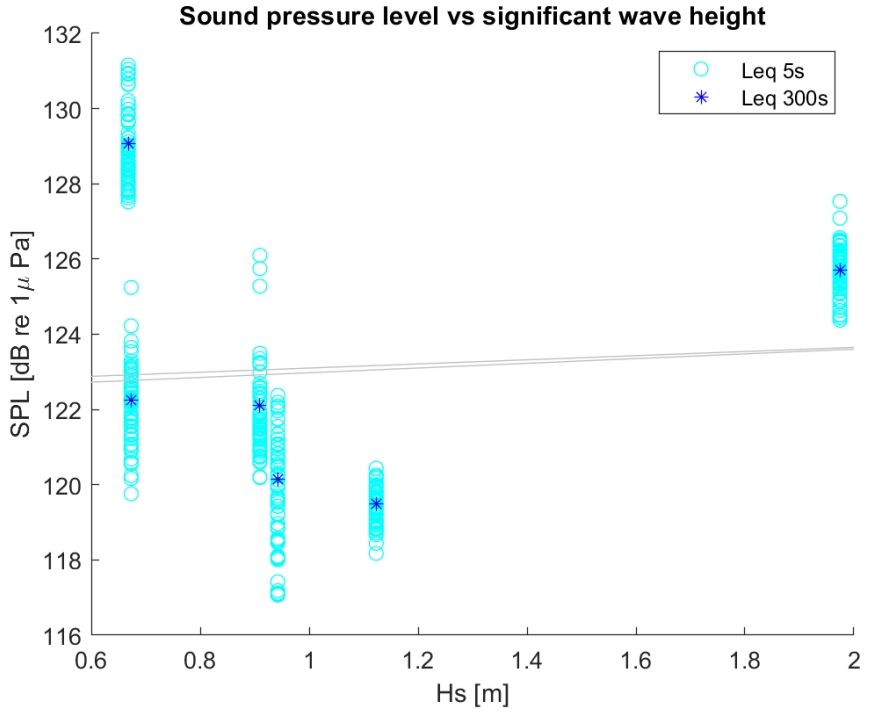

Figure 5.10: Sound pressure levels Leq averaged at 5 seconds and 300 seconds, sorted against corresponding wave height [m] from NORA3. The line is showing a linear fit of the scattered data points

Table 5.3: Correlation coefficients of mean values of Leq and Lpeak for the bulks of 5 seconds and 300 seconds against wind speed and against significant wave height.

Data	**Correlation**
Wind vs Leq 300s	0.67
Wind vs Leq 5s	0.65
Wave vs Leq 300s	0.07
Wave vs Lpeak 5s	0.08

The values in the table show correlation coefficients of approximately 0.67 for wind and only 0.07 for wave. This does not show any significant correlation between them, however, for increasing wind speeds it could imply a relationship with increasing sound pressure levels. It is important to note that by only studying the 15th and 16th of November, we have very limited input to do such an analysis. By studying more dates at different months of the year, as well as more continuous measurement series, we would have a better baseline for determining this relation.

Measurements Throughout 2011

To get an overview of how the data would change throughout the year, we further studied measurements from a broader period. As with the previous measurements, we studied the filtered and unfiltered averaged sound pressure levels. We then studied the corresponding wind and wave data from NORA3. Interactions from wind and wave on the acoustic data is better to perform with more data from different seasons, as environmental conditions change a lot during an entire year. In this case we have the measurement segments from the 15th of every month in 2011.

In the following figures, the Leq and Lpeak values are presented, both with filtered and unfiltered data. The difference between them are also shown. A summary of these results are given in Table 5.4.

Table 5.4: Summary of mean values of Leq and Lpeak for the bulks of 5 seconds and 300 seconds, for the 15th of every month in 2011. Showing both unfiltered and filtered, as well as the difference between them. Decibels [dB] are re 1 μPa.

SPL	**Original [dB]**	**Filtered [dB]**	**Difference [dB]**
Leq 300s	130.92	122.56	8.36
Lpeak 300s	147.20	142.48	4.72
Leq 5s	128.88	121.08	7.80
Lpeak 5s	138.82	134.03	4.79

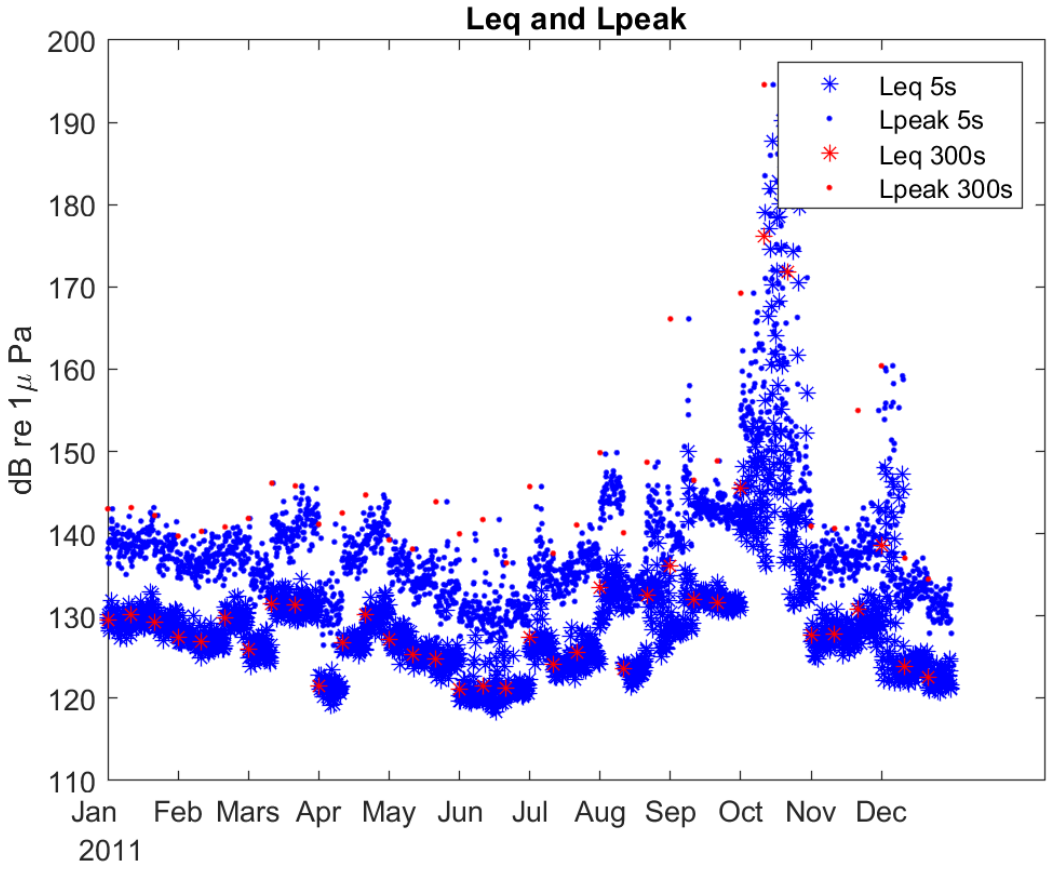

Figure 5.11: Sound pressure levels, equivalent and peak values for bulks of 5 seconds and 300 seconds. The blue colour is indicating values for the 5 seconds bulks of data, and the red colour indicates the bulks of 300 seconds.

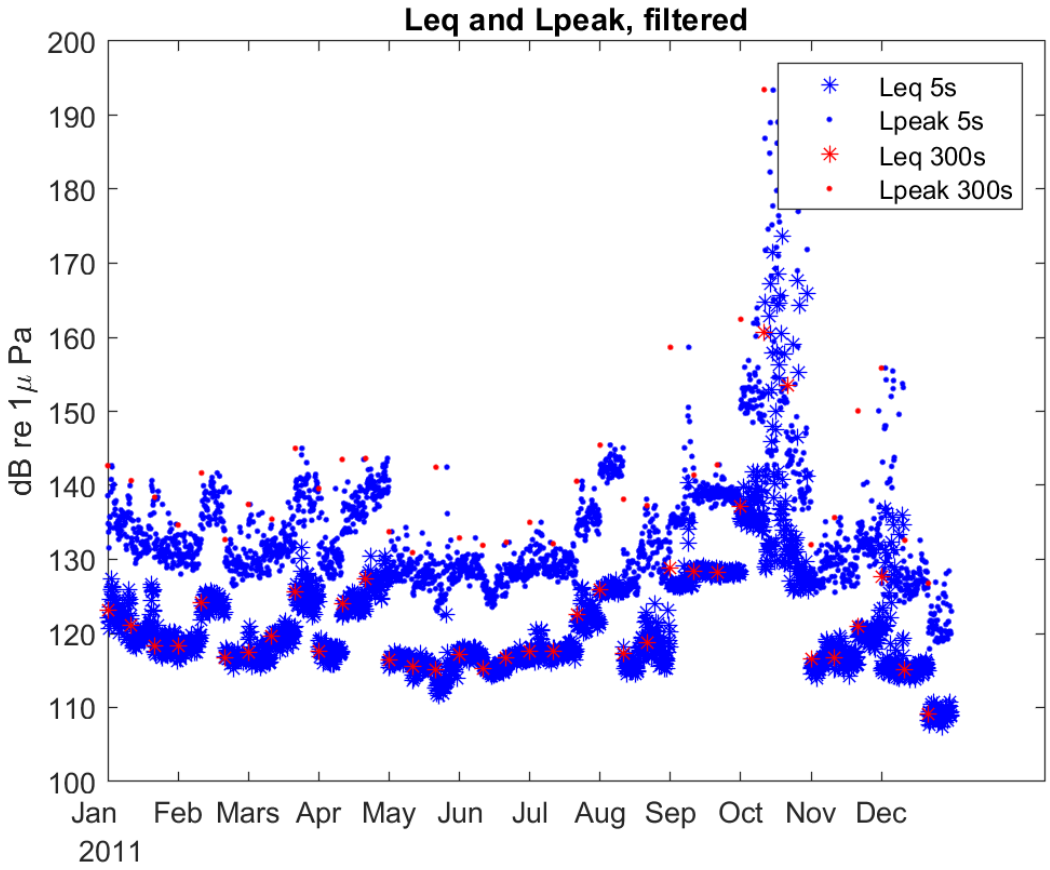

Figure 5.12: Sound pressure levels Leq and Lpeak made with filtered data for bulks of 5 seconds and 300 seconds. The blue colour is indicating values for the 5 seconds bulks of data, and the red colour indicates the bulks of 300 seconds.

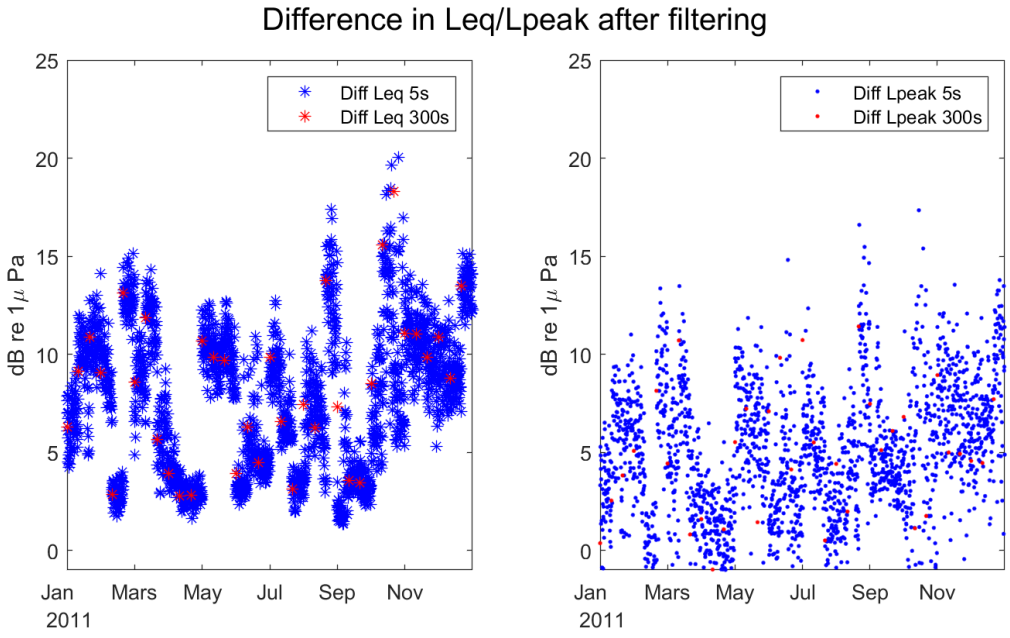

Figure 5.13: Difference in Leq and Lpeak after filtering the data set.

As with the first dataset, we also compared these new values to corresponding data about wind and wave from NORA3. These results are displayed in Figures 5.14 and 5.15.

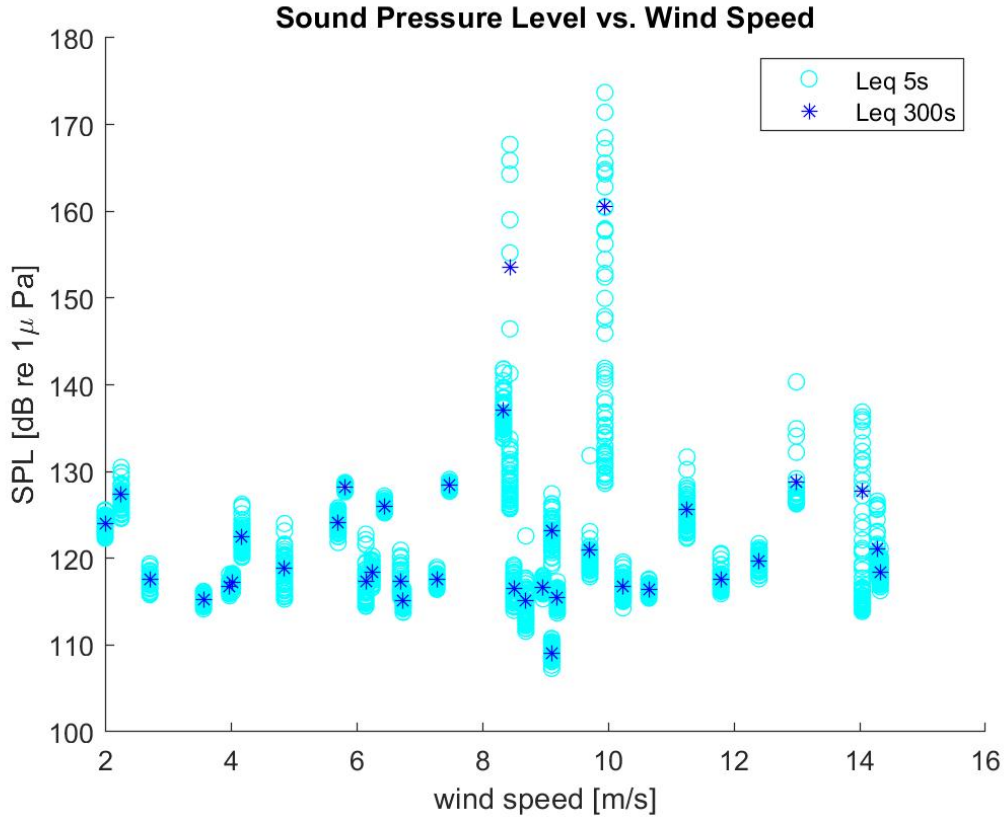

Figure 5.14: Sound pressure levels Leq averaged at 5 seconds and 300 seconds, sorted against corresponding wind speed [m/s] at 10m height from NORA3.

The sound is determined by the background noises. From the Radecke and Benesch (2012) report, they state that the sound level drops for higher wave heights. The reason being that there is less ship traffic in the vicinity, and because there are more air bubbles at higher waves which attenuate distant noise. We could therefore expect the same results if we analysed more measurements than what was provided.

For a wind farm, we would expect standstill performance for strong environmental forcing conditions. Therefore, at some distance, the underwater sound level could be higher for these conditions than the full load hours where the environmental conditions are calmer, based on the conclusions of the report.

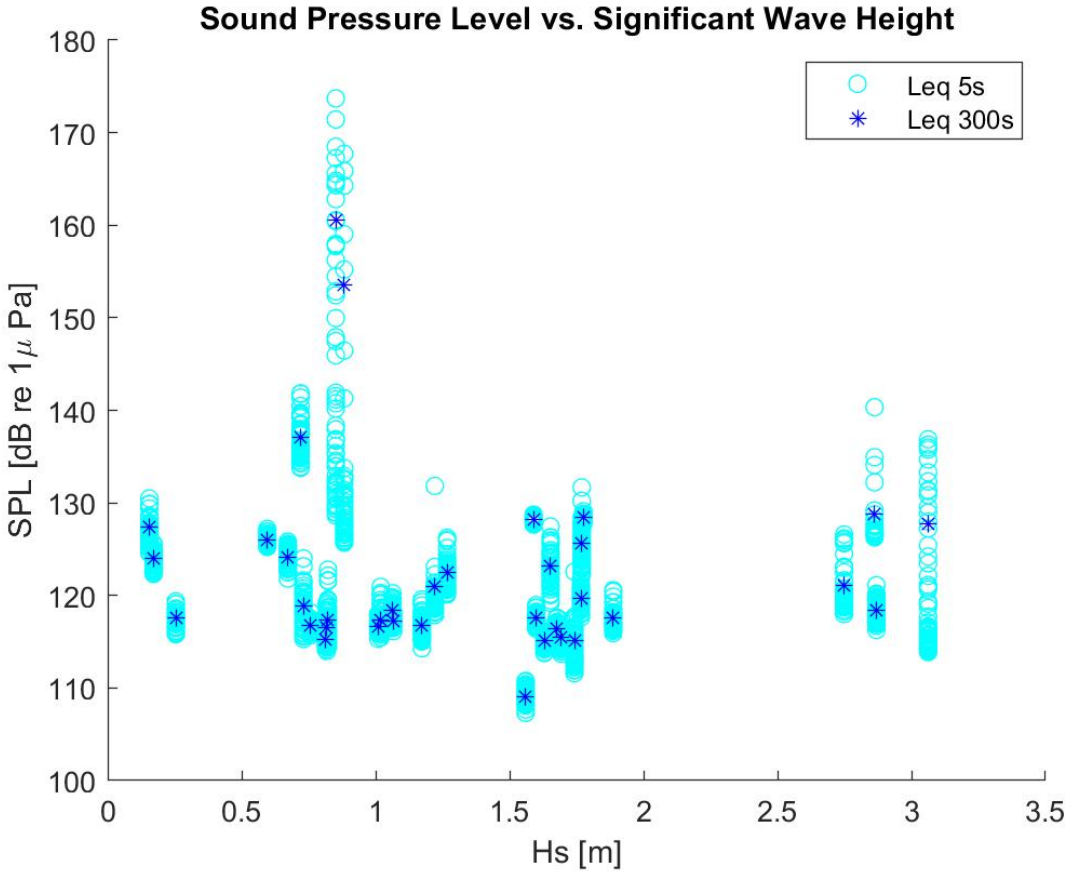

Figure 5.15: Sound pressure levels Leq averaged at 5 seconds and 300 seconds, sorted against corresponding wave height [m] from NORA3.

In Figures 5.14 and 5.15 we don't see any significant correlation between wind speed or wave height as the plots are very scattered. The correlation coefficient was only 0.1, with a positive "correlation" for wind speed, and a negative one for significant wave height. Determining the wave age or other wave characteristics could be better for the overall understanding than what significant wave height provided in this study. On the other hand, the big spikes from the October data, most likely from ship traffic, are influencing this correlation study and the results could have been different if these data were ignored. Even though we study sound pressure levels for a long period and in different seasons, we still have fewer measurement points than other reports, and it is, therefore, reasonable to not get the exact same results as other studies such as the report from Radecke and Benesch (2012).

10-day Period during November 2010

Since the long term period in 2011 consisted of a random selection of measurements throughout that year, it did not form an ideal basis for studying how sound pressure levels may change with the weather conditions. In order to study the correlation between sound pressure levels and forcing conditions in more detail, we also looked closer into a continuous period of 10 days. The following results will be based on the time period 12th-21st of November 2010.

Figure 5.16 provides an overview of the forcing conditions during this 10-day period. The red dots marks where we have measurements from the hydrophone. We have already studied the 15th-16th of November, and we provide a broader time series this time to get a better overview of the overall sound pressure development in time. From the figure, we can observe that the 12th of November has strong forcing conditions.

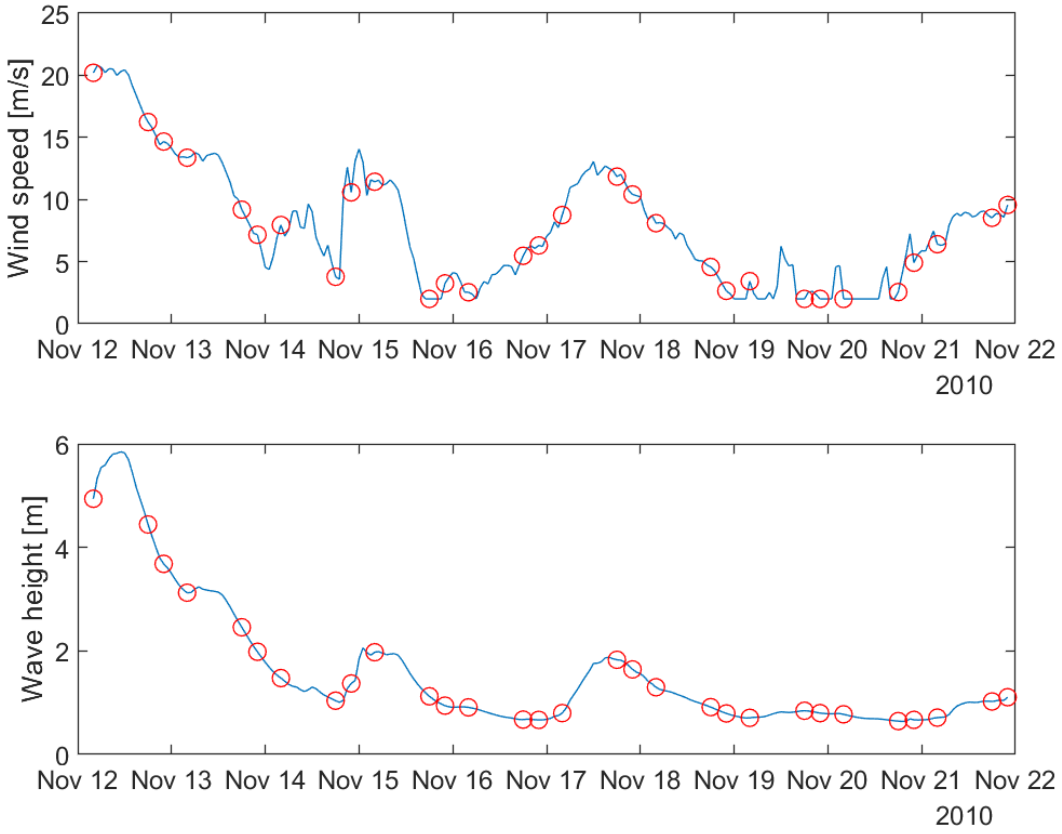

Figure 5.16: Wind speed and wave height for the period of 12th-21st of November 2010. Data are extracted from the NORA3 reanalysis. The red circles indicate where in the time series we have available hydrophone measurements.

The results of the calculated equivalent- and peak sound pressure levels, averaged at bulks of 5 seconds and 300 seconds, are shown in Table 5.5. The results are also displayed in Figure 5.17, where we show both the filtered and unfiltered sound pressure levels.

Table 5.5: Summary of mean values of Leq and Lpeak for the bulks of 5 seconds and 300 seconds, for a 10-day period in 2010. Showing both unfiltered and filtered, as well as the difference between them.

SPL	**Original [dB]**	**Filtered [dB]**	**Difference [dB]**
Leq 300s	125.97	119.31	6.66
Lpeak 300s	141.81	137.43	4.38
Leq 5s	125.16	118.62	6.54
Lpeak 5s	135.00	131.34	3.66

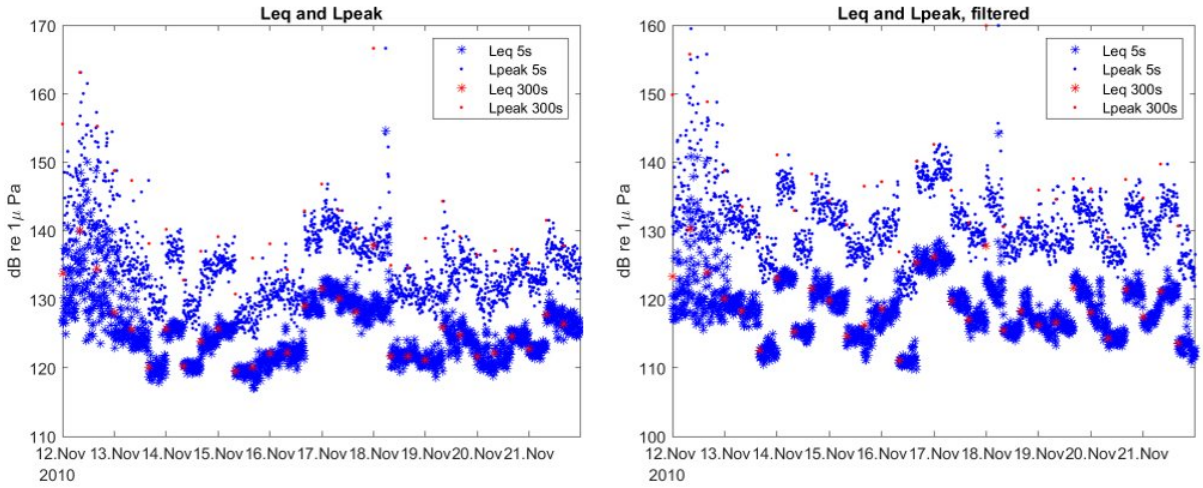

Figure 5.17: Sound pressure levels for a 10-day period in 2010. Red points are the 300 seconds averaged equivalent and peak sound pressure levels, and the blue points are for the averaged 5 seconds bulks. Left panel are unfiltered measurements, and right panel is bandpass filtered measurements.

From Figure 5.17, we see that the sound pressure levels are quite scattered throughout the ten days. If we look at the averaged value Leq 5s from Table 5.5, it has a value of **118.62 dB re** $1\mu Pa$. In the report by Radecke and Benesch (2012), their analysis resulted in an averaged value of 118 dB re $1\mu Pa$, so in this particular case we have good agreement with their study.

How the sound pressure levels are distributed against the wind and wave conditions are shown in Figure 5.18 and Figure 5.19 respectively. The grey line in the figures displays a linear fit of the scattered data points. From that line, we can see a slight positive slope as the values of both wind, wave and sound pressure levels increase. The correlation coefficients for this study are 0.51 for wind and 0.43 for wave. That is not a very significant correlation, but we can see a slight relationship between them. In this case, the wind and wave data themselves are very correlated, indicating that the waves are mainly wind-induced.

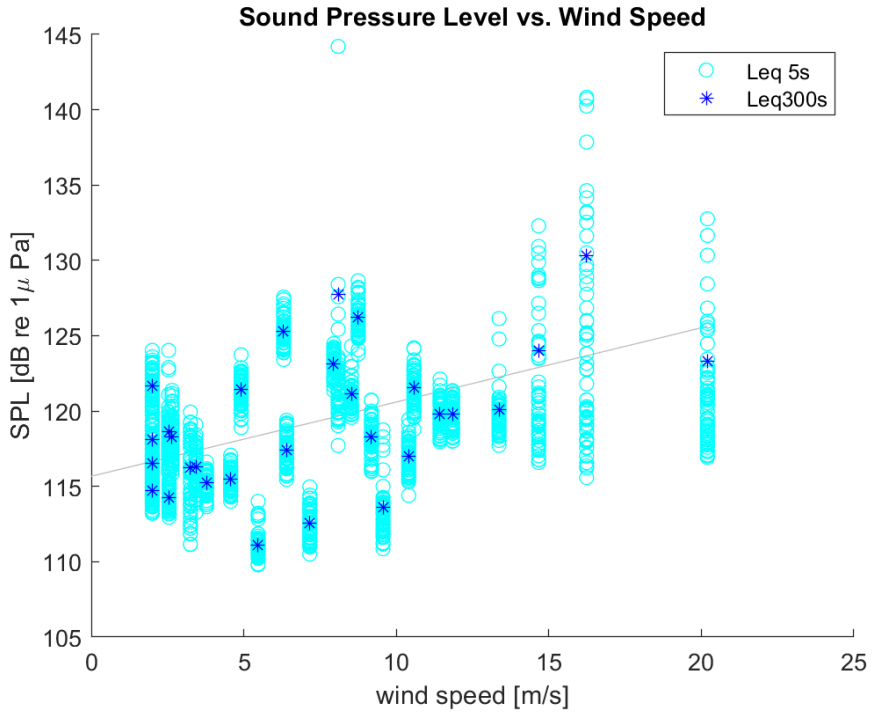

Figure 5.18: Sound pressure levels against the corresponding wind speed 12th-21st of November 2010. The grey line is a linear fit of the scattered data points.

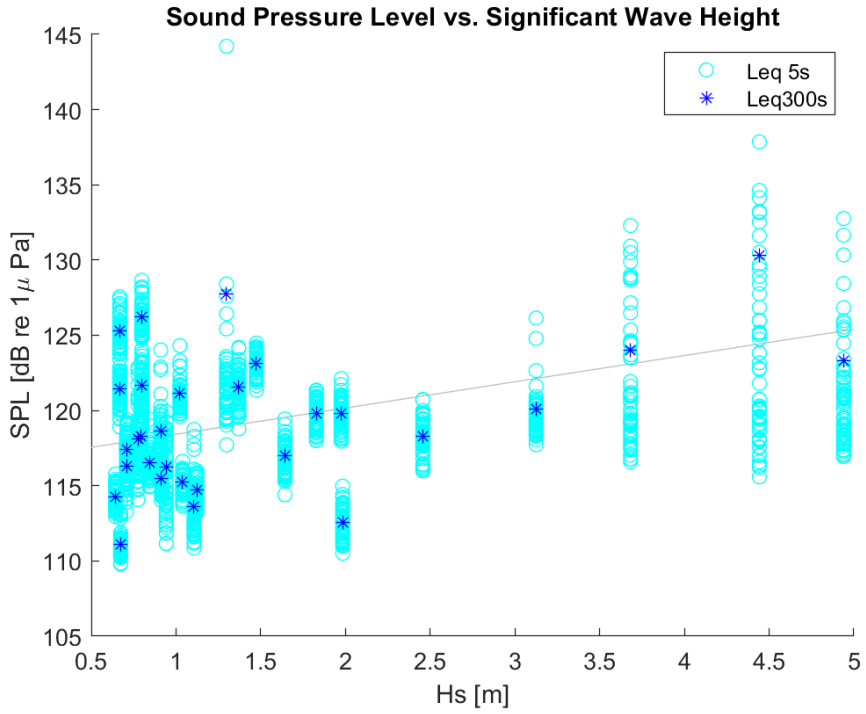

Figure 5.19: Sound pressure levels against the corresponding wind speed 12th-21st of November 2010. The grey line is a linear fit of the scattered data points.

Extreme Forcing Events

Since we wanted to study the noise propagation during selected forcing events, we further studied extreme events. By finding the largest values of wind speed and wave height from NORA 3 during 2010 and 2011, we identified two extreme events. These are the 12th of November 2010 and the 8-9th of December 2011. At these times, cyclone Carmen (2010) and cyclone Friedhelm (2011) passed in the vicinity of the farm.

We performed the same analysis on these data as previously. Even though the wind speed was high, the turbine's dominant tone of 90 Hz could still be seen in most of the narrow band spectra. The narrowband spectra are displayed in Figure 5.20. Common for all spectra are that they generally have a higher spectral density than for the previous measurement series that we studied.

The turbine closest to the FINO1 platform is a REpower 5-MW Offshore wind turbine. It has a cut-off wind speed of 30 m/s. It could therefore still be operating in rough conditions. However, for one of the measurements on the 9th of December 2011, the 90 Hz peak was not visible. For these spectra, the energy levels were generally higher than for the other spectra, and without the peak at 90 Hz. It is, therefore, reasonable to assume that the higher background level came from natural contributions from the rough weather and that the wind turbine was not operating at this exact time.

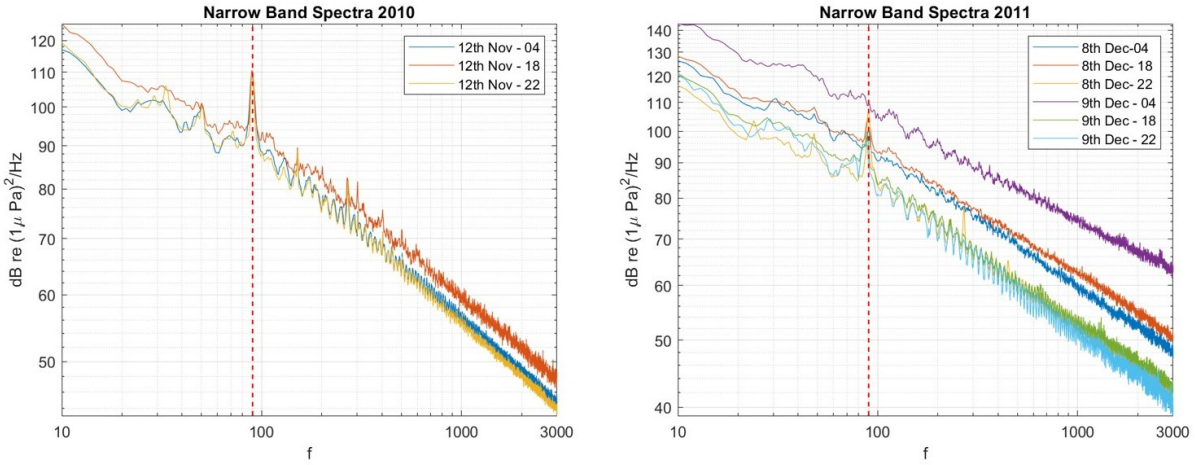

Figure 5.20: Narrowband spectra for the extreme events of 2010 and 2011. The red dashed line is showing the turbine's dominant frequency of 90 Hz.

The results of the calculated equivalent- and peak sound pressure levels, averaged at bulks of 5 seconds and 300 seconds, are shown in Table 5.6. The results are also displayed in Figure 5.21, where we show the filtered levels only for simplicity. For these events, both the unfiltered and filtered sound pressure levels lie beyond those previously studied. The differences in the filtered calculations are also greater, meaning that the frequencies lying outside of the filter have a bigger contribution to the overall sound pressure levels. In addition, the levels are also more scattered than in previous measurements. This could imply that the continuous operational noise is less prominent and masked by other natural contributions.

SPL	Original [dB]	Filtered [dB]	Difference [dB]
Leq 300s	136.09	125.87	10.22
Lpeak 300s	158.01	151.18	6.83
Leq 5s	132.64	122.18	10.46
Lpeak 5s	143.96	136.15	7.81

(a) 12th of November 2010

SPL	Original [dB]	Filtered [dB]	Difference [dB]
Leq 300s	139.73	130.96	8.77
Lpeak 300s	162.30	157.45	4.85
Leq 5s	135.19	125.76	9.43
Lpeak 5s	146.47	139.67	6.80

(b) 8-9th of December 2011

Table 5.6: Summary of mean values of Leq and Lpeak for the bulks of 5 seconds and 300 seconds, for the extreme events of a) 2010 and b) 2011. Showing both unfiltered and filtered, as well as the difference between them.

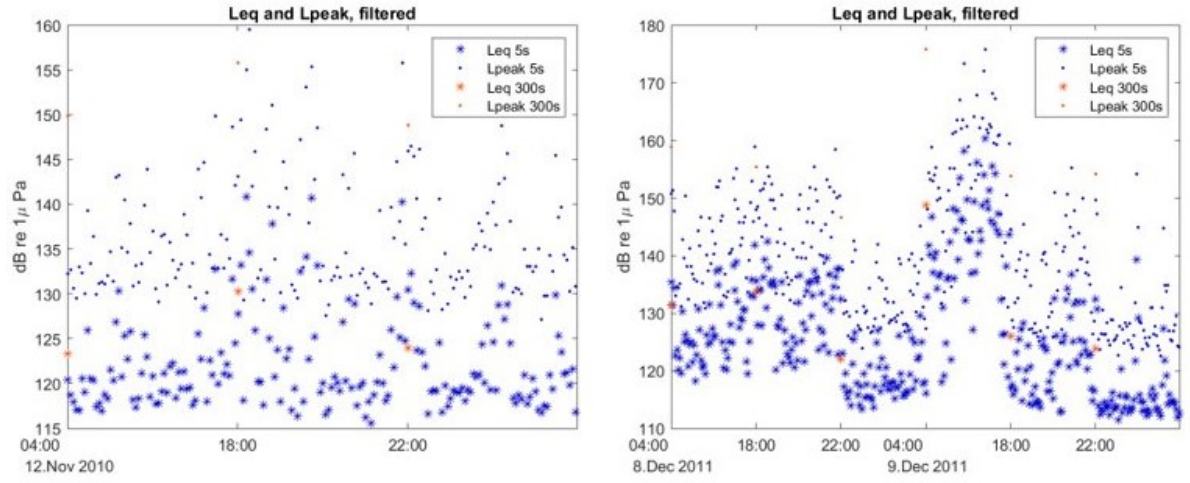

Figure 5.21: Sound pressure levels for the extreme events of 2010 and 2011. Orange points are the 300 seconds averaged equivalent and peak sound pressure levels, and the blue points are for the averaged 5 seconds bulks.

Further, we studied how the sound pressure levels were distributed against wind speed and wave heights. The results of these events for 2010 and 2011 are shown in Figure 5.22 and Figure 5.23 respectively. For 2010 the sound pressure levels overall didn't increase with the wind and wave data. The highest values are found in the middle range of both wind and wave data. However, the difference is not very significant. In 2011 we find the highest sound pressure levels in the most extreme conditions. This is also when the turbine is shut off.

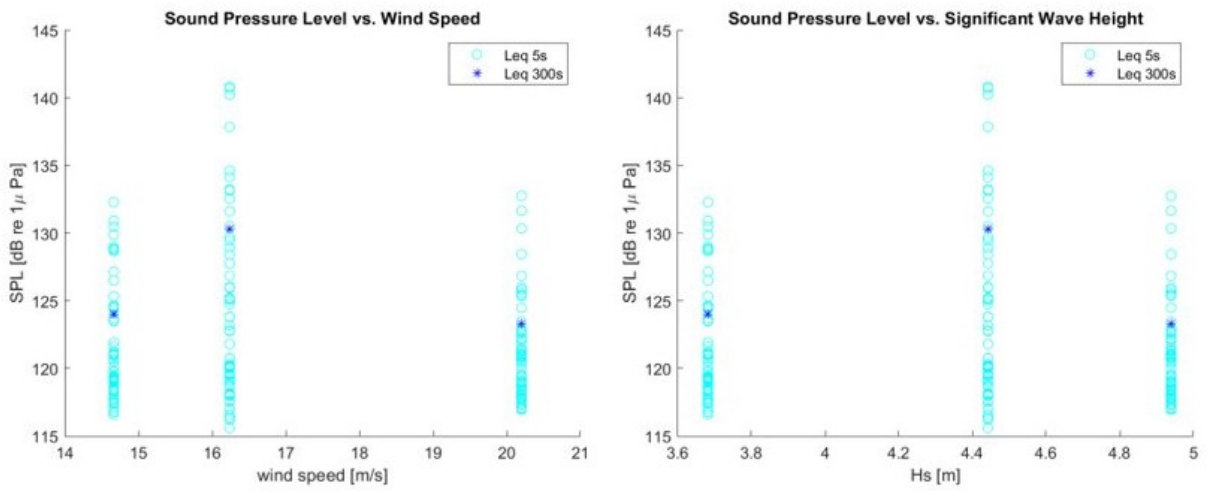

Figure 5.22: Sound pressure levels against wind speed (left) and significant wave height (right). These measurements are taken during the extreme event in 2010.

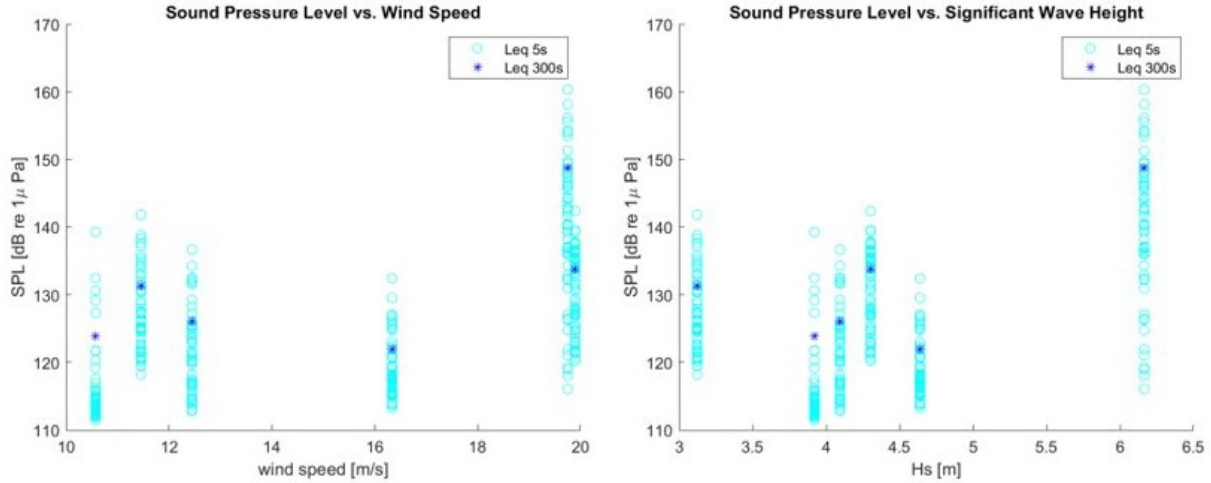

Figure 5.23: Sound pressure levels against wind speed (left) and significant wave height (right). These measurements are taken during the extreme event in 2011.

In Radecke and Benesch (2012) it was pointed out that large waves could attenuate sound from the turbines. In such a case, the sound pressure level from the turbines would decrease with increasing wave heights. In extreme environmental conditions, the turbines are shut off and the operational sound would therefore not be present in such cases. This was the case for one of the measurements on the 9th of December 2011, and we saw that the overall sound pressure level was larger in these extreme conditions even though the operational sound was absent. Increasing sound from natural contributions corresponds well to the Wenz curves in Figure 1.2 where we see that the sound pressure levels rise for increasing sea states.

5.1.2 Propagation Modelling

For our next step, we did sound propagation modelling at the study site of FINO1 offshore platform. We used the BELLHOP model as described in both the theory and method sections of this thesis. The BELLHOP model produces a shade file that allows us to display the propagation. The altimetry formed by the wave conditions are also accounted for and plotted in all displayed propagation figures.

From the observational data, we revealed a peak frequency of 90 Hz from the narrowband spectra in Figure 5.4, something that we also validated by Radecke and Benesch (2012) and Betke (2014). In our study, we are interested in the propagation of turbine induced noise. For the sound propagation modelling, we therefore look at how this frequency will propagate. To also demonstrate how various frequencies can propagate differently, we also model for the 4th, 5th and 7th harmonics of the turbines frequency of 90 Hz, which is 360 Hz, 450 Hz and 630 Hz. The displayed propagation in Figure 5.24 is based on the daily averaged oceanic data for the 15th of Novemeber 2015.

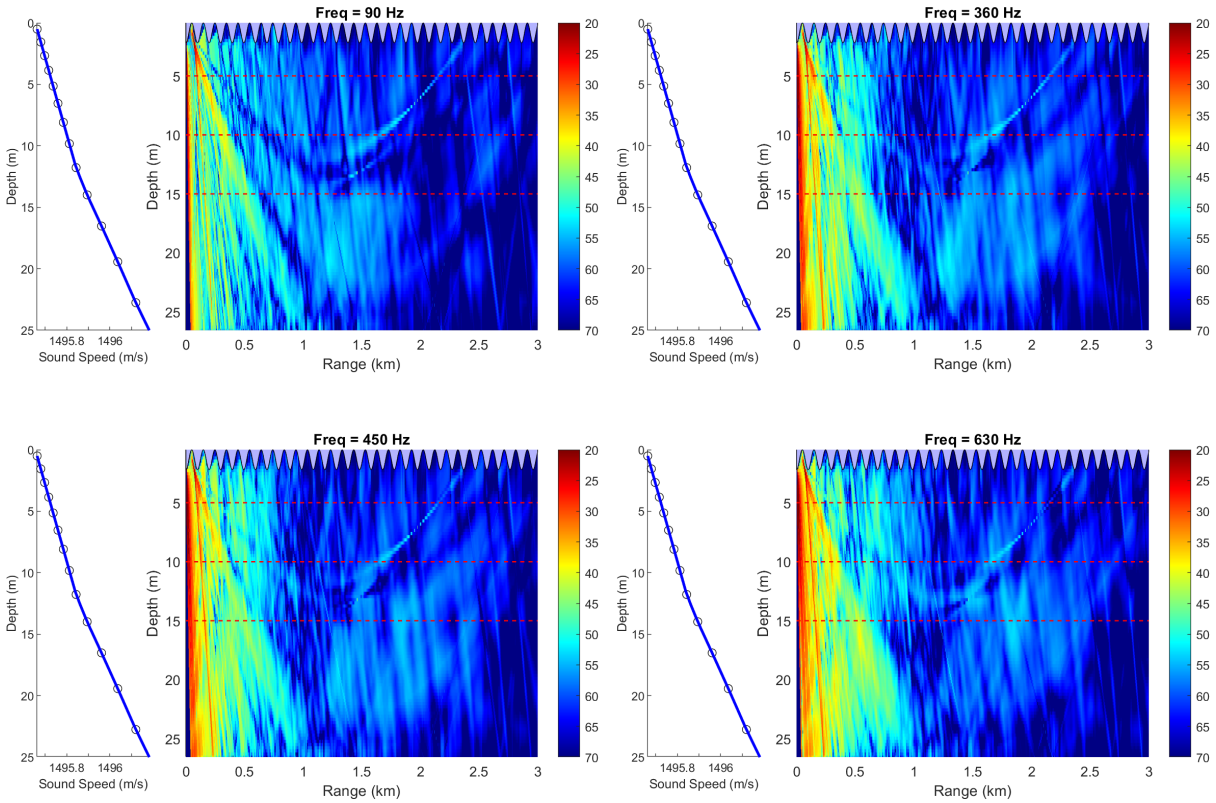

Figure 5.24: Propagation modelling of the dominant frequency of 90 Hz and its harmonics at the FINO1 location, with source depths of 5-20 meters. The colour bar is showing transmission loss [dB]. Left of the propagation panels are the corresponding sound speed profile. The red dashed lines mark the depths of 5, 10 and 15 meters.

From the BELLHOP model, we have information about transmission loss for every depth and range we have modelled for. This allows us to study transmission loss at a certain location, as well as looking at slices of transmission loss for both depth and range. The red dashed lines in Figure 5.24 mark depths of 5, 10 and 15 meters. Further, we will look at how transmission loss changes for different depths, as well as for the various frequency at a constant depth.

From Radecke and Benesch (2012), it is explained that a simple equation of transmission loss in the North Sea can be expressed as:

$$TL = 15 \cdot log(r), \tag{5.1}$$

where r is the sound propagation distance in meters. This equation is not following a cylindrical or spherical geometric loss equation, but something in between. Another adapted approximation for the North Sea and the Alpha Ventus location is:

$$TL = \left[10 + 2 \cdot \log(f) + \left(2,5 \cdot 10^{-8} \cdot f + 2,0 \cdot 10^{-5}\right) r\right] \cdot \log(r), \tag{5.2}$$

where r is the sound propagation distance in meters and f is the frequency in Hz.

As a theoretical expression of transmission loss, we also have the equations presented in Section 2.3.3, where we can use for instance Equation (2.12) for cylindrical spherical loss together with the attenuation from seawater given by Equation (2.15).

In Figure 5.25, we consider transmission loss depth slices of a 90 Hz frequency. The transmission loss equations mentioned above are displayed in the same figure for comparison. From the figure we can observe that the transmission loss differs depending on which depth we consider.

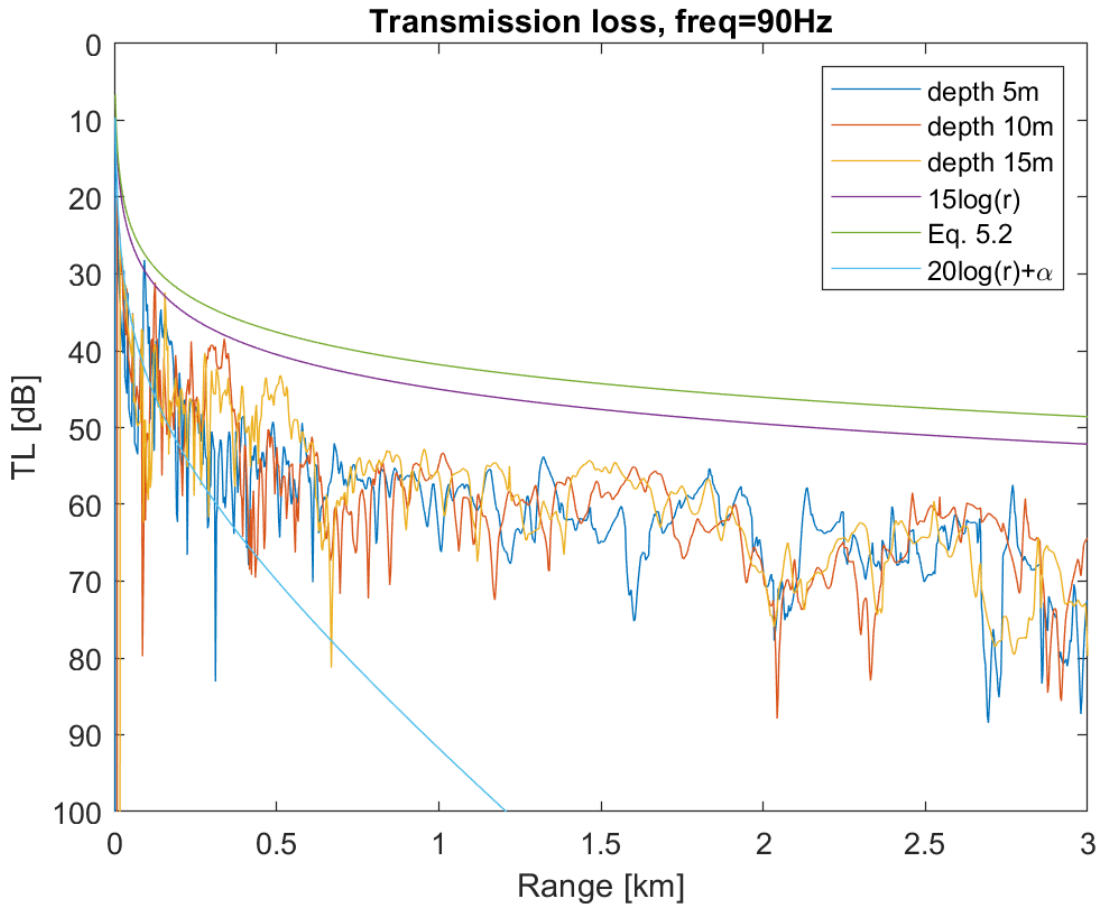

Figure 5.25: Transmission loss of a 90 Hz source frequency at slices of different depths, plotted together with theoretical values for comparison.

Having knowledge about how frequencies will propagate in different conditions is very important because sound can travel very far in certain circumstances, something we should consider when addressing turbine induced noise. From Figure 5.25 we can observe that the BELLHOP transmission loss estimations are somewhere in between the values of the theoretical approximations. Equation (5.1) is a very simple approximation that doesn't account for the attenuation of different frequencies. Equation (5.2) is frequency-dependent, but in this case, it behaves pretty similarly. They both underestimate the transmission loss compared to BELLHOP, but follow a similar shape. The spherical spreading together with the frequency-dependent attenuation from seawater overestimates the transmission loss after a couple of hundred meters. None of these theoretical values accounts for wave influence, something we accounted for in the BELLHOP modelling.

In Figure 5.26, we see how the various frequencies develop with range, at a fixed depth of 15 meters. From the theory presented in Section 2.3.3, we studied that the attenuation from seawater increases for higher frequencies, making the transmission loss greater. In our case, all frequencies are low, and at such a short-range this theory is not that noticeable. However, we can still see, together with Figure 5.24 that the propagations of the frequencies are different. Compared to the simplified approximation of Equation (5.1), the transmission losses calculated by BELLHOP are greater for all these frequencies.

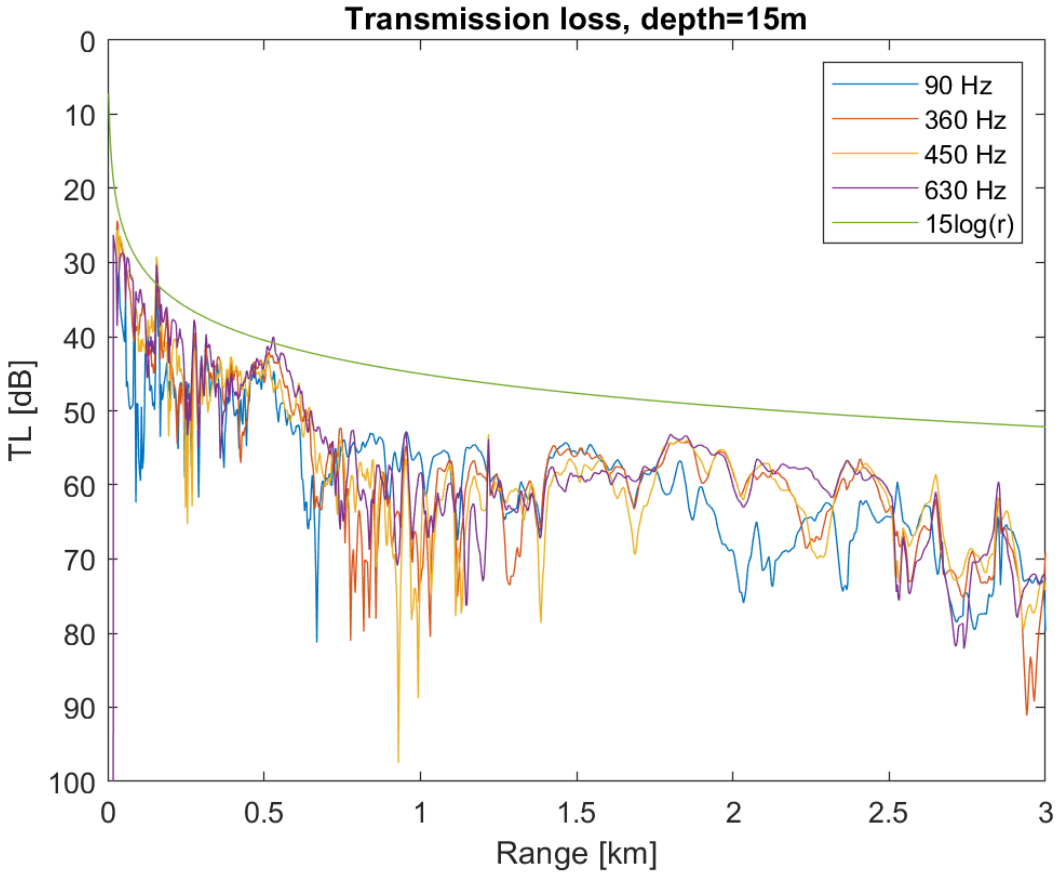

Figure 5.26: The transmission loss of various frequencies at a depth of 15m, plotted together with a theoretical value for comparison.

The hydrophone we obtained data from was mounted on a tripod of 3 meters in height. Since the seabed is of approximately 27 meters depth we assume that the receiver depth is then 24 meters. From the shade file generated by BELLHOP we extract the transmission loss for the receiver depth at range of 450 meters away. This gave a transmission loss of **55.12 dB** for the 15th of November.

In Table 5.7, we see the calculated transmission loss values for a signal of 90 Hz at a range of 450 meters, using these equations.

Table 5.7: Transmission loss calculated using different approximations, as well as the BELLHOP modelling output. This is for the 15th of November 2010, at the hydrophone location.

TL approximation	**TL [dB]**
$15log(r)$	39.80
Eq. (5.2)	36.93
$20log(r) + \alpha r_{km}$	67.35
BELLHOP	55.12

As we can see from the table, the results are as expected after studying the transmission loss slice in Figure 5.25. The theoretical spreading laws don't account for stratification in the ocean. This stratification is important for how the sound propagates. BELLHOP accounts for this stratification which we gave as an input file. Another thing to take note of is that the BELLHOP transmission loss function has a lot of fluctuations throughout the range. Depending on our location of interest, the calculated transmission loss could be at a peak of these fluctuations, potentially giving us both small and large values depending on the location. The most important result is, however, that the amount of transmission loss at our location of interest is highly determined by the environment, as we can see from the modelled output.

Measurements throughout 2011

Further, we also did BELLHOP for a longer time period in 2011. That is, every 15th of each month in 2011 for the FINO1 location. The oceanic information downloaded from CMEMS has daily averaged profiles of temperature and salinity. We also accounted for wave conditions based on NORA3 data at noon for each day we modelled. As with the previous modelling we also chose a source frequency of 90 Hz. The source depths are still 5m, 10m, 15m and 20m. The results of the propagation model are shown in Figure 5.27.

We see that the frequency propagates differently depending on which month we model for. This is because the ocean environment is very important for how sound propagates. From the environmental information about temperature and salinity, we calculated the sound speed in the ocean. This is displayed on the left of each panel in Figure 5.27. From Snell's law (Equation (2.10) in Section 2.3) we know that the rays will bend towards minimal sound speed. How the sound speed profile looks depends on the season, as the temperature changes throughout the year.

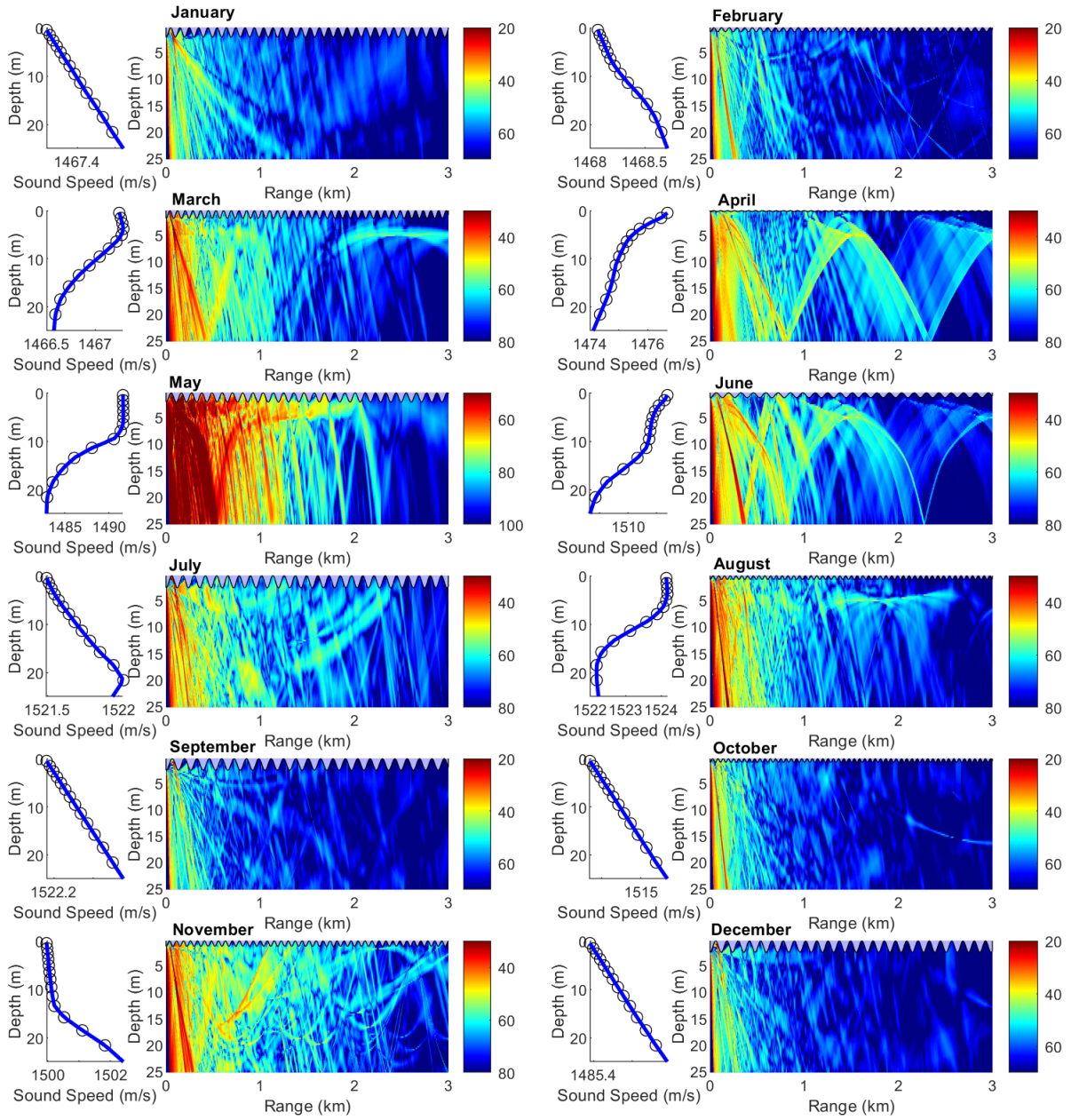

Figure 5.27: BELLHOP propagation model FINO1 area of 90 Hz. The colour bar is showing transmission loss [dB]. We have modelled for the 15th of each month in 2011. Besides the propagation panel is the corresponding sound speed profile.

From the left panels of each displayed propagation, we see that the sound speed profile has its minimum values at the top for some months and on the bottom for other months. This corresponds to the modelled propagation in Figure 5.27, where we see that the rays sometimes stay closer to the surface, and in other months the rays propagate down to the bottom. The waves at the surface also influenced the propagation, and the modelled output would be slightly different if this had not been accounted for.

From the model, we also calculated the transmission loss at the same location (24 meters depth, 450 meters range). The result of the transmission loss is displayed in Figure 5.28. We plotted the transmission loss against wind and wave, in addition to a time series. This was to see if there was any immediate correlation. The correlation coefficients were -0.74 and -0.75 for wind and wave respectively. Based on these selected measurements, the transmission loss against wind speed and wave height are negatively correlated, meaning that the transmission loss decreases with increasing wind and wave. This does not correspond to the theory that waves can attenuate sound. However, this random selection of measurements does not provide an ideal baseline for such a study. In addition to that, the ocean salinity and temperature profiles are averaged daily and did therefore not correspond to the exact profile for the same time as the wind and wave data. The calculated transmission loss is extracted from a location close to the bottom because this is the point where our hydrophone data is from. These wind and wave interactions on sound propagation and transmission loss are more interesting closer to the surface.

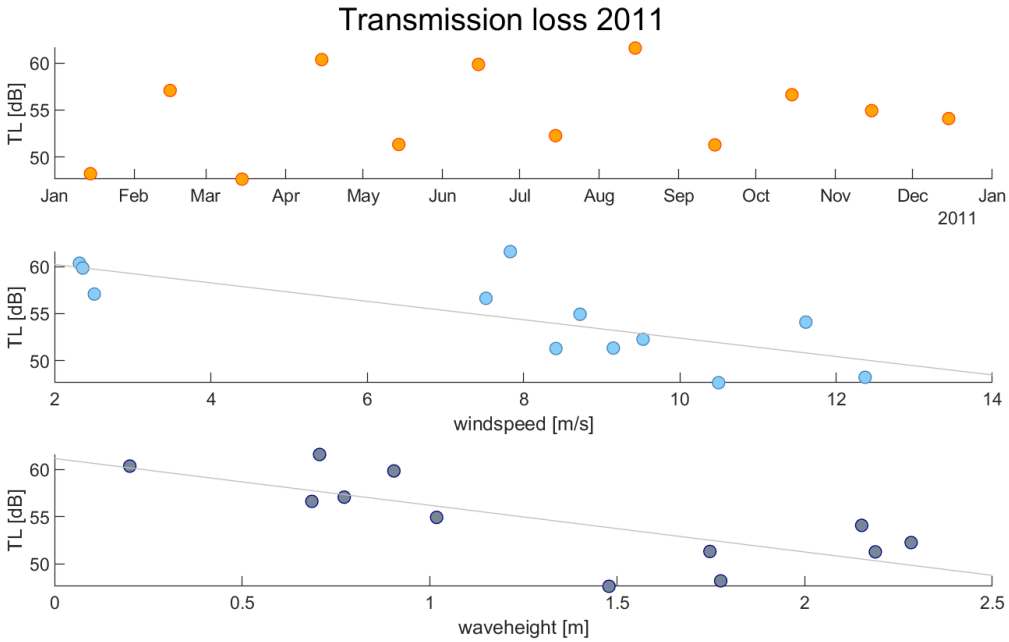

Figure 5.28: Transmission loss [dB] from BELLHOP at the FINO1 hydrophone location. Top panel is a time series, and the next two panels display transmission loss against wind speed and wave height respectively. The grey line is a linear fit of the scattered data.

10-day Period during November 2010

For the continuous 10-day period in November 2010, the results of the propagation's of the 90 Hz source frequency are shown in Figure 5.29.

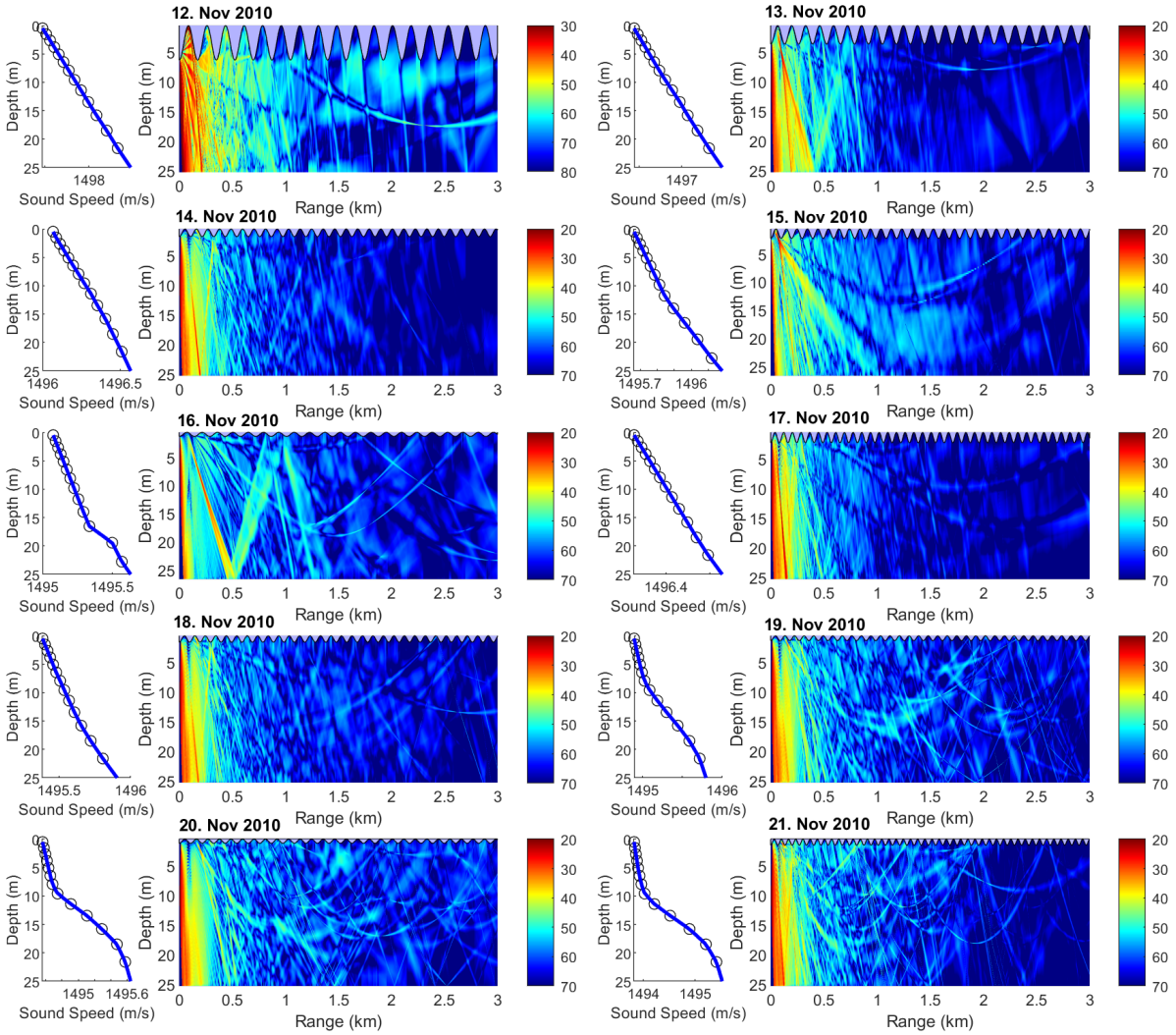

Figure 5.29: BELLHOP propagation model for 12th-21st of November 2010. Sound speed profile is shown on the left panel, and the propagation of a source frequency 90 Hz is shown besides it.

The sound speed profiles does not change much since we only study 10 days, but we still see difference in the way the acoustic signal is propagating throughout the investigated time period. This indicates that the altimetry has affected the propagation pattern. If we look at the colour bar for the 12th of November, we see that the bar limits are higher than for the other plots. This suggest that the overall transmission loss is higher for this event, and as we saw in Section 5.1.1 we had strong forcing conditions at this date.

To further study this relationship, we have plotted the transmission loss against the wind and wave conditions. The calculated transmission loss is also here from the location of the hydrophone (24 meters of depth, 450 meters of range). The results are shown in Figure 5.30.

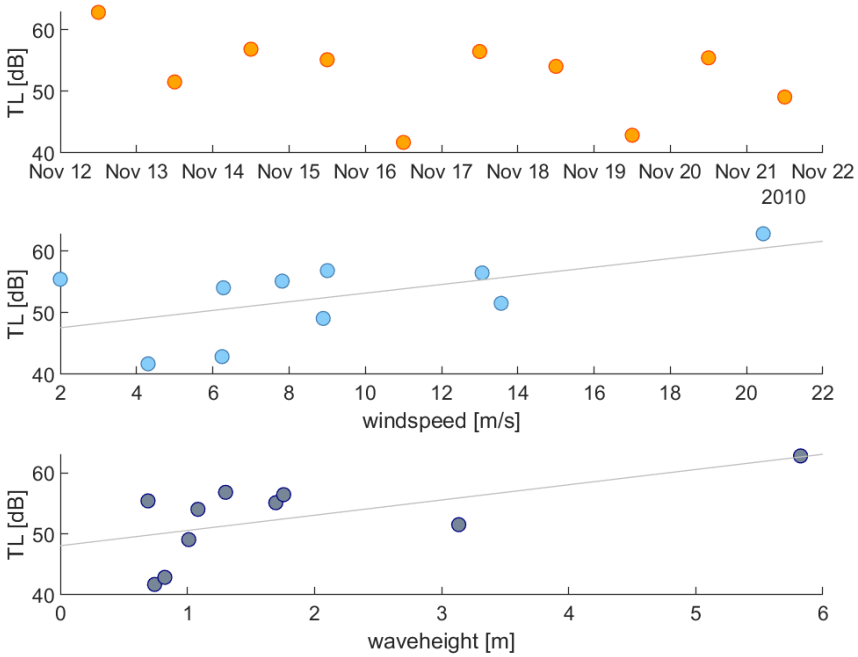

Figure 5.30: Transmission loss [dB] from BELLHOP at the FINO1 hydrophone location. Top panel is a time series, and the two panels below display transmission loss against wind speed and wave height respectively. The grey line is a linear fit of the scattered data.

From Figure 5.30, we see that there is a positive relationship between sound pressure levels and forcing conditions, as the sound pressure levels increase as the wind and wave conditions get stronger. The correlation coefficients for sound pressure levels and wind and wave conditions are 0.58 and 0.61 respectively. The largest correlation is thereby found between sound pressure level and wave height. This corresponds well with the Wenz-curves from Figure 1.2 in Section 1.2, and in this case we got results that were as expected. If we compare this result to the result for the long 2011 series in Figure 5.28, we observe that the results are very different. This is most likely due to the fact that the longer series from 2011 was not continuous and had a random selection of measurements. This stress the fact that detailed studies are important for obtaining good an reliable results. Since the transmission loss is greater, it is natural to assume that even the low frequency turbine induced noise will not propagate very long when the forcing conditions are high, given that the turbine is operation in those conditions.

Extreme Events

As a last part of the analysis of the FINO1 location, we also did BELLHOP for the selected extreme events. The results are shown in Figure 5.31 for the extreme events of 2010 and 2011.

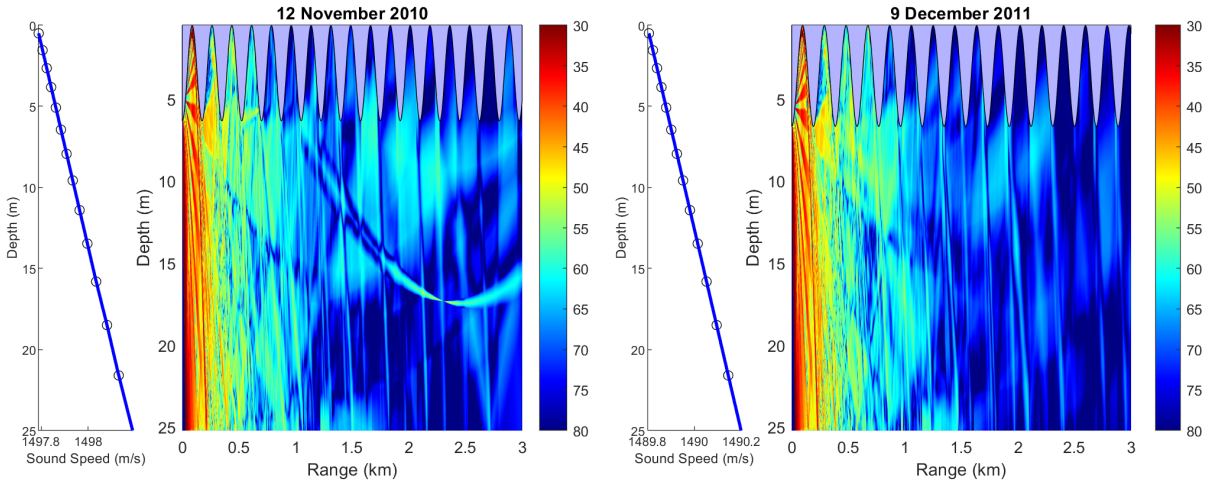

Figure 5.31: BELLHOP propagation model for 12th of November 2010 (left) and 9th of December 2011 (right). Sound speed profile is shown on the left panel, and the propagation of a source frequency 90 Hz is shown besides it.

The propagation pattern looks somewhat like what we would expect for these months, compared to the propagation pattern in Figure 5.27. However, the transmission losses are higher for these extreme events. For the 12th of November 2010, the transmission loss by the hydrophone was **62.81 dB**. For the 9th of December, the transmission loss was **64.12 dB**. This indicates that even if we assume that our turbine is operating, a lot of the turbine noise will be attenuated by the waves caused by these extreme forcing conditions.

From the sound pressure level results at the same time periods, we saw the overall sound pressure levels were high. Even when the turbine was not operating, we still experienced a high level of sound. This indicates that wind and waves contribute to higher underwater noise. Even in the presence of operational noise induced by the turbines, this type of noise may not be the biggest contributor.

5.2 Sound Propagation at Hywind Tampen Area

For this study, we selected an extreme event by finding the peak values of wind speed and wave height from our NORA3 data set for Tampen location in 2016. The peaks found corresponded to the extreme weather "Tor" in January 2016. The full 2016 time series is shown in Figure 5.32, with red lines a few days around this event. On the night of the 29th of January 2016, a low pressure developed north of the Atlantic Ocean into the south of the Norwegian Sea. Wind measurements showed storms and hurricanes along the coast, as well as strong wind gusts on land from Hordaland to Helgeland. By the 30th of January it was no longer extreme wind as the low pressure weakened (MET (2016)).

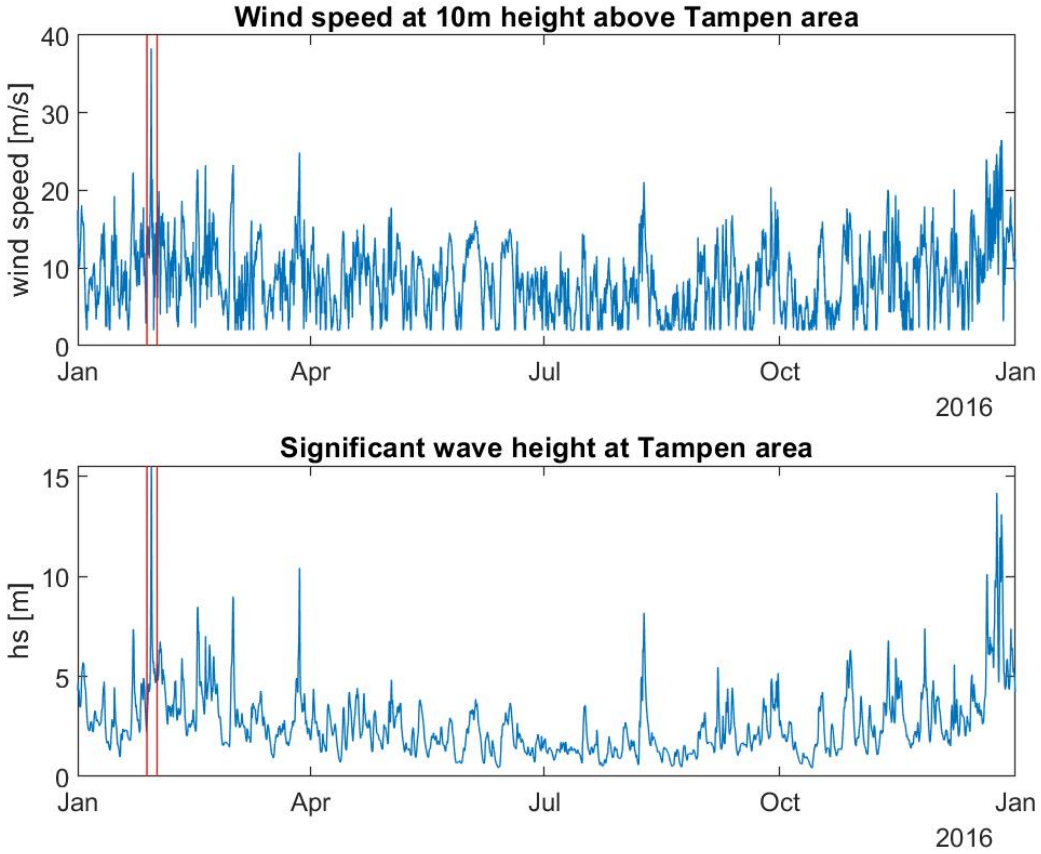

Figure 5.32: NORA3 data of wind speed and significant wave height for the year of 2016 at the Hywind Tampen location. The red lines show the period 28-31. Jan 2016, a few days around the extreme weather "Tor".

Further, we modelled for a few days around this extreme event. For the environmental input we also here used corresponding data from CMEMS to calculate the sound speed profile in each case. In the following cases, we have also accounted for the bathymetry of the location. However, for the short propagation distance of 3 kilometres, it could also be considered constant. From the noise assessment by Weissenbergen (2019), a prominent tone of 25 Hz where assumed to be excited by the floating turbines. Therefore we have modelled for this frequency to propagate, and the source depths are set to 10, 15, 20 and 30 meters.

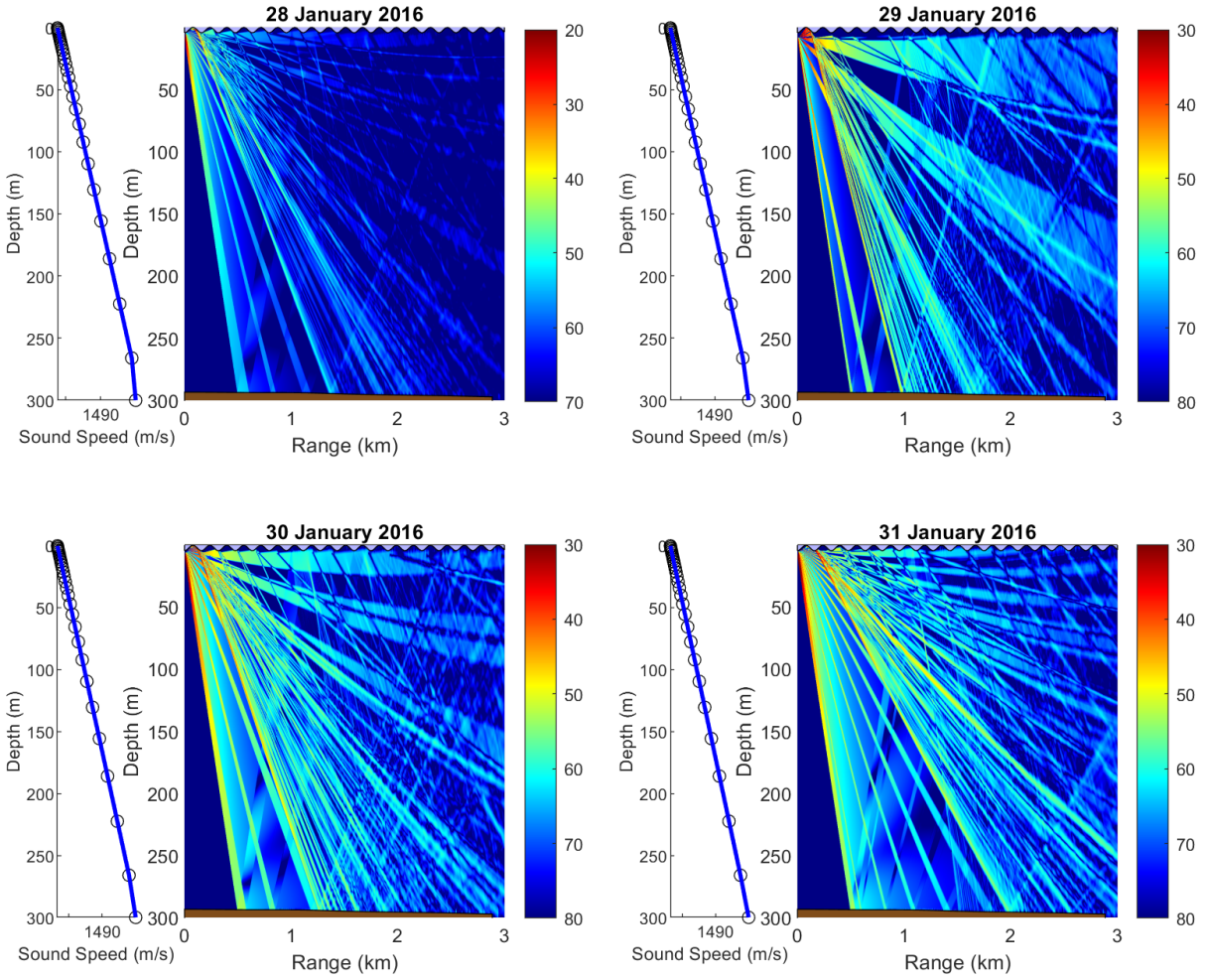

Figure 5.33: Modelled propagation of a source frequency equal to 25 Hz. Modelled for 28-31th of January 2016 around the extreme weather Tor. Left of the propagation panel is the corresponding sound speed profile.

At a first glance of Figure 5.33, we can see that the sound rays are being spread out from the source differently throughout the extreme event. In all cases, we can see that the surface waves are reflecting the sound waves. From Snell's law, we would expect the sound waves to propagate along the surface since the sound speed profile is at its minimum at the surface. Since we only model for a range of 3 kilometres, this is not very clear, but at a longer distance, this will be visible.

If we look closely at the surface, we can see that some of the sound rays propagate towards the surface and are being reflected town towards the bottom. When we modelled for complete still conditions (not displayed here) the sound waves had a more even propagation in shade, whereas we, in this case, observe a more "streaky" propagation from the source. Together with the reflections from the surface, it is clear that waves affect how acoustic signals propagate in the ocean. Since wind turbines will operate in various forcing conditions, this is important to be aware of.

Further, we extracted the modelled transmission loss for two locations. We stayed closer to the surface, at a depth of 20 meters and at the ranges of 500 meters and 1 kilometre. The results are presented in Table 5.8.

Table 5.8: Transmission loss at depth 20 meters, during the extreme weather "Tor" in 2016.

Date/Range	**500 meters**	**1 kilometer**
28 Jan 2016	57.73	46.86
29 Jan 2016	70.22	65.17
30 Jan 2016	46.23	56.21
31 Jan 2016	58.92	46.86

From Table 5.8, we see that the highest transmission losses are found on the 29th of January, the day corresponding to the highest wave heights and wind speeds. In Figure 5.34 we have plotted the transmission losses against the wind and wave conditions. The wind and wave data are extracted from noon each day, and do not correspond to the highest forcing in the period. In this case, the data are very correlated, especially the wave height compared to transmission loss at depth of 20 meters and a range of 1 kilometre. Studying correlation for such a few data points doesn't necessarily indicate a relation, but for these data, we see clearly that the transmission loss increases as the forcing conditions get stronger.

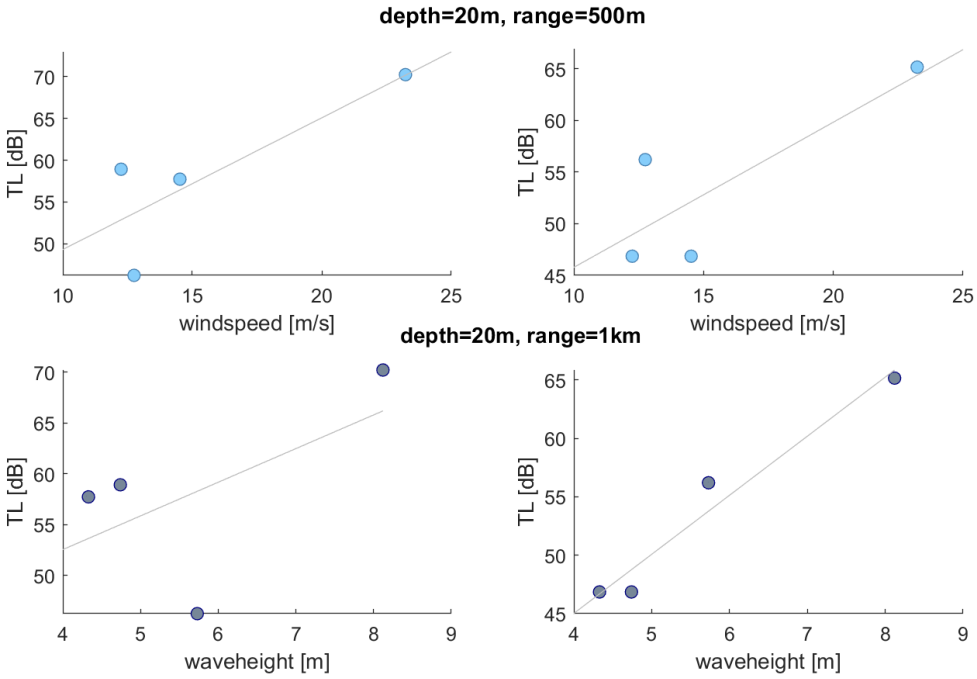

Figure 5.34: Transmission loss calculated at a depth of 20 meters, plotted against wind and wave data during "Tor" extreme weather. The top panels are transmission loss at a range of 500 meters, and the bottom panels correspond to the transmission loss at 1 kilometre. The grey lines are a linear fit of the scattered data points.

It is important to state that on the days of the extreme forcing conditions induced by "Tor", the wind speed exceeded the operational limit for most offshore turbines, and this particular signal would potentially not be present. However, it is still interesting to look at how these low frequencies will behave under different conditions to increase the overall understanding. As technology develops, the cut-off speed for wind turbines might increase and in that case, such a study would still be highly relevant.

Since floating offshore wind is still a new technology, there are few studies on noise generation from these turbines, and in general, there are several things to address and consider as this technology expands in the energy market. One important finding from Betke (2014) was that the operating noise could be assigned to the turbines with tripod foundations, and not to the turbines with jacket foundations. One reason could be that the structures conduct the machinery vibrations differently, and that the jacket foundations do it less efficiently in comparison to the tripod foundations. Another reason could be the difference in the machinery of the turbines, as the type of generator and gearbox excite different frequencies. As offshore wind technology develops it is not straightforward how these changes will correspond to the changes in sound generation and propagation. As already discussed in Section 2.2.2, the mechanical resonance is likely to change with the size of the tower and choice of foundation and gearbox technology. Hywind Tampen will consist of floating turbines and the foundations are based on spar buoy design. The foundations discussed in this section are shown in Figure 5.35.

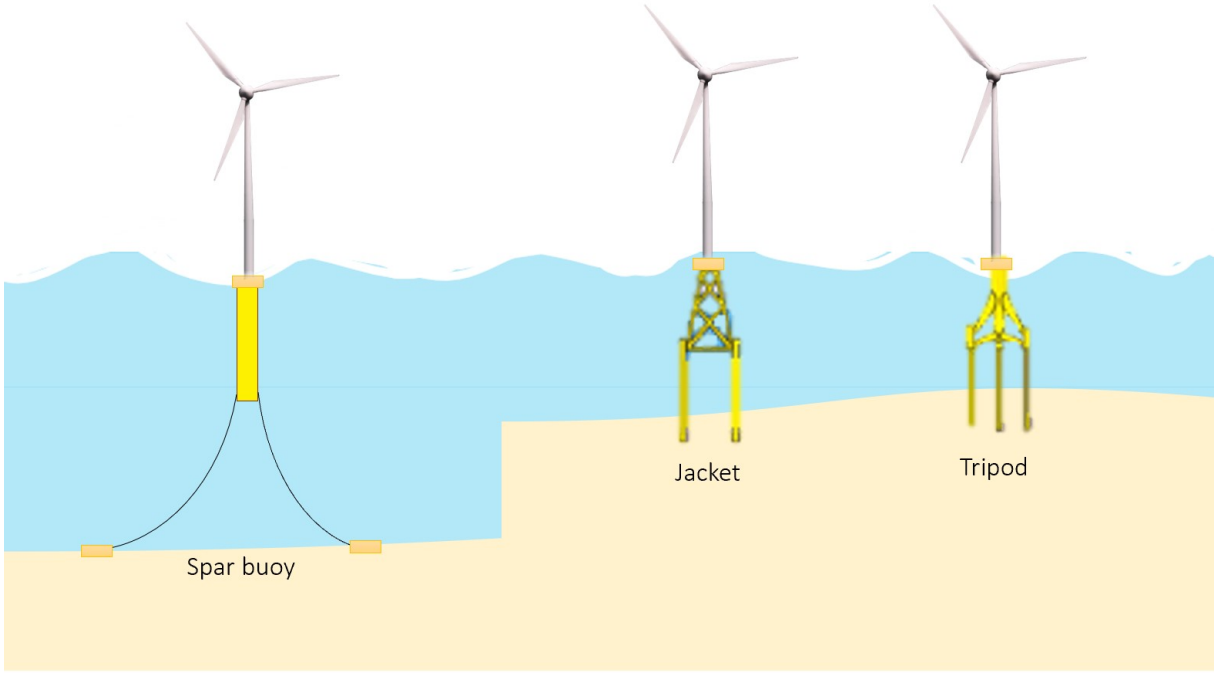

Figure 5.35: Different foundations for offshore wind, here showing a tripod and jacket foundations for bottom-fixed offshore wind turbines, as well as the spar buoy used for Hywind floating wind turbines.

Even with newer and more quiet gearbox technology, floating offshore wind still raises important questions regarding noise generation. This is because the turbines' mooring lines, in addition to the floaters, could be a source of producing noise. The sound characterization report for Hywind Scotland by Burns et al. (2022), revealed a significant amount of mooring noise, however it was less impulsive that the mooring noises from Hywind Demo. The floating turbines are anchored, and depending on how this anchoring is performed, noise from drilling during the construction of the wind farms could also be a concern for the floating wind farms. There will also be increased ship traffic in the construction of floating offshore wind farms and when conducting service on the turbines during their operational phase, just as with the bottom-fixed farms. On the other hand, the general ship traffic noise in the area might be reduced as commercial shipping routes may deviate from the wind farm area.

Chapter 6

Further Discussion

6.1 Importance of Noise in the Licensing of Offshore Wind Farms

How the strategic decisions for the development of offshore wind farms are made, differs from one country to another. So does the regulatory framework. The geographical location of the sea in which the wind farms are installed, determines which legislative framework that applies. As an example, states such as the UK, Denmark and Germany all apply national regulations to activities in their exclusive economic zone (DNV (2021)).

Close to the shore, within the range of the baseline, the municipalities are responsible for making coastal zone plans on how areas are going to be used for which activities. Offshore wind production within the baseline follow the provisions of the Energy Act (Energiloven). In the Norwegian Economic Zone (waters from the baseline and 200 nautical miles off shore) there exists quite a different governmental regime compared to the approval of activities in the coastal zone. The licensing process under the Offshore Energy Act will be explained below. Outside the range of the Economic Zone is the High Sea where no state has jurisdiction. The United Nations has made a very important convention regarding the use of the high sea; the United Nations Convention on the Law of the Sea (UNCLOS, UN (1982)). So far, the question of using the high sea for energy production and installing wind turbines in international territories has not been addressed in the UNCLOS.

Schütz (2018) points out in her paper that "Regarding the geographical scope of the EEA agreement, Norway has taken the position that it only applies on Norwegian "territory", which means that the agreement is not relevant to legislation primarily meant for areas outside the territorial border 12 nautical miles beyond the baseline". When comparing the licence system under the Offshore Energy Act with decisions made in the coastal zone, we see that it is the Ministry of Oil and Energy that has the power to decide who to give licence and on which conditions. This secures a more holistic approach in the decision-making process compared to activities on land or in the coastal zone where decisions are made by municipalities. It might be rather challenging when activities are situated in several municipalities or to take due consideration to the interest of fisheries or the environment not limited only to one municipality.

Offshore wind in Norway is very new, and the regulatory framework for offshore wind energy in Norway is still under development. In Norway, the main framework for offshore renewable energy production is defined by the Offshore Energy Act (Havenergilova). The act is applicable to Norwegian sea territory outside the baseline and on the continental shelf (§2-1(2)). The first step when developing offshore wind parks is a strategic impact analysis made by the Norwegian Water Resources and Energy Directorate (NVE). The next step is the decision of which areas to open for offshore wind production. In 2020 the government decided to open Sørlige NordsjøII for bottom-fixed or floating wind turbines, and Utsira Nord for floating wind turbines. The provisions regarding the strategic and environmental impact assessments under the Offshore Energy Act are based on EU law, but also on the so-called OSPAR Convention (OSPAR convention (1992)) which aims to protect the marine environment in the North-East Atlantic Ocean. The authorities must consider the five main phases in the lifespan of an offshore wind park: location, licensing, surveillance, construction and operation, and decommissioning.

In principle, the right to utilize renewable offshore energy resources belongs to the Norwegian State (§1-3). A license by the Ministry is required to build, own or operate production facilities; in practice for the production of offshore renewable energy (§3-1). The Ministry has given a regulation and a guide regarding further details about the licensing process (Havenergilovforskrifta and " *Veileder for arealtildeling, konsesjonsprosess og søknader for vindkraft til havs*"). The content of the impact assessment is described in further detail in §6 of the regulation and the guide. Among other things, it states that the impact of the energy plant on the environment, such as fish and ecosystems, must be described in the impact assessment. A noise assessment would therefore be natural to include in this part of the licensing process.

Since we have considered Hywind Tampen as part of this study, it is interesting to look at the importance of noise in the licensing of this project. As mentioned earlier, Hywind Tampen floating wind farm will provide electricity to the two oil and gas fields nearby. It is therefore considered as "an extension" of these existing installations and regulated under the Petroleum Safety Authority's regulations for petroleum activities (Petroleumslova, Petroleumsforskrifta). The provisions concerning environmental impact are quite similar to those for the Offshore Energy Act.

A section about noise and marine mammals can be found in the summary of consultation responses to the impact assessment for the Hywind Tampen project (Equinor (2019)). Here, the Norwegian Environment Agency emphasized that there was a strong focus on noise and marine mammals in terms of both possible impacts on communication, food search and behavioural changes. They consider the Marine Mammal Noise Exposure Criteria by Southall et al. (2019) in Aquatic Mammals as an "international standard" for determining possible noise impacts. Equinor's noise impact assessment for Hywind Tampen (Weissenbergen (2019)) used criteria prepared by NOAA (2018), which are similar to the ones carried out by Southall et al. (2019). In the assessment, it was addressed that there would be continuous sound from the operating turbines. However, it was considered unlikely that animals would stay within a short enough distance for a long enough time to exceed the threshold limits for injury. The overall risk for marine mammals from sound from Hywind Tampen was evaluated as non-existing.

6.2 Marine Environment and Recommendations

The book Ecological Research at the Offshore Windfarm Alpha Ventus by Betke (2014) targets many important aspects of challenges and perspectives regarding offshore wind farms. Amongst them are wind turbine sound and its effects on marine mammals and fish. Construction noise is of great concern as it produces a strong and impulsive sound that can be harmful to species nearby. Production noise is a lot less intense, but since it is permanent it also raises questions about impacts in terms of both injury and behaviour changes on marine mammals and fish.

By German Law, the pile driving strike should not exceed a sound exposure level of 160 dB re 1 $\mu Pa^2 s$ within a 750 meters radius in order to get a licence from the Federal Maritime and Hydrographic Agency (BSH)(Müller et al. (2019)). At the Alpha Ventus Wind Farm this threshold was exceeded. Even at great distances from the pile driving, the noise level was clearly above the ambient noise even though it was a lot weaker than close to the construction. By these results, it is therefore clear that such limits are hard to reach without any form of noise mitigation measures.

The operational noise exceeded the hearing threshold for harbour porpoise, but this threshold was also surpassed by the background noise regardless of the turbines. Whether the presence of these turbines would have an impact on the behaviour of marine mammals are therefore hard to know. It revealed that the operational noise could be assigned to the tripod turbines only. The prominent tone had a frequency of 90 Hz with sound pressure levels up to 120 dB re $1\mu Pa$ at a distance of 100 meters from the turbine. These values varied slightly depending on the environmental conditions.

In Norway, The Institute of Marine Research (IMR) provides advice for all operations at sea that involves the use of sound sources that can affect marine ecosystems. These operations include scientific research, seismic surveys, petroleum activities and the operation of offshore wind farms. In regards to the licensing of offshore wind farms, IMR aims to have an advisory role, based on The Norwegian Water Resources and Energy Directorate's (NVE) request for advice about potential effects on the marine environment (Sivle et al. (2022)).

In conjunction with the expected growth of offshore wind, a report was made by IMR that summarized the current knowledge and potential impacts of wind farms on the marine ecosystem (Sivle et al. (2022)). Potential effects include effects from new structures, electromagnetism from cables and off-course the sound produced from turbines during both construction and operation. Physical changes are also included and in addition to increased ambient noise levels, changes in ocean currents and patterns of up-welling and down-welling are also discussed, something we also studied in Section 2.1.2.

Regarding the effects, they are not all negative. Several species are attracted to the bottom-fixed farms. The submerged part of the turbine can act as an artificial reef where species establish themselves. As a response from the new reef, this can also alter the surrounding seabed by increasing food ability (Degraer et al. (2020)). When considering noise from the turbines, it is important to consider every phase of the turbine's life cycle. In this thesis, we have considered operational sound for our study, which is important as noise will be emitted for a long time period. The construction phase is also important because actions such as pile driving can emit a lot of sounds which could be damaging even though it is for a shorter amount of time.

Hawkins and Popper (2016) considered multiple problems of assessing the impact on marine species. An important issue that has been overlooked when assessing these impacts is particle motion. In addition to the actual sound pressure, a lot of marine species are sensitive to the particle movement that follows. It can be challenging to measure this particle motion, and few environmental assessments have taken particle motion into consideration. Research within this concern should therefore have greater importance in the future.

In the IMR report, they also present recommendations regarding the implementation of offshore wind farms in Norwegian water. However, they point out the lack of knowledge about the environmental effects of offshore wind farms, and therefore expect that the advice will change in the coming years as more knowledge becomes available. de Jong et al. (2020) concludes that with the state of current knowledge it is impossible to predict the total impact of offshore wind farms on underwater life. Controlled experiments and field studies are stressed as ways to close these knowledge gaps.

As it is urgent to obtain comprehensive research on the environmental effects of offshore wind farms, IMR will investigate the Hywind Tampen area to get a good overview before the wind farm starts operating. Marin scientists will investigate which fish species are present in the area, as well as to what extent. With this documentation they aim to look at possible environmental effects by comparing studies before and after the operation phase is starting (Hommedal (2022)).

6.3 Stakeholders' Acceptance of Offshore Wind Farms

As the ocean is a huge resource, many different stakeholders are competing over the same areas. Examples of such stakeholders are fisheries and aquaculture, petroleum activities, marine transport and naval forces. As offshore renewable energy is expected to expand in the coming years, management plans aiming to ensure sustainable use of this resource in harmony and coexistence between all interested parties are crucial.

Politics are an important driver for the development of offshore wind energy projects. Stakeholders' opinions and acceptance might influence decisions about this prevalence. In the case of scepticism and lack of acceptance, the effectiveness of licensing offshore energy projects might diminish. Increasing dialogue and knowledge between all interested stakeholders are therefore important for the development of offshore renewable energy.

Offshore wind turbines increase in size and prevalence, and spacing between turbines makes them take up larger marine areas. In addition to that, sub sea cables and mooring lines limit the possibilities to do trawling and other traditional marine activities in the area of a wind farm. Shipping vessels may not enter the farm, and naval forces firing ranges cannot be combined with a wind farm (Norwegian Government (2009)). This makes area up-take by offshore wind farms one of the big conflicts limiting the acceptance by other stakeholders. Turbine noise may therefore not be the biggest concern for all interested parties, but it will still contribute to the overall acceptance of offshore energy projects.

One stakeholder that would be interested in our field of study is fisheries. There are many drivers for conflict between fisheries and offshore wind energy farms. As already mentioned, limited possibilities to do fishing inside a wind farm is the biggest conflict, however, another main concern are in regards to the potential negative impact wind turbines have on fish and the marine environment. For fisheries, marine areas are not only of big economic value, but also of social value as it has long traditions and are a cultural identity for many countries, including Norway. Environmental assessments covering the overall impacts, seabed mapping and consequences for important fishing areas would therefore be of interest for fisheries. As already discussed, The Institute of Marine Research (IMR) stresses the importance of comprehensive research investments on this topic, something that would potentially increase the acceptance from the fisheries.

To take advantage of the areas more efficiently, offshore power may be combined with other energy concepts or stakeholders activities as options. An example of such synergies is to implement the production of human food or animal feed in the area of an offshore wind farm (Buck (2007)). The integration of aquaculture may pose numerous positive benefits to that industry, as the quality of the water far offshore is better for the aquaculture's environment, and the offshore turbines can act as artificial reefs (WWF (2014)). In such a context, where aquaculture is placed in so close vicinity to wind turbines, it is clear that the determination of turbine sound levels and their impact on marine ecosystems should be comprehensively addressed and clarified.

Chapter 7

Conclusion

In this study, we have performed several processing methods for analysing the available hydrophone data. The acoustic data was given by RAVE, a research initiative for the Alpha Ventus wind farm in Germany. The available data was from the years 2010 and 2011 by a hydrophone close to the FINO1 offshore platform.

The modelled results showed that the environmental conditions alter the propagation and transmission of acoustic signals. Oceanic parameters such as temperature and salinity determine the sound speed profile which, by Snell's law, has a huge influence on sound propagation. The presence of surface waves induced by the strong forcing conditions also alters the propagation and transmission loss of acoustic signals.

Not all results confirmed a good agreement with theory. However, the more detailed and continuous measurements/modellings gave expected results; that the sound pressure levels and the transmission loss increased with the presence of wind forcing and strong waves at the surface.

The floating wind farm Hywind Tampen was one of the locations of interest. For this study site, we didn't have observational data since the wind farm is not operational yet. The processing tools used on the FINO1 observational acoustic data, as well as the propagation model, will therefore be useful applications in the future that could contribute to more research within this field of study.

Throughout this study, we have also discussed the importance of noise in the legal framework for offshore wind. It is clear that determining environmental impact is important in order to get a license for constructing new wind farms in the ocean. How the turbine induced noise will affect fish and marine mammals is a crucial part of this assessment. When prominent tones and sound pressure levels from the wind turbines are determined, as well as how they behave in terms of propagation, it is possible to compare this to the hearing and injury thresholds for marine species in order to assess the overall impact.

As the ocean is a huge resource, many different stakeholders are competing over the same areas. Fisheries are one of these stakeholders, and it is important to assess the influence a wind farm will have on other parties in order to obtain a balance suitable for everyone. Increasing research on problems that both people and stakeholders are interested in can help with the overall understanding and acceptance of offshore wind farms.

Chapter 8

Future Work

The processing tools performed on our available hydrophone data are relevant for any similar studies in the future. When Hywind Tampen offshore wind farm starts its operation it would be of great interest to process any available sound pressure data from the turbines. Since these turbines have floating foundations, doing studies like this on Hywind Tampen could close some big knowledge gaps as discussed in previous sections.

Bibliography

Environmental impacts of offshore wind power production in the north sea, 2014. URL https://www.wwf.no/assets/attachments/84-wwf_a4_report___havvindrapport.pdf.

Mostafa Bakhoday-Paskyabi. *Offshore wind farm wake effect on stratification and coastal upwelling*, volume 80. Elsevier B.V., 2015. doi: 10.1016/j.egypro.2015.11.415. URL http://dx.doi.org/10.1016/j.egypro.2015.11.415.

F. Bertucci, M. Breitzke, E. Ciappiand, A. Cresci, E. Debusschere, C. Ducatel, T. Folegot, C. Juretzek, F-P. Lam, J. OâBrien, and M.E. dos Santos. Addressing underwater noise in Europe: Current state of knowledge and future priorities. *Future Science Brief 7*, 7, 2021. ISSN 2593-5232. doi: 10.5281/zenodo.5534224.

Klaus Betke. *Underwater construction and operational noise at alpha ventus*, pages 171–180. Springer Fachmedien Wiesbaden, Wiesbaden, 2014. ISBN 978-3-658-02462-8. doi: 10.1007/978-3-658-02462-8_15. URL https://doi.org/10.1007/978-3-658-02462-8_15.

Klaus Betke, Manfred Glahn, and Rainer Matuschek. Underwater noise emissions from offshore wind turbines. pages 1–2, 03 2004. URL https://tethys.pnnl.gov/sites/default/files/publications/Betke-2004.pdf.

Subhamoy Bhattacharya, Domenico Lombardi, and David Muir Wood. Similitude relationships for physical modelling of monopile-supported offshore wind turbines. *International Journal of Physical Modelling in Geotechnics*, 11, 04 2011. doi: 10.1680/ijpmg.2011.11.2.58.

E. A. Bossanyi. The design of closed loop controllers for wind turbines. *Wind Energy*, 3(3): 149–163, 2000. doi: https://doi.org/10.1002/we.34. URL https://onlinelibrary.wiley.com/doi/abs/10.1002/we.34.

David L. Bradley and Richard Stern. Underwater sound and the marine mammal acoustic environment: A guide to fundamental principles, July 2008. URL https://www.mmc.gov/wp-content/uploads/sound_bklet.pdf.

Bela Hieronymus Buck. Farming in a high energy environment: potentials and constraints of sustainable offshore aquaculture in the german bight north sea, 2007. ISSN 1866-3192.

R.D.J. Burns, S.B. Martin, M.A. Wood, C.C. Wilson, C.E. Lumsden, and F. Pace. Hywind scotland floating offshore wind farm: Sound source characterisation of operational floating turbines. Technical report Version 3.0 FINAL, by JASCO Applied Sciences for Equinor Energy AS, 2022. Document 02521.

Begum Yurdanur Dagli, Yesim Tuskan, and Ümit Gökkus. Evaluation of offshore wind turbine tower dynamics with numerical analysis. *Advances in Civil Engineering*, 2018: 11, 2018. doi: https://doi.org/10.1155/2018/3054851. URL https://www.hindawi.com/journals/ace/2018/3054851/.

Karen de Jong, Henning Steen, Tonje Nesse Forland, Henning Wehde, Daniel Nyqvist, Anne Christine Utne Palm, Kjell Tormod Nilssen, Tone Falkenhaug Jon Albretsen, Martin Biuw, Lene Buhl-Mortensen, and Lise Doksæter Sivle. Potential effects of offshore wind farms on the marine environment. *Rapport fra havforskningen*, 42, 2020. ISSN 1893-4536.

Steven Degraer, Drew A. Carey, Joop W.P. Coolen, Zoë L. Hutchison, Francis Kerckhof, Bob Rumes, and Jan Vanaverbeke. Offshore wind farm artificial reefs affect ecosystem structure and functioning: A synthesis. *Oceanography*, Vol. 33, No. 4, December 2020. URL https://doi.org/10.5670/oceanog.2020.405.

DNV. Regulators and legislation for offshore wind legislation in selected countries. Report 2021-0524, Rev 1, DNV Energy Systems, 06 2021.

Dosits. Why is sound important to marine animals?, Apr 2018. URL https://dosits.org/animals/importance-of-sound/why-is-sound-important/.

Dosits. Introduction to signal levels, 2021. URL https://dosits.org/science/advanced-topics/introduction-to-signal-levels/.

Edis Osmanbasic. The future of wind turbines: Comparing direct drive and gearbox, 2020. URL https://www.engineering.com/story/the-future-of-wind-turbines-comparing-direct-drive-and-gearbox.

Energiloven. LOV-1990-06-29-50.

Equinor. Oppsummering av høringssvar til konsekvensutredning for hywind tampen prosjektet, 2019. URL https://www.equinor.com/content/dam/statoil/documents/impact-assessment/hywind-tampen/equinor-hoeringsuttalelser-til-konsekvensutredning-for-hywind-tampen.pdf. Last accessed 4 May 2022.

Equinor. Hywind tampen: the worlds first renewable power for offshore oil and gas, 2022. URL https://www.equinor.com/en/what-we-do/hywind-tampen.html.

European Comission. An EU Strategy to harness the potential of offshore renewable energy for a climate neutral future. Technical report, EUROPEAN COMISSION, Brussels, 2020.

Adrian Farcas, Paul M. Thompson, and Nathan D. Merchant. Underwater noise modelling for environmental impact assessment. *Environmental Impact Assessment Review*, 57: 114–122, 2016. ISSN 01959255. doi: 10.1016/j.eiar.2015.11.012. URL http://dx.doi.org/10.1016/j.eiar.2015.11.012.

F.H. Fisher and V.P. Simmons. Sound absorption in sea water. *The Journal of the Acoustical Society of America*, 62, 1977. doi: 10.1121/1.381574.

Havenergilova. LOV-2010-06-04-21.

Havenergilovforskrifta. FOR-2020-06-12-1192.

Anthony D. Hawkins and Arthur N. Popper. A sound approach to assessing the impact of underwater noise on marine fishes and invertebrates. *ICES Journal of Marine Science*, 74(3):635–651, 12 2016. ISSN 1054-3139. doi: 10.1093/icesjms/fsw205. URL https://doi.org/10.1093/icesjms/fsw205.

Stine Hommedal. Havvind: Hi skal kartlegge fiskebestander før utbygging, 2022. URL https://www.hi.no/hi/nyheter/2022/mars/havvind-hi-skal-kartlegge-fiskebestander-for-utbygging. [Online; Published March 24, 2022. Accessed May 9, 2022].

Roy M. Howard. *A signal theoretic introduction to random processes*. John Wiley Sons, Inc., 2016.

Finn B. Jensen, William A. Kuperman, Michael B. Porter, and Henrik Schmidt. *Computational Ocean Acoustics, Second Edition*. Springer, 2011.

Prof. Neenu Maria Jose and Dr. Alice Mathai. Study on natural frequency of offshore wind turbine in a layered soil. *International Journal of Engineering Research Technology*, 5 (5), 2018. URL https://www.irjet.net/archives/V5/i5/IRJET-V5I5270.pdf.

Lawrence E. Kinsler, Austin R. Frey, Alan B. Coppens, and James V. Sanders. *Fundamentals of Acoustics, Fourth Edition*. John Wiley Sons, Inc., 2000.

H Lindell. Utgrunden off-shore wind farmâmeasurements of underwater noise. Technical Report Report No. 11-00329-03012700, Ingemansson Technology AB, Gothenburg, Sweden, 2003.

Peter Madsen, Magnus Wahlberg, Jakob Tougaard, Klaus Lucke, and Peter Tyack. Wind turbine underwater noise and marine mammals: Implications of current knowledge and data needs. *Marine Ecology Progress Series*, 309:279–295, 03 2006. doi: 10.3354/meps309279.

MET. Ekstremverrapport — Hending: Tor 29-30. januar 2016. Technical Report METinfo nr.14, The Norwegian Meteorological Institute, Bergen, 2016.

A. Müller, C. Juretzek, and M. Boethling. Monitoring and assessment of the effectiveness of noise mitigation measures to reduce impact by percussive pile driving in german waters. part one: Noise abatement strategy, thresholds, standards, legislative and administrative actions. Technical report. Order Nr. 10036955, Bundesamt für Seeschiffahrt und Hydrographie (BSH), 2019.

Sophie L. Nedelec, James Campbell, Andrew N. Radford, Stephen D. Simpson, and Nathan D. Merchant. Particle motion: the missing link in underwater acoustic ecology. *Methods in Ecology and Evolution*, 7(7):836–842, 2016. doi: https://doi.org/10.1111/2041-210X.12544. URL https://besjournals.onlinelibrary.wiley.com/doi/abs/10.1111/2041-210X.12544.

NOAA. 2018 revisions to: Technical guidance for assessing the effects of anthropogenic sound on marine mammal hearing (version 2.0): Underwater thresholds for onset of

permanent and temporary threshold shifts. Technical Report 167 p, National Marine Fisheries Service, U.S. Dept. of Commer., NOAA. NOAA Technical Memorandum NMFS-OPR-59,, 2018.

NOAA. What is a hydrophone?, 2021. URL https://oceanservice.noaa.gov/facts/hydrophone.html.

A Norro, B Rumes, and S Degraer. Chapter 3 . Characterisation of the operational noise , generated by offshore wind farms in the Belgian part of the North Sea. *Offshore wind farms in the Belgian part of the North Sea.*, page 327, 2009.

Norwegian Government. Ot.prp. nr. 107 (2008-2009): Concerning an act on offshore renewable energy production (the offshore energy act), 2009.

Norwegian Government. Norway opens offshore areas for wind power [press release], 2020. URL https://www.regjeringen.no/en/historical-archive/solbergs-government/Ministries/oed/press-releases/2020/norway-opens-offshore-areas-for-wind-power/id2705986/.

Norwegian Government. Ambitious offshore wind initiative [press release], 2022a. URL https://www.regjeringen.no/en/aktuelt/ambitious-offshore-wind-power-initiative/id2912297/.

Norwegian Government. 65 millionar kroner til havvind-undersøkingar [press release], 2022b. URL https://www.regjeringen.no/no/aktuelt/hv-pk-rnb/id2912306/.

OSPAR convention. Convention for the protection of the marine environment of the north-east atlantic. 1992: text as amended July 1998, updated May 2006., 1992. URL https://www.ospar.org/site/assets/files/1290/ospar_convention-1.pdf.

Tanja Pangerc, Peter D. Theobald, Lian S. Wang, Stephen P. Robinson, and Paul A. Lepper. Measurement and characterisation of radiated underwater sound from a 3.6 mw monopile wind turbine. *The Journal of the Acoustical Society of America*, 140(4):2913–2922, 2016. doi: 10.1121/1.4964824. URL https://doi.org/10.1121/1.4964824.

Petroleumsforskrifta. FOR-1997-06-27-653.

Petroleumslova. LOV-1996-11-29-72.

MB Porter. The bellhop manual and user's guide: Preliminary draft. *Heat, Light, and Sound Research, Inc., La Jolla, ...*, pages 1–57, 2011. URL http://oalib.hlsresearch.com/Rays/HLS-2010-1.pdf.

Michael B. Porter. Bellhop3D User Guide. page 72, 2016.

Hermann Radecke and Michael Benesch. Messung der betriebsgeräusche von offshore-wea zur bestimmung des schalleintrags durch die schallübertragungsfunktion zwischen turm und wasser an anlagen im testfeld offshore : Schlussbericht ; dieses forschungsvorhaben wurde unter der bezeichnung rave betriebsschall im rahmen der forschungsinitiative rave - research at alpha ventus durchgeführt, 2012. URL https://www.tib.eu/de/suchen/id/TIBKAT%3A798349069.

Sigrid Eskeland Schütz. Marine spatial planning - prospects for the arctic. *Arctic Review*, 9:44–66, Feb. 2018. doi: 10.23865/arctic.v9.899. URL https://arcticreview.no/index.php/arctic/article/view/899.

Peter Sigray and Mathias H. Andersson. Particle motion measured at an operational wind turbine in relation to hearing sensitivity in fish. *The Journal of the Acoustical Society of America*, 130(1):200–207, 2011. doi: 10.1121/1.3596464. URL https://doi.org/10.1121/1.3596464.

Lise Doksæter Sivle, Tonje Nesse Forland, Karen de Jong, Geir Pedersen, Guosong Zhang, Tina Kutti, Kate McQueen, Henning Wehde, and Endre Grimsbø. Advice from the Institute of Marine Research on anthropogenic noise in the sea. - Knowledge basis, evaluations and advice for 2022. *Rapport fra havforskningen*, 1, 2022. ISSN 1893-4536.

I. M. Solbrekke, A. Sorteberg, and H. Haakenstad. The 3 km norwegian reanalysis (nora3) – a validation of offshore wind resources in the north sea and the norwegian sea. *Wind Energy Science*, 6(6):1501–1519, 2021. doi: 10.5194/wes-6-1501-2021. URL https://wes.copernicus.org/articles/6/1501/2021/.

Brandon L. Southall, James J. Finneran, Coleen Reichmunth, Paul E. Nachtigall, Darlene R. Kneten, Ann E. Bowles, William T. Ellison, Douglas P. Nowacek, and Peter L. Tyack. Marine mammal noise exposure criteria: Updated scientific recommendations for residual hearing effects. *Aquatic Mammals*, 45(2):125–232, 2019. doi: 10.1578/AM.45.2.2019.125.

S. Sowmiya. Mitigation of underwater vibration due to offshore wind turbines. *International Journal of Engineering Research Technology*, 6(14), 2018. URL https://www.ijert.org/research/mitigation-of-underwater-vibration-due-to-offshore-wind-turbines-IJERTCONV6IS14091.pdf.

Robert Z. Szasz and Laszlo Fuchs. *Chapter 5: Wind Turbine Acoustics*, volume 44. WIT Press 05: Transactions on State of the Art in Science and Engineering, 2010. doi: 10.2495/978-1-84564-205-1/.

Lynne D. Talley, George L. Pickard, William J. Emery, and James H. Swift. *Descriptive Physical Oceanography: An introduction, Sixth Edition*. Elsevier Ltd., 2011.

Jakob Tougaard, Line Hermannsen, and Peter T. Madsen. How loud is the underwater noise from operating offshore wind turbines? *The Journal of the Acoustical Society of America*, 148(5):2885–2893, 2020. doi: 10.1121/10.0002453. URL https://doi.org/10.1121/10.0002453.

H. Tu, Y. Wang, Q. Lan, W. Liu, W. Xiao, and S. Ma. A Chebyshev-Tau spectral method for normal modes of underwater sound propagation with a layered marine environment. *Journal of Sound and Vibration*, 492, 2020. doi: https://doi.org/10.1016/j.jsv.2020.115784.

UN. The united nations convention on the law of the sea. Division for ocean affairs and the law of the sea, 1982. URL https://www.un.org/depts/los/convention_agreements/texts/unclos/unclos_e.pdf.

Von Lencer. by von lencer at wikipedia: Lage und detailkarte des windparks alpha ventus (mit umspannplattform und fino 1) in der nordsee, 2009. URL https://de.wikipedia.org/wiki/Alpha_ventus#/media/File:Windpark_alpha_ventus_Lagekarte.png. [Online; accessed April 29, 2021].

Jürgen Weissenbergen. Noise Impact Assessment Hywind Tampen Noise Impact Assessment Hywind Tampen Jürgen Weissenberger. pages 1–25, 2019.

Gordon M. Wenz. Acoustic Ambient Noise in the Ocean: Spectra and Sources . *The Journal of the Acoustical Society of America*, 34, 1962. doi: 10.1121/1.1909155.

WindEurope. Scaling up Floating Offshore Wind towards competitiveness. Position Paper, November 2021.

Chun-Mei Yang, Zong-Wei Liu, Lian-Gang Lü, Guang-Bing Yang, Long-Fei Huang, and Ying Jiang. Observation and comparison of tower vibration and underwater noise from offshore operational wind turbines in the east china sea bridge of shanghai. *The Journal of the Acoustical Society of America*, 144(6):EL522–EL527, 2018. doi: 10.1121/1.5082983. URL https://doi.org/10.1121/1.5082983.